The University Of Sheffield.

Investigating Novel Molecular Regulators of the Ribbon Synapses of Mammalian Inner Hair Cells.

By:

Oliver Houston

A thesis submitted in partial fulfilment of the requirements for the degree of Doctor of Philosophy

The University of Sheffield

Faculty of Science

Department of Biomedical Science

December 2015

Acknowledgements:

To begin I would like to thank both of my supervisors; Professor Walter Marcotti, for providing me with a project and a technique that I could master when my chromaffin cells were quite literally floating away and Dr Elizabeth Seward, for teaching me “the art of the patch”.

I am also grateful to my advisors, Professor David Strutt and Professor Matthew Holley, for testing me, reviewing my work and putting me back on track when I needed it.

My thanks also go to the Marcotti lab members, who made the lab an enjoyable place to work for 3 years and provided endless support and encouragement when the preparation technique seemed impossible. In particular, Dr Stuart Johnson, for answering an endless string of technical questions tirelessly and Dr Alison Wood, for figuring out how to genotype even the trickiest strains of mice.

Finally I would like to acknowledge Sarah, who I cannot thank enough for the support, the home, the coffee and constantly reminding me that there is a world out there.

Abstract:

The auditory ribbon synapse is highly specialised to regulate the release of glutamate from IHCs and generate action potentials in auditory afferent fibres in response to small and graded changes in the receptor potential of IHCs. This is essential for maintaining the fidelity of auditory stimuli over wide range of frequencies and intensities. This study was aimed at identifying possible novel molecular regulators for the development and function of auditory ribbon synapses. I have used patch-clamp electrophysiology to record calcium currents and changes in membrane capacitance from IHCs to monitor vesicle fusion at the auditory ribbon synapse.

The ubiquitously expressed calcium-sensor for vesicle priming, DOC2B was considered to be a potential priming factor at the auditory ribbon synapse. I have found that it is not involved in fast, calcium-dependent exocytosis of synaptic vesicles at the auditory ribbon synapse.

The inositol 5'-phosphatase SynJ2 is required for the survival of auditory hair cells and is thought to regulate clathrin-mediated endocytosis. My results show that IHCs from SynJ2 KO mice display normal endocytic responses after exocytotic events and normal replenishment of the vesicle pools. Therefore, SynJ2 is not required for endocytosis, or vesicle recycling in IHCs.

Connexins 26 and 30 are subunits of heteromeric gap-junctions and hemichannels in supporting cells of the cochlea. Connexin mutations cause over 50% of cases of non-syndromic hereditary deafness in humans. IHCs from mice with severely reduced connexin expression display larger calcium currents and smaller exocytotic responses. Therefore expression of connexins in the cochlea is essential for presynaptic function at the auditory ribbon synapse.

Finally I have found that the transcriptional co-activator Wbp2 is not required for presynaptic function of mature IHCs, therefore Wbp2 is not involved in the transcription of key presynaptic molecules in IHCs.

Contents:

Figures:

Tables:

Abbreviations:

Abbreviation	Meaning
ABR	Auditory brainstem response
Cm	Membrane capacitance
CME	Clathrin mediated endocytosis
CNS	Central nervous system
Cx26	Connexin 26
Cx30	Connexin 30
DOC2B	Double C2 domain protein β
gL	Leak conductance
*I*h	Holding current
IHC	Inner hair cell
OHC	Outer hair cell
RRP	Readily releasable pool
Rs	Series resistance
SGN	Spiral ganglion neuron
SNARE	soluble n-ethylmaleimide-sensitive-factor attachment receptor
SRP	Secondary releasable pool
SynJ1 and SynJ2	Synaptojanin 1 and Synaptojanin 2
Wbp2	WW-domain binding protein 2

Chapter 1 - Introduction: The Ribbon Synapse is Essential for Hearing.

Hearing is one of the major senses in vertebrates, the loss of which can greatly impair the quality of life of humans and other vertebrates. It allows for ideas to be transferred from one person to many others using spoken language. It serves as an early warning system for dangers by detecting potential threats, allowing us to determine the location of a threat and what that threat may be. The auditory system detects stimuli across a wide range of intensities and frequencies with incredibly high temporal speed and precision (VanDewater et al., 1996). This is particularly important for sound localisation, where interaural time differences and interaural intensity differences, i.e. differences in the timing of sound waves reaching each ear, or the intensity of the sound waves at each ear, can be used by the central auditory system to determine the location of a sound source (Akeroyd, 2014). Therefore the auditory system is highly specialised to maintain the fidelity of incoming auditory stimuli.

The sensory cells of the auditory system are the hair cells, which are stimulated by deflection of a mechanosensitive hair bundle at their apex (Marcotti, 2012). Hair cells transduce these stimuli into an electrical signal that triggers the release of the neurotransmitter glutamate at the ribbon synapses at the base of the hair cell (Safieddine et al., 2012). Glutamate released from hair cells stimulates action potential firing in auditory afferent fibres that convey signals directly to the auditory centres in the central nervous system (CNS) (Glowatzki and Fuchs, 2002).

Perturbation of the sensory hair cells and their ability to transmit auditory signals to the afferent fibres - either by injury, disease or age-related processes – greatly impairs hearing in humans and other vertebrates. Recent studies have indicated the ribbon synapse is sensitive to both age-related and noise-induced damage, which leads to hearing loss (Kujawa and Liberman, 2009). A comprehensive understanding of the regulators of auditory ribbon synaptic function is vital to determine why it is sensitive to damage and may pave the way for future treatments for hearing loss.

1.1 Anatomy of the peripheral auditory system.

The peripheral auditory system has normally been described in three main parts: the outer, middle and inner ears. The outer ear comprises the pinna and the ear

canal that serve to direct air borne sound waves towards the tympanic membrane of the middle ear. The middle ear contains the tympanic membrane (eardrum) and three tiny bones called ossicles; the malleus, the incus and the stapes. The middle ear serves to transfer mechanical displacement of the tympanic membrane by sound waves to the cochlea of the inner ear by motion of the ossicles, amplifying the vibrations of the tympanic membrane, while maintaining their frequency profile (Fay and Popper, 1994). The inner ear is a complex structure within the temporal bone of the skull; it contains the vestibular system that detects movement and acceleration of the head, and the cochlea, which is the sensory organ for hearing. The cochlea is a coiled, fluid-filled organ encased in bone, which receives mechanical input from vibrations of the ossicles at the oval window (Figure 1.1) (Echteler et al., 1994).

The cochlear spiral.

The fluid-filled duct that creates the spiral structure of the cochlea is divided into three tubes; the scala vestibuli, the scala tympani and the scala media (Figure 1.1) (Echteler et al., 1994). The scala media lies between the scala vestibuli and scala tympani; it is separated from the scala vestibuli by Reissner's membrane and the scala tympani by the reticular lamina and the basilar membrane. At the apical tip of the cochlear spiral, the scala vestibuli and scala tympani are connected by a narrow opening, the helicotrema. The round window is a small opening at the basal end of the scala tympani, covered by the round window membrane. The scala vestibuli has a similar small opening called the oval window, which is covered by the oval window membrane and the footplate of the stapes bone (Echteler et al., 1994). The scala media contains endolymph, an extracellular solution with an unusually high concentration of potassium ions (157 mM) and low concentration of sodium (1.3 mM) and calcium (0.02 mM) ions (Dallos and Fay, 1996). The scala vestibuli and scala tympani contain perilymph, an extracellular fluid with normal concentrations of sodium (145 mM), potassium (5 mM) and calcium (1.3 mM) ions relative to interstitial fluid. To prevent the mixing of endolymph with perilymph or interstitial fluid, the many cell types surrounding the scala media form tight junctions that prevent diffusion of ions in/out of the scala media (Dallos and Fay, 1996).

Figure 1.1: Anatomy of the ear.

A) Anatomy of the peripheral auditory system, showing; the outer ear composed of the external pinna and the ear canal; the middle ear containing the ear drum and the ossicles; the inner ear containing the cochlea for hearing and the vestibular balance organ (Holley, 2000).

B) Schematic representation of a cross-section of the cochlear tube, showing endolymph in the scala media in green and perilymph in the scala tympani and scala vestibuli in blue. Also showing the organ of Corti, basilar membrane and tectorial membrane (Oarih, 2004).

A)

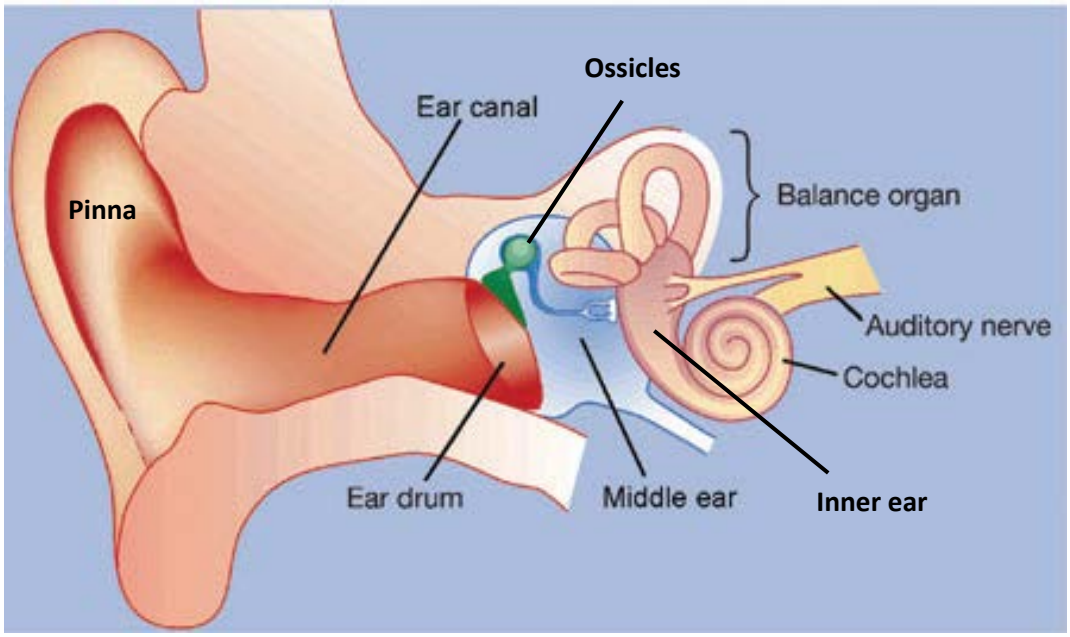
Ossicles
Ear canal
Pinna
Balance organ
Auditory nerve
Cochlea
Ear drum
Middle ear
Inner ear

B)

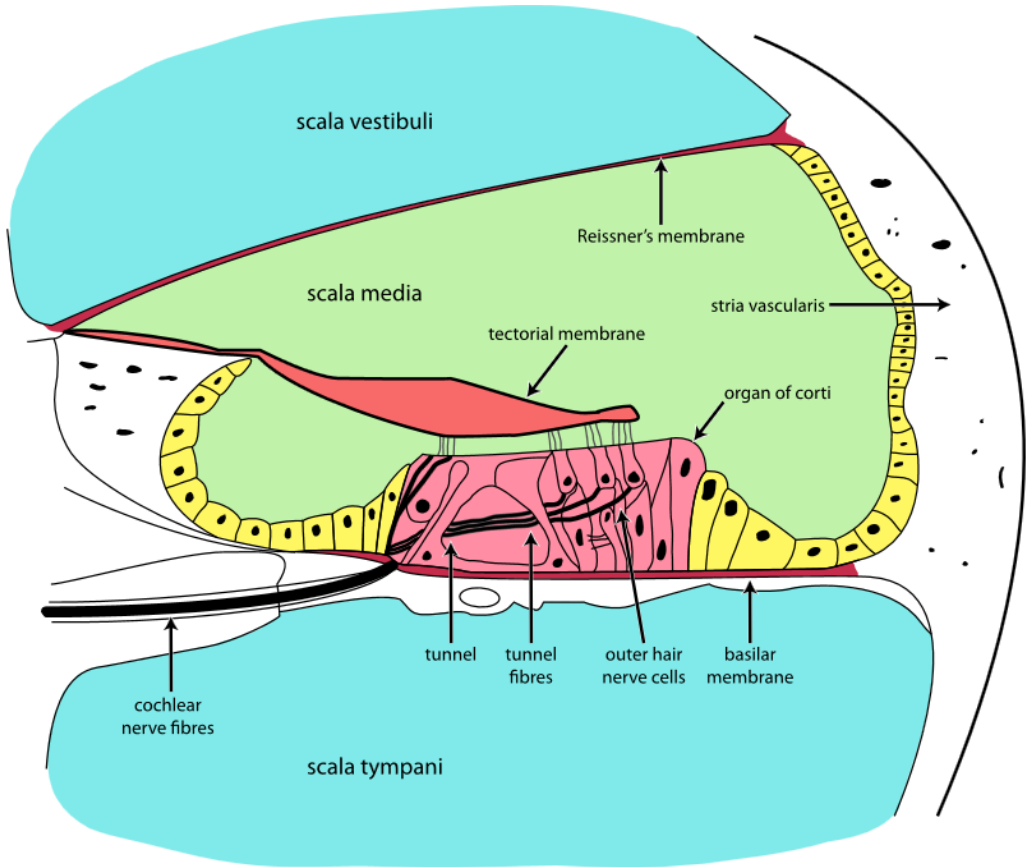
scala vestibuli
Reissner's membrane
scala media
stria vascularis
tectorial membrane
organ of corti
tunnel
tunnel fibres
outer hair nerve cells
basilar membrane
cochlear nerve fibres
scala tympani

The composition of endolymph is produced by secretion of potassium ions from the stria vascularis in the lateral wall of the scala media and is responsible for the endocochlear potential (EP) of +80 to +100 mV (Hibino et al., 2010).

The organ of Corti.

The organ of Corti is a region of the cochlear spiral that contains the basilar membrane, the sensory epithelium for hearing and the tectorial membrane. The basilar membrane is a stiff, yet pliable acellular membrane formed of densely packed collagen fibres (Guild, 1927; Cabezudo, 1978; Hudspeth, 2014). The tectorial membrane is a second acellular membrane in the cochlea composed of collagen fibres and glycoproteins (tectorins), it is attached to the surface of the spiral limbus and projects into the scala media above the sensory epithelium (Richardson et al., 2008). The sensory epithelium for hearing contains the sensory hair cells, associated supporting cells and the projections of afferent and efferent fibres of the cochlear nerve (Dallos and Fay, 1996). The basolateral membranes of cells in the sensory epithelium are bathed in perilymph that diffuses through the basilar membrane (Figure 1.2).

Sound waves within the cochlea.

When sound waves are transferred to the cochlea by the ossicles, they cause fluid displacements within the scala vestibuli and scala tympani. These fluid displacements set up travelling waves in the cochlea, displacing the basilar membrane (Figure 1.3) (Zerlin, 1969). Displacement of the basilar membrane leads to stimulation of the hair cells adjacent to the displaced portion of the basilar membrane (Dallos and Fay, 1996).

As the basilar membrane increases in width and pliability along its length (Guild, 1927), high frequency sounds cause peaks of displacement at the basal end of the cochlea, while lower frequency sounds lead to peak displacements closer to the apical end (Robles and Ruggero, 2001) (Figure 1.3). Crucially, this means there is a tonotopic gradient in the cochlea, where low frequency sounds stimulate hair cells at the apex of the cochlea and high frequency sounds stimulate hair cells at the base.

Figure 1.2: The organ of Corti contains sensory hair cells within the mammalian cochlea.

A schematic representation of the organ of Corti and its major components, notably the OHCs, with hair bundles connected to the tectorial membrane and the IHCs, with hair bundles projecting into the endolymph below the tectorial membrane (Holley, 2000).

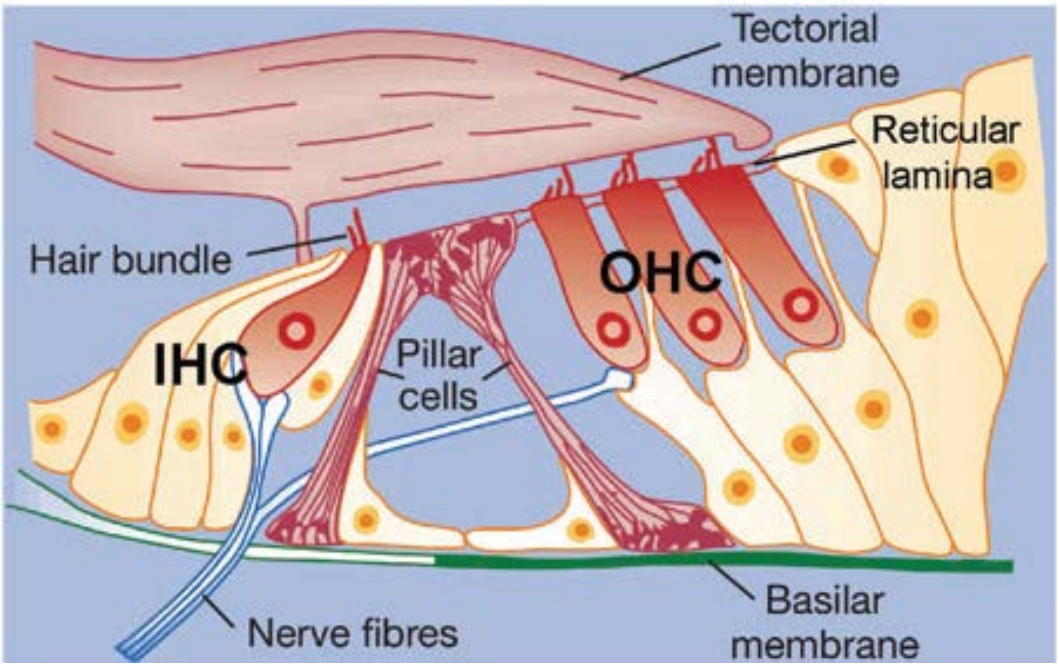

Figure 1.3: Displacement of the basilar membrane by sound waves in the cochlea.

A) Simple model of the cochlea as a tube of fluid separated into two compartments by the basilar membrane, densely packed fibres at the base of the basilar membrane make this region stiffer.

B) Travelling wave in the basilar membrane after a pure tone sound wave is transferred to the cochlea by the ossicles. The travelling wave creates a peak of displacement at different positions of the basilar membrane depending on the frequency of the sound wave. (Open University, 2013).

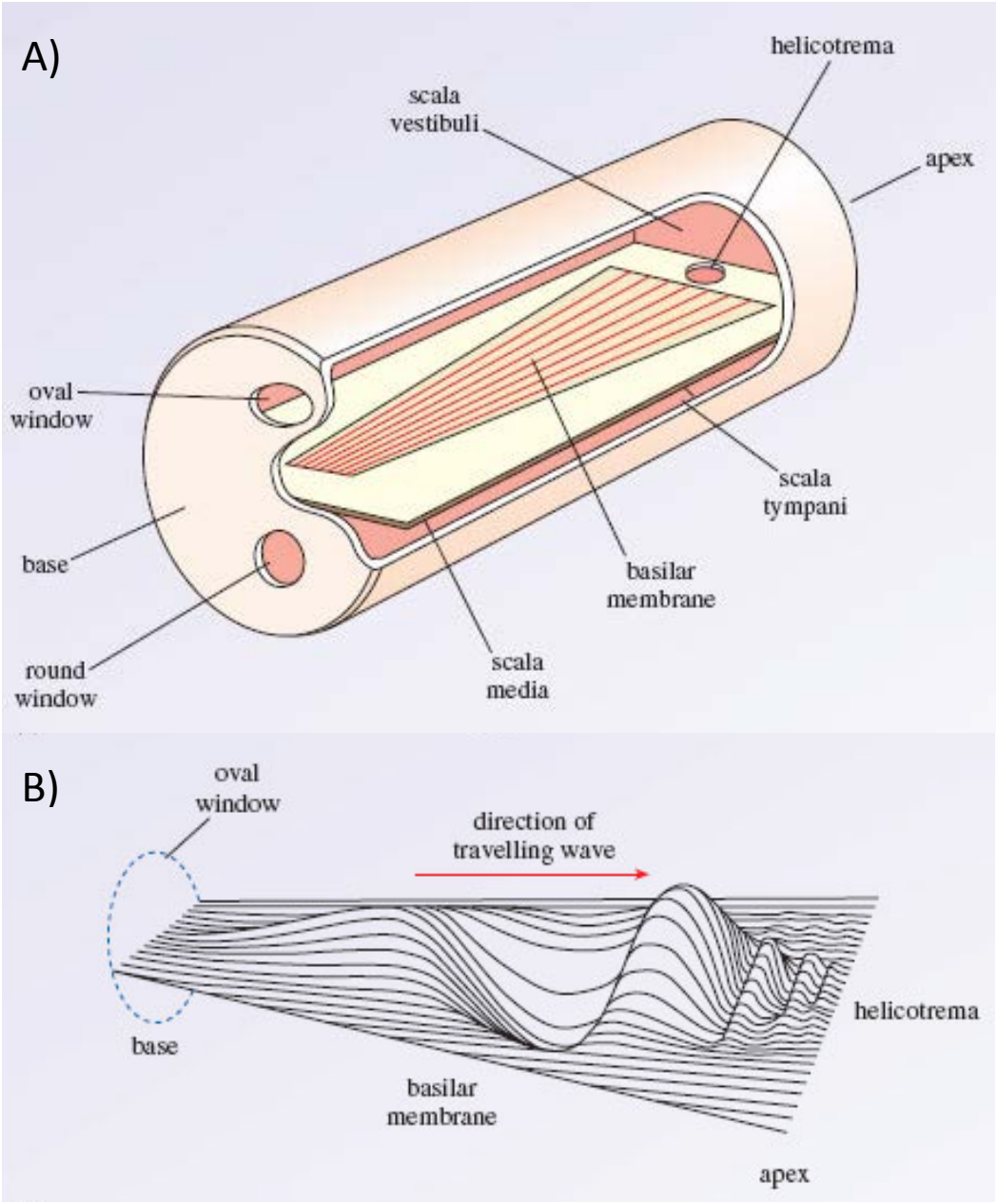

The spiral ganglion and the cochlear nerve.

The cochlear spiral surrounds the spiral ganglion, which contains the cell bodies of the auditory afferent fibres, the spiral ganglion neurons (SGNs) (Pujol et al., 1998). SGNs are bipolar neurons that receive input from synapses at the basal pole of sensory hair cells and transmit signals to the cochlear nuclei within the brainstem via the cochlear nerve. There are two types of SGN; type I SGNs, which receive synaptic input from inner hair cells (IHCs) and type II SGNs, which receive input from outer hair cells (OHCs) (Rubel and Fritzsch, 2002).

The cochlear nerve also contains efferent fibres, which carry inhibitory signals from the brainstem to the sensory epithelium. Medial and lateral olivocochlear efferent fibres originate in the medial and lateral superior olive – respectively – of the superior olivary complex in the brainstem (Rabbitt and Brownell, 2011). In the mature mammalian auditory system, the axons of medial olivocochlear neurons project into the cochlea, through the spiral ganglion and then radially through the tunnel of Corti and synapse with OHCs. The axons of the lateral olivocochlear neurons also project through the spiral ganglion, but form synapses with the afferent boutons of type I SGNs where they meet IHCs (Simmons et al., 1996).

1.2 Hair cells.

Hair cells are specialised sensory cells found in the auditory and vestibular systems of vertebrates. The hallmark feature of hair cells is the apical hair bundle that transduces mechanical stimulation into an electrical signal (Eatock, 2006). In auditory hair cells, the hair bundle projects through the reticular lamina into the endolymph filled scala media, where the endocochlear potential of +80 to +100 mV provides a large electrical driving force for potassium ions that carry the mechano-electrical transducer current. There are two types of auditory hair cell; the outer hair cells (OHCs), which form 3 rows in the organ of Corti and the inner hair cells (IHCs), which form a single row, medial to the OHCs (Dallos and Fay, 1996).

The hair bundle and mechanotransduction.

The hair bundles of both IHCs and OHCs are formed of 3-4 rows of stereocilia, neatly arranged in a staircase-like architecture and the tips of shorter stereocilia are connected to their taller neighbours by tip links (Figure 1.4) (Furness and Hackney, 2006). The elusive mechano-electrical transducer (MET) channels are located at the tips of shorter stereocilia, either near, or connected to, the base of the tip links. The MET channels are partially open at rest and can be further opened by tension generated by the tip links. It is currently unclear if tension is applied to the channel directly by the tip link, or via tension in the plasma membrane of the stereocilia (Fettiplace and Kim, 2014).

The stereocilia of hair cells are stiffened by bundles of actin filaments at their core that are anchored by a densely packed "actin gel", the cuticular plate, which fills the cytoplasmic space at the apical pole of the hair cell (Flock and Cheung, 1977; Derosier and Tilney, 1989). A narrowing at the base of the stereocilia provides flexibility, allowing deflection of the hair bundle (Tilney and Tilney, 1986). Deflection of the stereocilia in the excitatory direction moves taller stereocilia away from their neighbouring shorter stereocilia (Petit and Richardson, 2009). This generates tension in the tip links, increasing the flow of inward current through the MET channel and depolarising the hair cell. Stereocilia can also be deflected in the inhibitory direction, reducing tension in the tip links and closing the MET channel, leading to hyperpolarisation of the hair cell (Hudspeth and Corey, 1977; Fettiplace and Kim, 2014).

Outer hair cells and cochlear amplification.

The OHCS are often described as "the cochlear amplifier" because they are electromotile, contracting in response to depolarisation and extending in response to hyperpolarisation (Figure 1.4) (Brownell et al., 1985). The tips of the hair bundles of OHCs are connected to the tectorial membrane, allowing their contractions to amplify the displacement of the basilar membrane. This amplification of basilar membrane displacement increases the relative movement of fluid around the hair bundles of nearby IHCs (Kennedy et al., 2006). OHC electromotility is regulated by

Figure 1.4: Sensory hair cells within the organ of Corti.

A) Electron micrograph of orderly “staircase” like structure of the stereociliary hair bundle on a guinea pig cochlea hair cell. Scale bar equals 2μm (Marcotti, 2012).
B) High magnification electron micrograph revealing the tip links between stereocilia of adult rat cochlea hair cells. Scale bar equals 200nm (Marcotti, 2012).
C) Schematic of an OHC and prestin based electromotility. (Fettiplace and Hackney, 2006).
D) Schematic of an IHC, synaptic ribbons are in red, ribbon bound vesicles in yellow and docked vesicles in green. Blue shading represents the spread of calcium ions from spontaneously active presynaptic zones. Black lines illustrate spontaneous activity of the afferent fibres (Matthews and Fuchs, 2010).

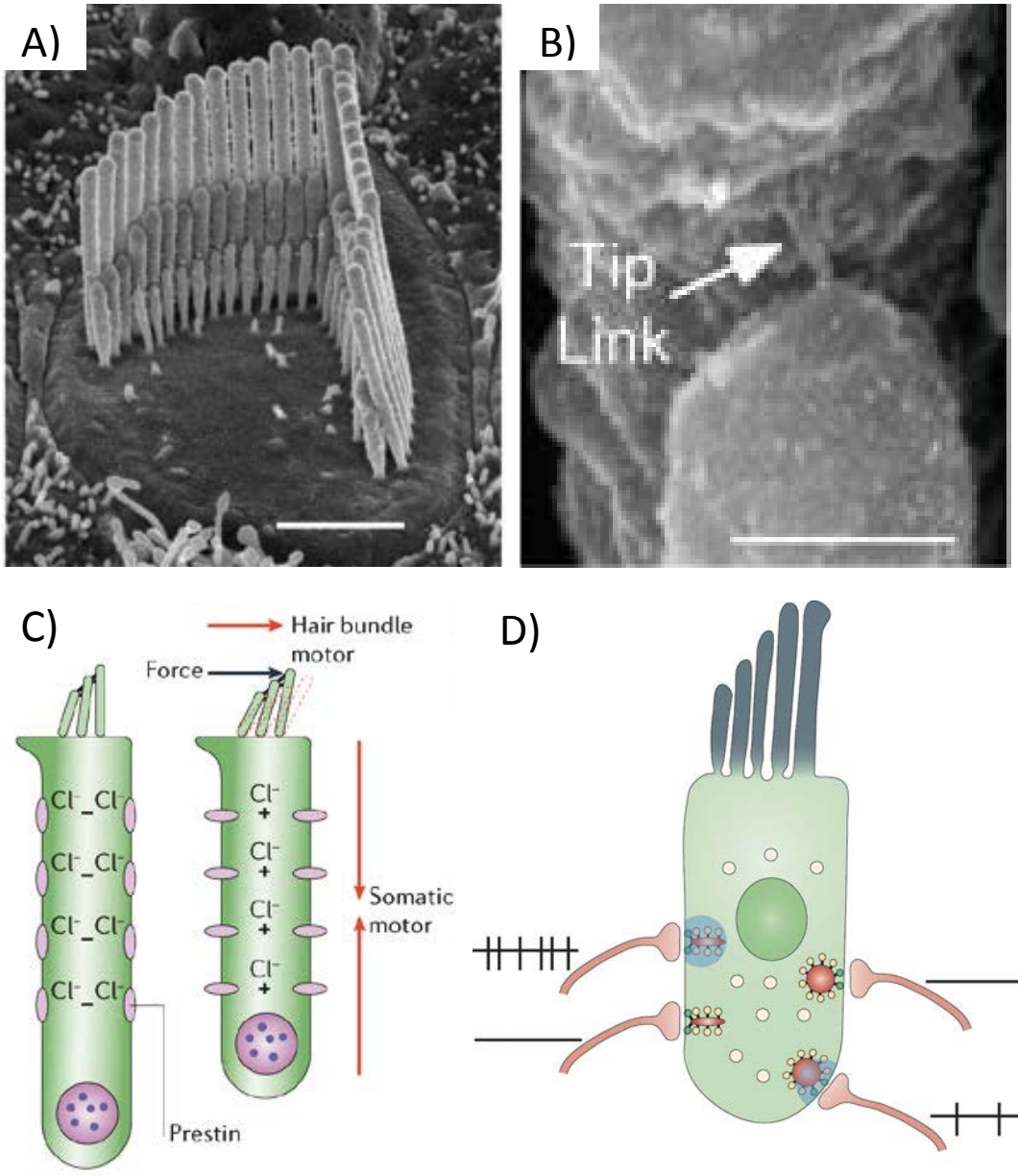
A)
B)
Tip
Link
C)
Hair bundle
motor
Force
Somatic
motor
Prestin
D)

the molecular motor prestin (Zheng et al., 2000). As OHCs are not considered to be sensory receptors for hearing and only form limited numbers of afferent synapses, they will not be considered further.

Inner hair cells.

IHCs are the primary sensory receptors for auditory stimuli. They are stimulated by displacement of the basilar membrane, which creates fluid movements around their hair bundle, opening and closing the MET channel. Depolarisation of IHCs by the influx of potassium and calcium ions through the MET channel triggers the release of glutamate from ribbon synapses (discussed in section 1.6) at the basolateral membrane (Moser and Beutner, 2000). Auditory stimuli are conveyed from the ribbon synapses of IHCs to the auditory brainstem in trains of action potentials by type I SGNs (Figure 1.4).

Unlike neurons, mature IHCs do not fire action potentials to trigger neurotransmitter release (see section 1.4), but instead display graded receptor potentials, varying with the intensity of the sound stimulation at the characteristic frequency (Russell and Sellick, 1977). Graded receptor potentials are responsible for modulating the fusion of synaptic vesicles at ribbon synapses by increasing the open probability of voltage-gated calcium channels localised to the presynaptic membrane (Glowatzki and Fuchs, 2002; Brandt et al., 2003; Goutman and Glowatzki, 2007). These processes will be discussed in detail over the following pages.

Spontaneous neurotransmission at auditory ribbon synapses.

At rest, IHCs release small amounts of glutamate, driving spontaneous activity in SGNs, thought to be due to inward current from the MET channel raising the resting potential of the IHC (Corey and Hudspeth, 1983; Glowatzki and Fuchs, 2002). The resulting partial depolarisation of the resting IHC means that there is a low, but significant open probability of the CaV1.3 channel, leading to occasional channel openings and the fusion of small numbers of vesicles. This low rate of tonic glutamate release is sufficient to drive firing activity in type I SGNs that has been described as spontaneous activity (Liberman, 1982).

1.3 Spiral ganglion neurons.

Type I SGNs convey sensory input to the CNS.

Auditory information is carried from the hair cells of the cochlea, to the cochlear nucleus in the brainstem by SGNs, of which there are two types. Type I SGNs, which receive input from a single auditory ribbon synapse and make up 90% of the fibres in the auditory nerve, are likely to carry the vast majority of auditory information to the CNS (Spoendlin, 1972; Perkins and Morest, 1975). Type II SGNs make up approximately 10% of the SGN population and receive input from the ribbon synapses of multiple OHCs (Kiang et al., 1982). Both type I and type II fibres project to the cochlear nuclei of the brainstem, where they bifurcate, sending projections to both the dorsal cochlear nucleus and ventral cochlear nucleus (Brown and Ledwith, 1990). Morphological studies show the fibres of type I SGNs are larger in diameter than fibres of type II SGNs and are myelinated (Kiang et al., 1982), further suggesting type I fibres are specialised to rapidly convey sensory information to the CNS. .

AMPA receptors mediate postsynaptic activity at the auditory ribbon synapse.

Excitatory glutamatergic AMPA receptors mediate postsynaptic currents and the generation of action potentials at the postsynaptic bouton of type I SGNs (Glowatzki and Fuchs, 2002). Electrophysiological recordings of EPSCs and action potentials at the afferent bouton of type I SGNs reveals that the majority of EPSCs are sufficient to generate action potentials in type I SGNs (Rutherford et al., 2012), suggesting that type I SGNs are highly specialised to fire action potentials with a low threshold for glutamate.

AMPA receptors have been shown to be arranged in a ring-like structure on the postsynaptic bouton of type I SGNs (Meyer et al., 2009) and the size of the AMPA receptor patch is inversely proportional to the size of the ribbon at the presynaptic active zone (Liberman et al., 2011).

Postsynaptic activity in auditory afferent fibres.

Single unit recordings from SGNs in the cat auditory nerve show that each neuron responds with bursts of spikes with maximal discharge rates at a characteristic sound frequency with a minimal sound threshold for activity (Galambos and Davis, 1943), supporting the idea that different IHCs are activated by different sound frequencies. In the absence of acoustic stimulation, action potentials can be recorded from type-I SGNs, described as spontaneous activity (Kiang et al., 1962).

Early studies combining electrophysiology and labelling, have shown that SGNs with high rates of spontaneous activity (20-100 spikes s^{-1}) have thicker fibres (0.8-1.2 µm) and tend to form synapses on the pillar side of the IHC. Fibres with low-spontaneous firing rates (0.5-10 spikes s^{-1}) have thinner fibres (0.3-0.8 µm) and tend to form synapses on the modiolar side of the IHC. In vivo high spontaneous rate fibres have been shown to have lower thresholds to acoustic stimulation than low spontaneous rate fibres (Liberman, 1978, 1980; Kiang et al., 1982).

Later work showed that for SGNs responding to relatively low-frequency sounds, spikes were clustered in groups according to the periodicity of the sound stimulus. This was termed phase-locking, where peaks in the sound wave are associated with clusters of action potentials in SGNs and troughs in the sound waves are associated with periods of quiescence in the SGN, suggesting inhibition of spontaneous activity (Rupert et al., 1963). Further work in squirrel monkeys showed that the discharge pattern of SGNs was phase-locked to the frequency of the sound stimulus up to 2.5 kHz, this link was maintained between 2.5kHz and 5kHz, but became progressively weaker (Rose et al., 1967). In guinea pigs, the receptor potential of IHCs has been shown to be phase-locked to sound stimulus, with periods of depolarisation occurring during peaks in the sound wave and hyperpolarisation occurring during troughs (Palmer and Russell, 1986), suggesting that phase-locking in type I SGNs is established by the receptor potential and glutamate release from the presynaptic IHC. Phase-locking deteriorates for high-frequency sounds as the time constant of IHC membranes limits the speed at which their membrane potential can change (Palmer and Russell, 1986).

1.4 Exocytosis, essential for neurotransmission.

Neurotransmission relies on the transfer of information between two cells, one of which is a neuron, via a specialised area where the two cells meet, the synapse. In the presynaptic cell, neurotransmitters are packaged into membrane bound vesicles and released when the vesicle membrane fuses with the presynaptic membrane by the process of exocytosis (Fuchs, 1996). Neurotransmitters diffuse across the synaptic cleft and bind to receptors on the postsynaptic membrane, leading to the stimulation, or inhibition of responses from the postsynaptic cell (Parnas and Parnas, 1994).

Synaptic exocytosis is a highly regulated process that involves several molecules forming the intricate “fusion machinery” (Sudhof and Rothman, 2009). The current hypothesis for canonical neuronal exocytosis suggests vesicles are brought to the presynaptic active zone, where they are docked in close proximity (≤100nm) to calcium channels. Once a vesicle is docked at the active zone, the fusion machinery is primed by the association of vesicular and plasma membrane SNARE proteins (soluble n-ethylmaleimide-sensitive-factor attachment receptor), with complexin and synaptotagmin (Wu et al., 2012). The association of SNAREs, synaptotagmins and complexins forms a prefusion complex that reduces the energy barrier for membrane fusion and prevents premature fusion of the vesicular and plasma membranes. Synaptotagmin is a calcium sensor that may act as the “fusion clamp”, preventing premature vesicle fusion by clamping the prefusion complex in a primed state until calcium ions bind to the C2 domains of synaptotagmin (Chapman, 2008).

In neurons, when an action potential reaches the presynaptic active zone, it depolarises the presynaptic membrane, increasing the open probability of voltage-gated calcium channels located here (Rama et al., 2015). This leads to more channel openings and an influx of calcium ions into the presynaptic active zone. When calcium ions bind to C2 domains of synaptotagmin, a conformational change in synaptotagmin triggers the fusion of the vesicle and plasma membranes, releasing neurotransmitters into the synaptic cleft (Figure 1.5) (Chapman, 2008). This could be due to removal of synaptotagmin’s clamp on the prefusion complex, allowing

SNARE proteins to “zip” together to drive fusion of the two membranes. Synaptotagmins may also further reduce the energy barrier to fusion by insertion of their C2 domains into the presynaptic membrane, inducing membrane curvature (Chapman, 2008; Sudhof, 2013).

While synaptotagmin-triggered, SNARE-mediated membrane fusion is the prevailing hypothesis for understanding vesicle fusion and neurotransmitter, other models exist. Recently, the “dyad hypothesis” has been proposed, suggesting that SNARE-proteins act simply as the docking mechanism for vesicles at presynaptic active zones, rather than drivers of fusion. According to the dyad hypothesis, synaptotagmins form dimers that act as the fusion machinery and insertion of their C2 domains into the presynaptic membrane is the driver for vesicle fusion (Gundersen and Umbach, 2013). While the dyad hypothesis is an interesting alternative to the prevailing SNARE-mediated fusion model, limited supporting evidence has been presented so far. However, it may serve as a useful model for cells where vesicle fusion relies on unconventional machinery, such as IHCs. Neurotransmitter release from the ribbon synapse of IHCs is likely to have some similarities to conventional synaptic exocytosis, but a number of differences have been described, which will be discussed further.

1.5 Ribbon synapses.

Ribbon synapses are highly specialised sensory synapses that have a large, electron-dense presynaptic structure, the ribbon, which is surrounded by small synaptic vesicles (Figure 1.6) (Sjostrand, 1958; Liberman, 1980). The bulk of the synaptic ribbon is composed of ribeye, which has a unique N-terminal A domain that facilitates the assembly of large structures and a C-terminal B-domain identical to the transcriptional repressor CtBP2 (Schmitz et al., 2000). The synaptic ribbon is tethered to the presynaptic membrane by the cytomatrix protein bassoon (Dick et al., 2003). Synaptic ribbons are found in hair cells of the auditory and vestibular systems , as well as photoreceptors and bipolar cells in the retina (Safieddine and Wenthold, 1999).

Figure 1.5: The synaptic vesicle cycle and exocytotic machinery.

A) Neurotransmitters (yellow) are loaded into synaptic vesicles, which are targeted to presynaptic active zones, where they dock, before being primed to form a stable prefusion complex. Calcium triggers a conformational change in synaptotagmin, which initiates the fusion of the vesicular and plasma membranes, releasing the neurotransmitters. Vesicular components are recovered by clathrin-mediated endocytosis.

B) The major components of the fusion machinery for classical neuronal exocytosis; the calcium sensor, synaptotagmin and the SNARE complex (SNAP-25, synaptobrevin and syntaxin). When calcium ions (red dots) bind to the C2 domains of the calcium sensor – synaptotagmin - a conformational change in synaptotagmin triggers vesicle fusion; either by the release of a clamp on the SNARE-complex, or by actively reducing the energy barrier for fusion.

Figure reproduced from: Synaptotagmin: A Ca^{2+} sensor that triggers exocytosis? (Chapman, 2002).

A)

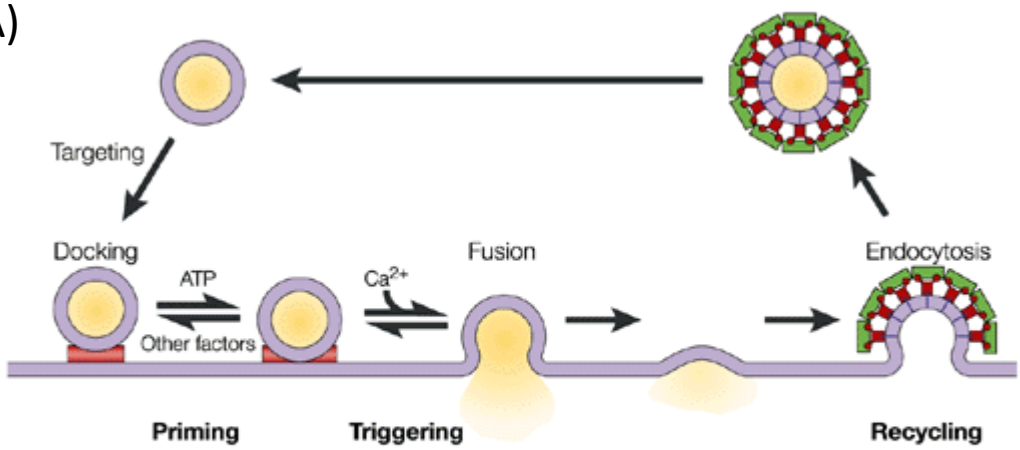
Targeting
Docking
ATP
Other factors
Ca^{2+}
Fusion
Endocytosis
Priming
Triggering
Recycling

B)

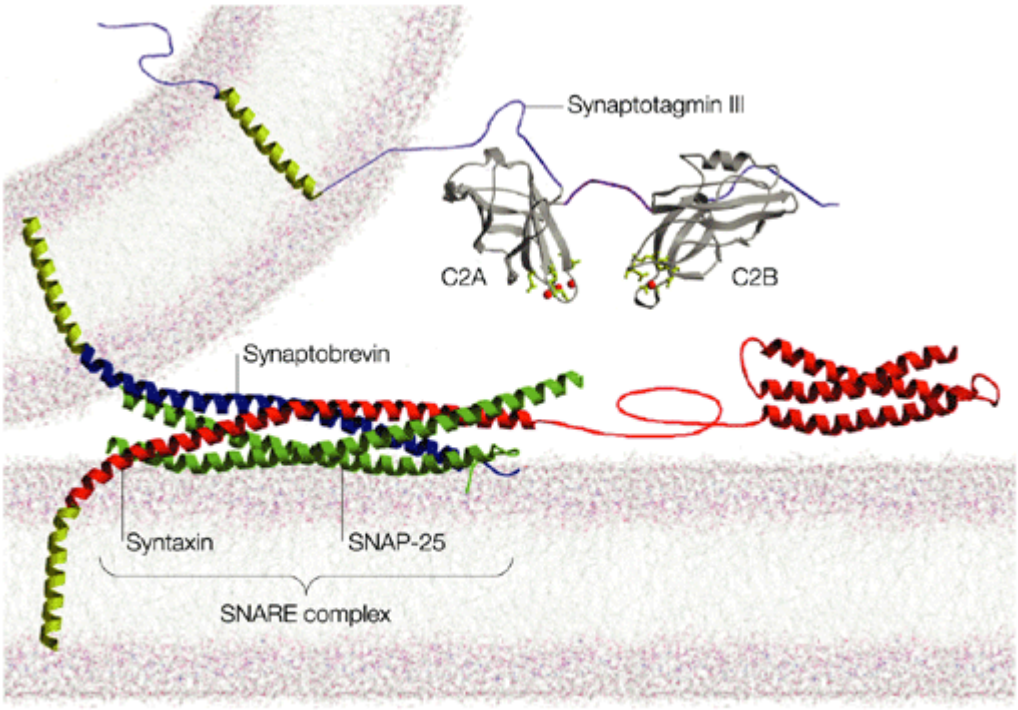
Synaptotagmin III
C2A
C2B
Synaptobrevin
Syntaxin
SNAP-25
SNARE complex

Hair cells and photoreceptors respond to sensory input with graded changes in their membrane potential (Russell and Sellick, 1978; Kurtz et al., 2001). Bipolar cells respond to synaptic input from photoreceptors and also show graded changes in their membrane potential (Barlow, 1953; Kaneko, 1970), however certain bipolar cells also show spiking activity similar to action potentials (Saszik and DeVries, 2012).

The presence of synaptic ribbons at the synapses of sensory cells, which display graded responses to sustained input, suggests the ribbon may be important for maintaining a rapid supply of synaptic vesicles to the readily releasable pool (RRP) during prolonged periods of activity. This has been suggested to be important for improving temporal acuity and fidelity over long periods of stimulation (Parsons et al., 1994). Alternatively, it has also been suggested that the ribbon tethers vesicles in close proximity with each other, so they can fuse together while simultaneously fusing with the presynaptic membrane, a process known as compound fusion (Heidelberger, 1998; Parsons and Sterling, 2003; Matthews and Sterling, 2008).

The role of auditory ribbon synapses.

In the mature mammalian cochlea, each IHC forms up to 20 ribbon synapses with type I SGNs, each ribbon synapse contains a single presynaptic ribbon and the single afferent bouton of one type I SGN, implying that each ribbon synapse is a single functional unit in the auditory pathway (Liberman et al., 1990).

In IHCs from bassoon knockout mice, the number of presynaptic active zones occupied by ribbons is reduced by about 80% (Khimich et al., 2005) and sound encoding is disrupted in vivo (Jing et al., 2013). The amplitude of the calcium current is significantly smaller in IHCs lacking bassoon, leading to a corresponding reduction in vesicle fusion. This is associated with a reduction in the clustering of calcium channels and synaptic vesicles at the presynaptic active zone of IHCs (Frank et al., 2010). Despite the dramatic loss of synaptic ribbons and exocytotic capacity observed in IHCs from bassoon KO mice, there is only a 20-30dB threshold shift in the auditory brainstem response (ABR), indicating that the limited presynaptic function remaining in these mutants conveys some auditory information to the

Figure 1.6: The ribbon synapse of the cochlear hair cell.

A) Electron micrographs of spherical electron dense ribbons at the synapses of immature IHCs, surrounded by tethered synaptic vesicles (Wong et al., 2014).

B) Immunostaining for the calcium channel CaV1.3 (red) and the C-terminal portion of the ribbon protein ribeye CtBP2 (green) in immature IHCs (Zampini et al., 2010).

C) Wedge shaped ribbons at the synapses of IHCs from adult (P20) mice (Wong et al., 2014).

D) Immunostaining for the calcium channel CaV1.3 (red) and the C-terminal portion of the ribbon protein ribeye CtBP2 (green) in mature IHCs shows increased colocalisation in mature IHCs, compared to immature IHCs (Zampini et al., 2010).

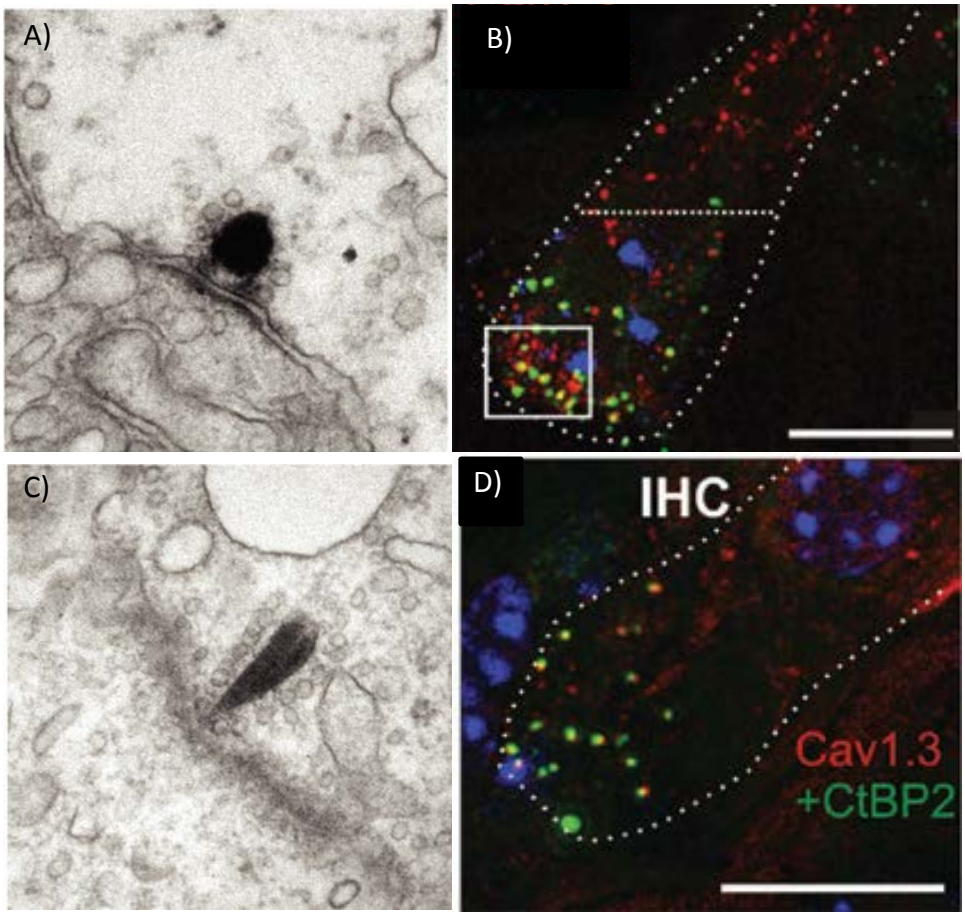

central auditory pathway (Khimich et al., 2005). The reduction in the exocytotic response of IHCs from bassoon KO mice appears to be due to the reduced calcium influx at the ribbon synapses, suggesting ribbons are not required for normal function of the fusion machinery. However vesicle pool replenishment was significantly slowed in these IHCs; suggesting either the ribbon, or bassoon is important for replenishment of the RRP at IHC ribbon synapses (Frank et al., 2010).

Modelling studies based on electrophysiological recordings from the hair cells and auditory nerves have suggested that synaptic ribbons are important for increasing the size of the readily releasable pool of vesicles and decreasing the latency between stimulation of the hair cell and action potential firing in the SGNs (Wittig and Parsons, 2008). This is supported by evidence that in bassoon knockout mice, short-term synaptic depression is enhanced at central neuronal synapses, suggesting bassoon is important for maintaining the supply of vesicles at synapses that lack ribbons (Hallermann et al., 2010).

The role of retinal ribbon synapses.

Evidence from salamander photoreceptors suggests that synaptic ribbons limit vesicle supply to release sites at ribbon synapses, suggested to improve visual acuity by regulating the number of vesicles released from the synapse in response to changes in stimulus intensity (Jackman et al., 2009). Further work in salamander photoreceptors and mouse bipolar cells showed that light induced damage to the synaptic ribbons disrupted fusion of vesicles from both the RRP and the secondary releasable pool (SRP), suggesting the ribbon is essential for vesicle fusion at retinal ribbon synapses (Snellman et al., 2011). Modelling of vesicle dynamics at bipolar cell ribbon synapses suggests that accumulation of vesicles at the ribbon can facilitate vesicle supply to the synapse by passive diffusion. This was used to suggest that the ribbon only transiently tethers vesicles near the active zone, passively increasing the concentration of vesicles, rather than actively directing vesicles towards the active zone (Graydon et al., 2014).

Comparing auditory and retinal ribbon synapses.

It is worth noting that there are a number of differences between the ribbon synapses of the auditory and visual systems.

In the retina, a single presynaptic photoreceptor ribbon can form synapses with multiple horizontal and bipolar cells, which may have different complements of postsynaptic glutamate receptors to act as inhibitory/excitatory synapses depending on the postsynaptic cell type (Euler et al., 2014; Schmitz, 2014). This is in contrast to the single excitatory postsynaptic bouton found at auditory ribbon synapses (Spoendlin, 1972).

Also, photoreceptors and auditory hair cells respond differently to stimulation by their respective sensory input; In the absence of auditory stimuli, IHCs are slightly depolarised by the resting MET current (Glowatzki and Fuchs, 2002), leading to some calcium channel activity and "spontaneous" fusion of synaptic vesicles at auditory ribbon synapses. This releases neurotransmitters that drive spontaneous spiking activity in type I SGNs at rates of less than 0.1Hz for low spontaneous rate fibres to over 100Hz for high spontaneous rate fibres (Liberman, 1982; Glowatzki and Fuchs, 2002; Heil et al., 2007). The rate of spontaneous activity in type I SGNs is likely to be proportional to the number of vesicles fusing at the ribbon synapse it receives input from. Depolarisation of the hair cell by auditory stimuli opens voltage-gated calcium channels closely colocalised with presynaptic ribbons, triggering synchronous exocytosis of multiple vesicles from a ribbon synapse, driving bursts of spike trains in SGNs (Moser and Beutner, 2000; Glowatzki and Fuchs, 2002; Brandt et al., 2005).

Similarly, photoreceptors are also depolarised at rest, however in response to stimulation by photons, they become hyperpolarised (Morgans, 2000).Crucially this means that photoreceptor ribbon synapses are most active at rest. In cone photoreceptors, it has been shown that 250 vesicles fuse per second in darkness, while saturating light reduces this to approximately 10 vesicle fusions per second (Choi et al., 2005).

Postsynaptically, the neurons of the visual and auditory system are also very different. In the visual system, bipolar cells display graded changes to their membrane potential in response to input from photoreceptor synapses (Barlow, 1953). Type I SGNs in the auditory system, by contrast display spiking responses to input from auditory ribbon synapses (Glowatzki and Fuchs, 2002).

Finally it is also clear that there are key differences in the molecular machinery for exocytosis at the different ribbon synapses of the auditory and visual system. For example, exocytosis at photoreceptor ribbon synapses relies on conventional synaptic machinery for exocytosis (Morgans, 2000). Conversely, many of the conventional synaptic proteins appear to be absent from the auditory ribbon synapse, e.g. synaptotagmins and SNARE proteins (Safieddine et al., 2012). The clear differences between the behaviour and molecular machinery of ribbon synapses from the auditory and visual systems make it impossible to generalise results from studies of one system to the other.

1.6 Exocytosis at the ribbon synapse of IHCs.

Exocytosis at the auditory ribbon synapse has a number of unusual characteristics; for example mature IHCs show an unusual linear relationship between the calcium influx during a depolarising stimulus and the corresponding exocytotic response (Johnson et al., 2005). Later studies showed that IHCs from the high frequency (≈30kHz) region of the gerbil cochlea displayed linear calcium-dependencies for exocytosis, while IHCs from the low frequency (≈300Hz) region display a high-order calcium dependency of exocytosis, similar to conventional synapses and immature IHCs (Johnson et al., 2008). The linear calcium dependency of exocytosis is possibly due to tight coupling between the calcium channels and exocytotic machinery on the vesicle surface allowing the opening of small numbers of calcium channels to trigger the release of synaptic vesicles (Brandt et al., 2005; Zampini et al., 2010). However it has also been suggested that the calcium-dependency of exocytosis is only quasi-linear due to the summation of different high-order saturating calcium-dependencies of exocytosis at different active zones within the same cell (Heil and Neubauer, 2010). However the linear relationship between calcium influx and

exocytosis is established, the presynaptic machinery at the auditory ribbon synapses is highly specialised to convey a wide range of exocytotic responses to small changes in the receptor potential of the IHC. This is likely to be important for coding sound intensity as low intensity stimuli appears to only activate low threshold SGNs (discussed below).

Calcium channels regulate exocytosis at auditory ribbon synapses.

L-type calcium channels were shown to be essential for hearing when mice lacking the α1D subunit were shown to be profoundly deaf (Platzer et al., 2000). This was later confirmed to be a defect in the IHC as there was a 90% reduction in the calcium current in IHCs from mice lacking the L-type CaV1.3 channel. The remaining calcium current is carried by an unidentified L-type calcium channel, likely to be CaV1.4 (Brandt et al., 2003). CaV1.3 channels colocalise with synaptic ribbons in mature IHCs, where the opening of small numbers of channels is suggested to create nanodomains of high calcium concentrations that stimulates the release of vesicles from the RRP docked at the ribbon synapse (Brandt et al., 2005). The number of calcium channels in mature IHCs has been estimated to be approximately 1700 channels with 80 at each ribbon synapse using nonstationary fluctuation analysis of mouse IHCs (Brandt et al., 2005), or approximately 2800 channels with 180 at each ribbon synapse using single-channel (unitary) current data from gerbil IHCs (Zampini et al., 2013). The discrepancies in the estimations seem to be due to differences in the estimation of the open probability (Po) of the channels during depolarisation (Po = 0.82 and Po = 0.21 respectively). Unitary current analysis also showed that CaV1.3 channels open with a very short opening latency (50μs) and have two different gating modes; one mode is characterised by brief infrequent openings, the other by longer openings, or high-frequency bursts of openings, which is suggested to support phase-locking of vesicle release to sound stimuli (Zampini et al., 2013). Similar gating modes of calcium channels have previously been described in other systems, where they have been linked to intrinsic modulators of calcium-channel activity (Kamp and Hell, 2000; Carabelli et al., 2001). CaV1.3 channels are essential for driving neurotransmitter release at the

ribbon synapse of IHCs in response to sound and are also likely to be important for spontaneous activity at the ribbon synapse.

Fusion machinery for exocytosis at the ribbon synapse

The molecular machinery governing exocytosis at the IHC ribbon synapse has been the focus of many intense electrophysiological studies in recent years, unfortunately, many studies have yielded more questions than answers. Early evidence for unique exocytotic machinery at the ribbon synapse was the absence of synapsins and synaptophysins in IHCs (Safieddine and Wenthold, 1999). Synaptophysin is thought to be involved in regulating SNARE-complex assembly due to its binding to synaptobrevin, preventing the association of synaptobrevin with SNAP-25 and syntaxin (Edelmann et al., 1995), possibly regulating the availability of certain vesicles for exocytosis to maintain the vesicle supply during periods of sustained synaptic activity (Becher et al., 1999). Synapsins are also thought to have a role in maintaining reserve pools of vesicles in synaptic terminals and in vesicle transport, accelerating the transition of vesicles from reserve pools to the (Li et al., 1995; Rosahl et al., 1995). The lack of these molecules suggests IHCs express a unique set of molecules that regulate exocytosis at the auditory ribbon synapse.

Further evidence for the unique fusion machinery at ribbon synapses is that SNARE-cleaving fragments of botulinum neurotoxins fail to block vesicle fusion at the IHC ribbon synapse (Nouvian et al., 2011); suggesting exocytosis from IHC ribbon synapses is not mediated by neuronal SNAREs.

Exocytosis from ribbon synapses is not only independent of SNARE-proteins; the classical calcium sensors for fast exocytosis – synaptotagmins I and II – are not detectable in mature IHCs. Interestingly, both are expressed in immature IHCs and are downregulated during maturation. Synaptotagmin-II is down-regulated by P8, while synaptotagmin-I is down-regulated progressively in a basal to apical fashion from P10 to P21 (Beurg et al., 2010).

While synaptotagmins do not play their conventional role as calcium sensors for fast synchronous exocytosis at mature ribbon synapses, they do appear to support the functional ribbon synapse; mature IHCs express the calcium-insensitive

synaptotagmin-IV and IHCs from synaptotagmin-IV null mice fail to develop a linear calcium-dependency of exocytosis in IHCs (Johnson et al., 2010). Synaptotagmin-II is also expressed in the cholinergic efferent system, which form transient synapses with immature IHCs (Simmons et al., 1996; Katz et al., 2004). IHCs from mice lacking functional efferent input, either by the loss of synaptotagmin II, or the loss the nicotinic acetylcholine receptor α9nAChR also fail to develop a linear calcium-dependency of exocytosis (Johnson et al., 2013a).

To counter the loss of synaptotagmins, there needs to be an alternative calcium sensor for exocytosis at the auditory ribbon synapse. Currently the only candidate molecule is the multi-C2 domain protein otoferlin. Mutations in otoferlin are responsible for nonsyndromic, hereditary hearing loss in humans (Yasunaga et al., 1999). Otoferlin is expressed in multiple isoforms in hair cells of the auditory and vestibular system, as well as in neurons in the brain (Yasunaga et al., 2000; Schug et al., 2006). Otoferlin has been proposed to have many roles in IHCs including; the calcium sensor for exocytosis (Roux et al., 2006), organisation of the basolateral compartment of IHCs via interactions with myosin VI (Heidrych et al., 2009), vesicle pool replenishment (Pangrsic et al., 2010), and as a coupler for endocytic reuptake of synaptic vesicles (Duncker et al., 2013). While otoferlin's role at the ribbon synapse is still controversial, it is clearly an important molecule in the functional IHC. Mice lacking otoferlin show a greatly reduced exocytotic response to increases in intracellular calcium (Roux et al., 2006). The many proposed functions of otoferlin have led to the suggestion that it is a multifunctional regulator of the vesicle cycle in IHCs (Pangrsic et al., 2012).

Activity at different synapses of a given IHC may encode sound intensity.

Recording activity in the afferent neurons of type I SGNs has revealed that fibres with different rates of spontaneous activity respond to acoustic stimulation by their characteristic frequency with different thresholds (Kiang, 1966). This was later shown to correlate with differences in the morphology of the fibres: high spontaneous rate fibres tend to be thicker and form synapses on the pillar face of an IHC, while fibres with low spontaneous rates tend to form synapses on the

modiolar face of an IHC (Kiang et al., 1982). This suggests that the intensity of auditory stimuli is encoded by activity in different type I SGNs, possibly due to differences in the output from the different ribbon synapses of IHCs responding to a given frequency.

The ribbon synapses of a single IHC have been shown to have both presynaptic and postsynaptic specialisations, such as larger ribbons and smaller postsynaptic AMPA receptor patches at synapses on the modiolar side of the IHC, compared to those on the pillar side of the IHC (Liberman et al., 2011). This supports the idea that sound intensity is encoded by afferent output from different ribbon synapses, with low intensity sounds stimulating spike trains from the "low-threshold, high spontaneous rate fibres", while high intensity sounds may stimulate both low and high-threshold fibres for a given frequency.

1.7 Vesicle recycling.

Presynaptic cells require an efficient means of retrieving phospholipids and vesicular proteins from the presynaptic membrane in order to replenish the pools of synaptic vesicles during repetitive stimulation. The uptake of plasma membrane and extracellular molecules is known as "endocytosis". At synapses, the recycling of synaptic membranes to produce synaptic vesicles is termed "vesicle recycling" and is thought to be largely dependent on clathrin-mediated endocytosis (CME) (Heuser and Reese, 1973; Rizzoli, 2014).

Clathrin-mediated endocytosis

The uptake of plasma membrane, membrane components and extracellular cargo by CME is arguably the best understood mechanism for internalisation in any cell type and has been reviewed in great detail (McMahon and Boucrot, 2011; Rizzoli, 2014). It is particularly important at synapses, where it is essential for replenishment of synaptic vesicle pools during prolonged synaptic activity. Briefly, there are a number of processes essential for CME to occur. First the nucleation of endocytic regulator complexes and the invagination of an endocytic pit. Second the selection of cargo and concurrent recruitment of clathrin molecules by the adaptor protein AP-2 and accessory proteins. Clathrin molecules self-assemble into

hexagonal or pentagonal lattices, leading to the formation of a clathrin-coated pit on the intracellular surface of the cells membrane. As the pit continues to invaginate, the curvature of the clathrin coated pits increases, leading to recruitment of the Bin1/Ampiphysin/RVS167 (BAR) domain proteins endophilin and dynamin. Vesicle scission appears to be mediated by enzymatic action of dynamin, but the precise mechanism remains unclear. This leads to the formation of a clathrin-coated vesicle. The clathrin coat is then rapidly disassembled, resulting in a vesicle that can either be recycled back into a synaptic vesicle, or targeted to intracellular organelles, such as endosomes, for sorting.

Endocytosis at the ribbon synapse

Endocytosis at the ribbon synapse of IHCs has received little attention compared to exocytosis, even though the time course of endocytosis was measured in one of the first studies to use capacitance changes as a measure of exocytosis from the ribbon synapse of IHCs (Moser and Beutner, 2000). However, recent studies are beginning to shed light on the mechanisms and regulation of endocytosis at auditory ribbon synapses.

An in-depth study of endocytosis in IHCs suggests two modes of endocytosis with distinct kinetics mediate the reuptake of vesicular membranes and components in-vitro. Short depolarisations, used to elicit the fusion of relatively small numbers of vesicles and small increases in membrane capacitance are followed by a slow, linear decrease in membrane capacitance. This decrease is thought to represent the removal of vesicle membranes from the presynaptic membrane and can be blocked by inhibitors of dynamin and CME. Long depolarisations that lead to a greater increase in membrane capacitance trigger both a slow linear decrease and a faster, exponential decrease in membrane capacitance, believed to the formation of bulk endosomes by bulk endocytosis. High-pressure freeze-fracture electron microscopy reveals the presence of clathrin-coated pits and vesicles as well as endosomes after prolonged stimulation of IHCs with high external potassium (Neef et al., 2014). Furthermore, inhibitors of CME prevent efficient replenishment of the SRP in response to trains of 1s depolarising voltage steps (Duncker et al., 2013). These

results suggest that CME is the primary mechanism for membrane reuptake at auditory ribbon synapses, but during periods of high activity, bulk endocytosis can be used to rapidly remove vesicular membranes and components.

The molecules regulating endocytosis at the ribbon synapses of hair cells are also beginning to receive some attention. The inositol 5-phosphatase protein synaptojanin-1 is important for maintaining synaptic transmission at ribbon synapses of zebrafish lateral line hair cells (Trapani et al., 2009) and is thought to be important for the uncoating of clathrin coated vesicles after endocytosis (Cremona et al., 1999). The ENU-mutagenised *mozart* mouse shows progressive hair cell death and hearing loss due to a point mutation in the phosphatase domain of synaptojanin 2, also thought to regulate CME, (Manji et al., 2011).

Otoferlin has been shown to couple to AP-2, an adaptor protein for CME (Duncker et al., 2013), implicating otoferlin in the regulation of reuptake of vesicular membranes at auditory synapses. This may be the reason IHCs from mice carrying the *pachanga* mutation in otoferlin are unable to effectively replenish the vesicle pools (Pangrsic et al., 2010).

1.8 Development of the inner ear.

Morphological development of the cochlea.

The inner ear develops from a small region of ectoderm adjacent to the neural tube, the otic placode, which invaginates to form the otocyst before an intense period of proliferation and morphogenesis to produce the complex architecture of the inner ear (Torres and Giraldez, 1998). In mice, the external coiled structure of the cochlea appears at embryonic day 12.5 (E12.5) and continues to grow until E17 (Morsli et al., 1998), approximately 4 days before birth. After this point, maturation of the cells within the cochlea leads to changes in the internal architecture that are required for development of the functional cochlea. For example, growth of the inner and outer pillar cells leads to the opening of the tunnel of corti at postnatal day 4 (P4) (Ito et al., 1995).

The sensory epithelium of the cochlea develops simultaneously with extension of the cochlea coil. Terminal mitosis in the prosensory region occurs between E11.5 and E14, beginning at the apex of the cochlea and progressing towards the base. Hair cells begin to differentiate at the mid-basal region at approximately E13.5 and differentiation progresses apically and basally along the cochlea until approximately E15.5 (Kelley, 2006).

Differentiation of SGNs and synaptogenesis in the cochlea occurs simultaneously to hair cell differentiation in a similar progressive fashion; beginning at the basal coil of the cochlea at E11.5 and progressing until innervation of the apical coil occurs at E15.5 (Rubel and Fritzsch, 2002). SGNs develop from neuroblasts that delaminate from the developing otic placode, otocyst and the elongating cochlea (Rubel and Fritzsch, 2002). Afferent fibres of type I SGNs reach the organ of Corti at the same time as sensory hair cells begin to differentiate (Sher, 1971). Branched fibres of developing type I SGNs form multiple contacts with one or more IHCs and OHCs in the early postnatal cochlea (Echteler, 1992). At birth, both pre and post-synaptic molecules are expressed at many of these dendritic contacts (Huang et al., 2012). However during the first postnatal week, many of the dendrites are withdrawn, leaving a single dendrite, with a single afferent bouton for each type I SGN (Pujol et al., 1998).

The architecture of the inner ear is fully formed by E17 and after this, only small changes in the anatomy occur, e.g. synaptic pruning and opening of the tunnel of corti. However there is a critical period of maturation, where hair cells and SGNs undergo functional changes, leading to development of the functional cochlea.

Development of IHCs and ribbon synapses.

All of the hair cells in the mouse cochlea are present by E14.5, but are not fully functional until the onset of hearing around P12. During this 2-3 week period, considerable changes occur in the morphology and function of IHCs and their ribbon synapses. For example there is a high order-relationship between calcium influx and vesicle fusion in immature IHCs, which becomes linear by the onset of hearing (Johnson et al., 2005), as discussed previously.

Synaptic ribbons are present in IHCs from birth, but they change significantly in number and shape before the onset of hearing. The number of ribbons increases, while their shape changes from spheroid to plate-like as the IHC and ribbon synapse matures (Figure 1.6) (Sobkowicz et al., 1982; Wong et al., 2014). Immature ribbon synapses can have multiple presynaptic ribbons in each active zone, but by the onset of hearing, only one ribbon is found at each synapse (Sobkowicz et al., 1982).

Distribution of calcium channels also changes significantly in IHCs during the maturation period. During early postnatal periods, calcium channels are distributed throughout the plasma membrane of IHCs, but in mature IHCs, they are clustered with ribbon synapses in the basolateral portion of the IHC membrane (Zampini et al., 2010). The increase in colocalisation between calcium channels and ribbon synapses correlates with a decrease in the amplitude of the calcium current from around 500pA at P7 to around 150pA by P12 (Brandt et al., 2005; Johnson et al., 2005). This suggests that there are a larger number of calcium channels in immature IHCs and expressed throughout the plasma membrane, which are down-regulated before the onset of hearing. These “extra-synaptic” calcium channels in immature IHCs may be important for regulating spontaneous electrical activity observed in immature IHCs (Kros et al., 1998).

Spontaneous activity in the developing cochlea.

During the prehearing maturation period, IHCs display spontaneous and evoked action potentials (Kros et al., 1998). Unlike neuronal action potentials, spiking activity in immature IHCs relies on calcium ions (Marcotti et al., 2003b). Inner supporting cells in the developing organ of Corti also display spontaneous depolarisation events that can be augmented by ATP and inhibited by P2 purinergic receptor antagonists, suggesting they are triggered by endogenous release of ATP locally. These spontaneous events were linked to spontaneous changes in cell shape that propagated through Kollikers organ, the supporting cell region adjacent to IHCs, (Tritsch et al., 2007). ATP and mechanical damage have previously been shown to induce propagating calcium waves in supporting cells of the outer sulcus (adjacent to OHCs) (Gale et al., 2004; Piazza et al., 2007). Tritsch et al. showed that

connexin hemichannel blockers could inhibit spontaneous activity of developing supporting cells, suggesting that ATP release through these hemichannels drives this spontaneous activity. Purinergic receptor antagonists were also shown to reduce spontaneous activity in IHCs and spiking activity in SGNs, suggesting ATP released from the supporting cells of Kollikers organ during propagation of spontaneous activity is important for driving spontaneous activity in IHCs (Tritsch et al., 2007).

Later work showed that when IHCs were exposed to endolymph-like solutions in-vitro, the amplitude of the MET current was amplified due to increased open probability of the MET channel. This increased open probability led to an increased inward current at rest, which is suggested to be sufficient to depolarise the IHCs to approximately -55mV, very close to the threshold for triggering action potentials in immature IHCs (Johnson et al., 2012). Therefore in-vivo-like conditions, the resting transducer current is likely to be sufficient to intrinsically drive spontaneous activity in immature IHCs. The idea of "spontaneous" action potentials in immature IHCs being driven by ATP release from supporting cells is not mutually exclusive with the idea of intrinsic generation of action potentials. It is possible that there is a low level of intrinsically driven activity that can be augmented by ATP released from nearby supporting cells during propagating waves of calcium signalling, possibly synchronising activity of nearby IHCs. It is clear that spontaneous activity is important for development of auditory function and processing, as outlined below.

Spontaneous activity and the ribbon synapse.

The pattern of spontaneous activity of IHCs can be modulated by acetylcholine, which in vivo may be released from olivocochlear efferent fibres that form transient synapses with immature IHCs (Glowatzki and Fuchs, 2000). Spiking activity in IHCs from mice lacking functional nicotinic acetylcholine receptors is insensitive to acetylcholine and during maturation, these IHCs fail to develop a linear relation between calcium influx and exocytosis, suggesting modulation of spontaneous activity by acetylcholine is important for maturation of the ribbon synapse in IHCs (Johnson et al., 2013a).

Normal spiking activity in developing IHCs is dependent on the activity of the transiently expressed Ca^{2+}-activated small conductance potassium (SK2) channel (Kcnn2) (Marcotti et al., 2004; Johnson et al., 2007). IHCs from mice overexpressing the SK2 channel (SK2OE) display an increased frequency of developmental action potentials and fail to develop a linear calcium-dependency of exocytosis at the mature ribbon synapse (Johnson et al., 2013b). Interestingly, normal expression levels and activity of the SK2 channel could be restored in IHCs of the SK2OE mice by dietary administration of doxycycline. This was used to demonstrate that normal spiking activity during the second postnatal week (P6-P12) is critical for maturation of the presynaptic machinery (Johnson et al., 2013b). This correlates well with refinement of calcium channel expression that occurs during this period (Johnson et al., 2005; Zampini et al., 2010).

Spontaneous activity and the refinement of auditory circuits.

Spontaneous activity at peripheral synapses is known to be important for development of circuits in the central nervous system (Katz and Shatz, 1996; Stellwagen and Shatz, 2002; Blankenship and Feller, 2010). In the auditory system, spiking activity in immature IHCs is sufficient to trigger exocytosis from IHCs (Marcotti et al., 2003b; Tritsch and Bergles, 2010) and drives spiking activity in SGNs and neurons in the medial nucleus of the trapezoid body (MNTB) in the auditory brainstem (Tritsch et al., 2010).

The pattern of spontaneous activity in immature IHCs is dependent on the position of the IHC in the cochlea, with apical cells displaying short bursts of high frequency action potentials separated by long periods of quiescence, while basal IHCs display regular, non-bursting activity (Johnson et al., 2011). This suggests the pattern of spiking activity is important for refinement of tonotopic maps in the CNS.

In neonatal mice lacking the α9 subunit of nicotinic acetylcholine receptors, the overall level of spiking activity remains the same, but there are subtle shifts in the temporal regulation, such as an increase in the firing rate during bursts, but a reduction in the lengths of the bursts. At the onset of hearing, these mice display an increase in the number of synaptic boutons and spread of MNTB projections in the

lateral superior olive (LSO), indicating a reduction in developmental synaptic pruning and tonotopic refinement in the LSO (Clause et al., 2014). This demonstrates the importance of spontaneous activity in IHCs for the development of normal auditory circuits in the CNS.

1.9 Investigating the functional ribbon synapse of IHCs.

Recent electrophysiological studies have begun to provide insight into the molecular machinery for exocytosis at the ribbon synapse, such as the diverse roles for otoferlin and the apparent lack of a role for SNARE-proteins, or calcium-sensitive synaptotagmins at the mature ribbon synapse. However, there are still many questions to be answered to improve our understanding of this unique synapse. Notably, are there as yet unidentified mediators of vesicle fusion expressed at the presynaptic membrane of IHCs? Are these molecules neuronal SNARE proteins, or similar? Alternatively, if otoferlin is the calcium sensor for exocytosis at the auditory ribbon synapse, does it also mediate fusion? This could be achieved by insertion of one or more C2 domains into the presynaptic membrane driving fusion with the vesicle membrane, possibly similar to the proposed role for synaptotagmins in the dyad hypothesis (Gundersen and Umbach, 2013).

Are there other calcium-sensitive regulators of the vesicle cycle expressed at the presynaptic active zone of IHCs? These unidentified molecules may regulate rapid priming, or replenishment of synaptic vesicles to maintain the size of the vesicle pools during sustained periods of stimulation.

It is also not clear how maturation of the synaptic machinery at the auditory ribbon synapse occurs. It appears that expression of neuronal regulators of synaptic function is downregulated during a critical period of sensory-independent activity in the developing cochlea (Beurg et al., 2010; Johnson et al., 2013b). Is expression of alternative regulators of synaptic function upregulated during this period? Or do otoferlin dependent mechanisms for vesicle fusion mature to form the functional synaptic machinery of the post-hearing cochlea? Identifying regulators of sensory-independent activity in the developing cochlea may improve our understanding of

maturation of the synaptic machinery, allowing us to determine the molecules essential for this process. Furthermore, expression of specific molecules necessary for either the production, or maturation of the auditory ribbon synapse is likely to be controlled by highly regulated transcriptional pathways. Identifying the transcriptional regulators and pathways that control the expression of key ribbon synaptic molecules may provide insight into the unidentified regulators of ribbon synaptic function.

1.10 Aims and objectives.

This thesis will attempt to enhance our understanding of the molecular regulation of the auditory ribbon synapse by presenting the results of a number of investigations into possible novel regulators of ribbon synaptic function. I have used electrophysiology to monitor inward calcium currents and changes in membrane capacitance to assess the presynaptic function of IHCs from mice lacking a molecule of interest.

The calcium-sensor DOC2B:

The soluble calcium-sensor double C2 domain protein B (DOC2B) regulates synaptic vesicle priming and may regulate the transition of vesicles from reserve pools to the RRP (Pinheiro et al., 2013). Therefore, I considered DOC2B to be a novel candidate for regulating vesicle priming at the auditory ribbon synapse.

Objective: To assess the fusion of synaptic vesicles in IHCs from DOC2B KO mice and monitor the kinetics of fusion and replenishment of the vesicle pools.

Hypothesis: Vesicle priming will be slowed at the auditory ribbon synapse, impeding the replenishment of the RRP and the kinetics of vesicle fusion. This should reduce the fusion of vesicles from the SRP, as fewer vesicles will become "fusion competent".

The inositol 5'-phosphatase family member Synaptojanin2 (SynJ2):

SynJ2 has been shown to be expressed in IHCs, where it is essential for their survival (Manji et al., 2011) and is thought to regulate an early stage in CME (Rusk et al.,

2003). As the molecular regulators of CME at the auditory ribbon synapse are unknown, SynJ2 is a good candidate for a regulator of CME in IHCs.

Objective: To assess the internalisation of IHC membrane following exocytotic events in IHCs from SynJ2 KO mice and the replenishment of vesicle pools as a measure of vesicle recycling.

Hypothesis: CME will be prevented in IHCs from SynJ2 KO mice, either slowing the internalisation of presynaptic membrane, or accelerating it as bulk endocytosis becomes the major component of endocytosis in these IHCs. This will also affect vesicle recycling, reducing the ability of the IHCs to replenish the vesicle pools.

Connexin-based gap junctions in the cochlea:

Connexins 26 and 30 (Cx26 and Cx30) form homomeric and heteromeric gap junctions in the supporting cells of the cochlea (Maeda and Tsukihara, 2011), where they mediate developmental spontaneous activity (Tritsch and Bergles, 2010). Developmental activity is important for the maturation of the synaptic machinery (Johnson et al., 2007), therefore disruption of this developmental activity in the supporting cells may affect the maturation of synaptic machinery IHCs.

Objective: Assess the presynaptic function of IHCs from Cx30 KO mice that do not express Cx30 and with severely reduced expression of Cx26 (Ortolano et al., 2008).

Hypothesis: The presynaptic machinery of IHCs from Cx30 KO mice will not have matured normally; therefore they are likely to display a non-linear relationship between calcium-influx and fusion of synaptic vesicles.

The transcriptional co-activator Wbp2:

Finally, the transcriptional Co-activator Wbp2 has been identified as a possible regulator of the auditory system by the mouse genetics project at the Wellcome Trust Sanger institute (Buniello et al., Under Revision). Preliminary research showed abnormalities at the ribbon synapses in the mature cochlea of Wbp2 KO mice.

Objective: Assess the presynaptic function of IHCs from Wbp2 KO mice.

Hypothesis: Wbp2 regulates the expression of molecules essential for the mature presynaptic machinery in IHCs, therefore IHCs from Wbp2 KO mice, therefore IHCs from Wbp2 KO mice will display abnormal exocytotic responses, such as a nonlinear calcium-dependency of exocytosis, or altered kinetics of vesicle fusion.

Chapter 2 – Methods.

2.1 Changes in membrane capacitance represent fusion of synaptic vesicles:

To release neurotransmitters from the presynaptic active zone of a cell, vesicles containing the neurotransmitter fuse with the presynaptic membrane, expelling their cargo into the synaptic cleft. After fusion of the synaptic vesicles, the additional membrane added to the plasma membrane of the presynaptic cell increases the surface area of the cell proportionally to the number of vesicles that fuse (Lindau and Neher, 1988). On the other hand, when vesicle membranes are removed from the presynaptic membrane, the cells surface area decreases accordingly. Due to the insulating properties of the phospholipid bilayers of cell membranes, they can store charge as an electric field, acting as an electrical capacitor.

Capacitors, a brief introduction.

Capacitors are common components of electrical circuits where two conductors (e.g. wires/plates/solutions) are separated by an insulator (e.g. glass/ceramic/phospholipid membrane). Capacitors can store charge (measured in coulombs – Q) in a circuit as an electrical field at the insulator, where positive charge builds on one conductor and negative charge on the other (Horowitz and Hill, 1980). The amount of charge (Q) stored in a capacitor is the product of the size of the capacitor (C) (measured in Farads - F) and the voltage (measured in volts – V):

$$Q = CV$$

Therefore when the voltage changes in the circuit, the amount of charge stored in the capacitor changes accordingly, leading to capacitive transients at a step change in the voltage as the capacitor charges/discharges accordingly. The size of the transient is relative to the size of the capacitor and the change in voltage. The decay constant (τ, measured in seconds) of the transient is a product of the size of the capacitor © and the resistance in the circuit (R, measured in Ohm's - Ω):

$$\tau = RC$$

In patch-clamp electrophysiology, the glass wall of the patch pipette and the plasma membrane of the patched cell act as capacitors. The transients related to the capacitance of patch pipettes are relatively fast, due to the low resistance at the wall of the electrode and are known as fast-capacitive transients. The transients related to the cell membranes capacitance are relatively slow, due to the high resistance of the cell membrane (Hamill et al., 1981). Changes in the capacitance of a cells membrane can be measured using electrophysiology and used to quantify vesicle release and reuptake from a particular cell (Jaffe et al., 1978; Lindau and Neher, 1988)

2.2 Solutions:

Electrophysiological recordings of IHCs maintained in near physiological conditions in the acutely isolated cochlea, were carried out using the following solutions (For reagents, see table 2.1):

Normal Extracellular Solution (ECS) contained the following (in mM):

Sodium chloride (135), calcium chloride (1.3), potassium chloride (5.8), magnesium chloride (0.9) HEPES-buffer (10), glucose (5.6), sodium dihydrogen orthophosphate (0.7) and sodium pyruvate (2), supplemented with 20ml/L Amino Acids (from concentrate, 50X) and 10ml/L vitamins (from concentrate, 10X). Adjusted to pH 7.48 with sodium hydroxide, osmolality; 306 mOsm $Kg^{-1}H_2O$.

Extracellular solution with potassium channel blockers (ECS-B) contained the following (in mM):

Sodium chloride (107), calcium chloride (1.3), potassium chloride (5.8) magnesium chloride (0.9), HEPES-buffer (10), glucose (5.6), tetraethylammonium chloride (30) and 4-aminopyridine (15). Adjusted to pH 7.48 with hydrochloric acid, osmolality; 308 mOsm$Kg^{-1}H_2O$. Additional channel blockers were added on the day of the experiment depending on the age of the animal to be recorded from.

Table 2.1: Reagents.

Reagent	Manufacturer	Catalogue No.
4-aminopyridine	Aldrich	275875
Amino Acids*	Gibco	11130-036
Apamin	Tocris	1652
Calcium chloride	VWR	190464K
Cesium chloride	Aldrich	203025
Cesium hydroxide	Aldrich	232041
Ethylene-Glycol-Tetraacetic acid (EGTA)	Sigma	03777
Glucose	VWR	101174Y
Glutamic acid	Sigma	49449
Guanosine triphosphate	Sigma	51120
HEPES-buffer	Calbiochem	391338
Hydrochloric acid (HCl)	BDH	101252F
Linopirdine	Tocris	1999
Magnesium chloride	VWR	25108
Potassium chloride	VWR	26764
Potassium Hydroxide	VWR	102410V
Sodium ATP	Roche	1051998709
Sodium chloride	VWR	27810
Sodium dihydrogen orthophosphate	VWR	102454R
Sodium Hydroxide	VWR	28244
Sodium phosphocreatine	Sigma	27920
Sodium pyruvate	Gibco	11360-070
Tetraethylammonium chloride	Sigma	86614
Vitamins*	Gibco	11120-037

* For composition of these products, please refer to tables 2.3 and 2.3

Table 2.2: Composition of amino acids produced by Gibco in 2015.

Component	Concentration (mM)
L-Arginine hydrochloride	30.0
L-Cystine	5.0
L-Histidine hydrochloride-H2O	10.0
L-Isoleucine	20.0
L-Leucine	20.0
L-Lysine hydrochloride	19.8
LMethionine	5.1
L-Phenylalanine	10.0
L-Threonine	20.0
L-Tryptophan	2.5
L-Tyrosine	9.9
L-Valine	20.0

Table 2.3: Composition of vitamins solution produced by Gibco in 2015.

Component	Congentration (mM)
Choline chloride	100
D-Calcium pantothenate	100
Folic acid	100
Nicotinamide	100
Pyridoxial hydrochloride	100
Riboflavin	10
Thiamine hydrochloride	100
i-Inositol	200
Sodium Chloride (NaCl)	8500

Cesium-Glutamate based intracellular solution (Cs-ICS) contained the following (in mM):

Cesium-glutamate (106), cesium chloride (20), sodium phosphocreatine (10), magnesium chloride (3), ethylene glycol tetraacetic acid (EGTA) (1), sodium ATP (5), HEPES-buffer (5) and guanosine triphosphate (0.3). Adjusted to pH 7.28 with cesium hydroxide, osmolality; 294 mmol $Kg^{-1}H_2O$.

Potassium based intracellular solution (K-ICS) contained the following (in mM):

Potassium chloride (131), sodium phosphocreatine (10), magnesium chloride (3), sodium ATP (5), HEPES-buffer (5), EGTA (1). Adjusted to pH 7.28 with potassium hydroxide, osmolality; 294 mOsm $Kg^{-1}H_2O$.

Isolating calcium currents with pharmacological agents.

To record calcium currents (I_{Ca}) in isolation, from IHCs, ECS-B contains 15 mM 4-aminopyridine and 30 mM tetraethylammonium chloride, both of which block voltage-gated potassium channels that carry the delayed rectifier K^+ current ($I_{K,DR}$) and the rapidly activating large-conductance Ca^{2+}-activated K^+ current ($I_{K,f}$). Recordings from IHCs of pre-hearing mice were also performed in the presence of 300 nM apamin, a selective blocker of the transiently expressed small-conductance Ca^{2+}-activated (SK2) current (Marcotti et al., 2004), added to ECS-B on the day of experiments. IHC recordings from post-hearing mice were performed in the additional presence of 80 µM linopirdine added to ECS-B on the day of experiments to block the KCNQ4 channels, expressed in IHCs after the onset of hearing and carry the negatively activating delayed rectifier current ($I_{K,n}$) (Marcotti et al., 2003a).

2.3 Preparation of the cochlea:

Mice were killed by cervical dislocation according to schedule 1 of the animal and scientific procedures act 1986 and the entire vestibulocochlear system was removed from the temporal bone of the skull (Figure 2.1A). The bone/cartilage encasing the cochlea spiral was carefully removed in ice-cold ECS using fine forceps under a dissecting microscope (Leica, Germany). For immature cochlea (<P12), the

cochlear were separated from the modiolus before the stria vascularis was removed to allow access to the organ of Corti. The immature organ of Corti was then separated into apical and basal coils, with care taken to protect the portion to be studied. For mature cochlea (>P12), removal of the stria vascularis was carried out immediately after the bone was removed to expose either the apical or basal coil of the organ of Corti, which was then separated from the modiolus (Figure 2.1B). The apical or basal coil of the organ of Corti was transferred to a recording chamber filled with ice-cold ECS, where it was secured under a nylon mesh (strands approx. 1mm apart) stretched over a stainless steel ring (internal diameter approx. 21 mm). The tectorial membrane was removed using fine forceps to allow access to the IHCs (Figure 2.1C). The recording chamber containing the organ of Corti was mounted on a specialised stage of an experimental microscope (Figure 2.2).

2.3 Electrophysiological recordings of membrane capacitance changes and calcium currents in IHCs:

Visualising the organ of Corti.

To visualise the organ of Corti, the recording chamber was mounted on a custom made rotating stage that allowed easy access to cells at different positions along the cochlea. Cells were visualised using an upright microscope (Olympus BX51, Tokyo, Japan) with nomarski DIC optics (X60 water immersion objective and X15 eyepieces). To minimise mechanical noise, the microscope was mounted on an antivibration table (TMC, MA, USA). The setup was electrically isolated inside a custom made faraday cage (Figure 2.2).

Perfusion of the recording chamber.

The recording chamber was perfused with fresh normal ECS at 4-6 ml min^{-1} using a peristaltic pump (Cole-Palmer, IL, USA) and the cells were maintained in near physiological conditions (1.3 mM extracellular calcium, 35-37 °C). The peristaltic pump that perfused the recording chamber was located outside the faraday cage and the inlet and outlet tubes were connected to the ground to minimise electrical interference.

Figure 2.1: Preparation of the cochlea for electrophysiological recordings from apical coil IHCs.

A. The vestibulocochlear system removed from the skull of a P18 mouse, encased in bone. Note the spiral structure of the cochlea (arrow). The attached vestibular system (arrowhead) is used to hold the cochlea still during dissection.
B. The organ of Corti has been exposed by removing the bone and stria vascularis. The apical coil (arrow) has been protected from damage and will be removed from the modiolus (arrowhead).
C. The organ of Corti, containing IHCs in the sensory epithelium (arrow). Secured in the recording chamber by nylon threads (arrowhead).

A-C, Scale bars represent 1mm.

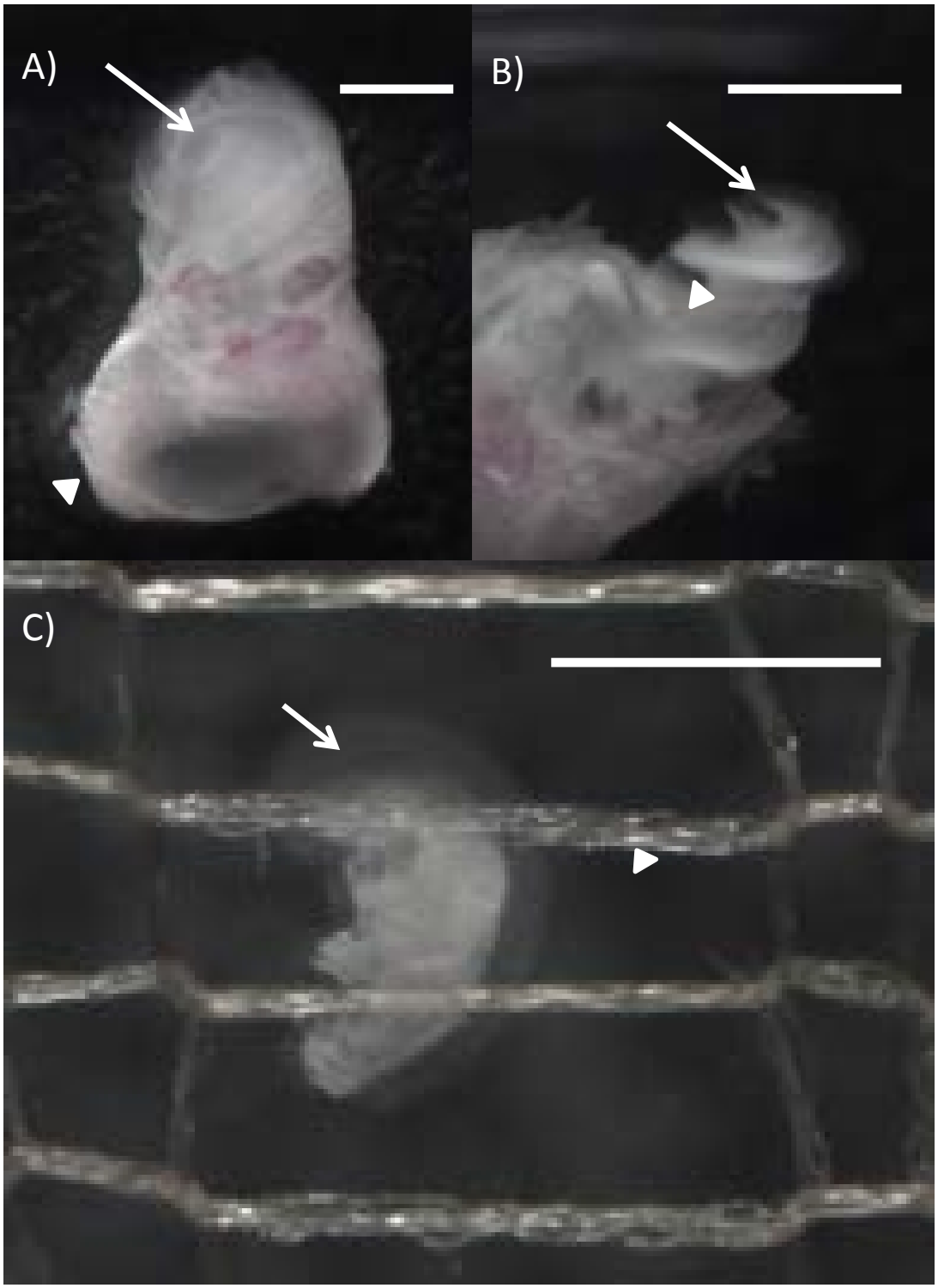
A)
B)
C)

To allow switching of solutions between ECS and ECS-B during experiments, a home-made gravity driven solution changer with a large diameter tip (500µm) was positioned in the recording chamber near the organ of Corti preparation (Figure 2.2). The solution changer was fed by three 10ml syringe reservoirs located inside the faraday cage, each of which was controlled using a three way tap. The flow rate was maintained at approximately 4-6 ml min^{-1} by keeping the height and volume of the reservoirs constant. Prior to establishment of the patch-clamp configuration, inflow from the peristaltic pump was diverted and normal ECS was perfused from the solution changer. After establishment of the patch-clamp configuration, the chamber was perfused with ECS-B.

Maintaining physiological temperature.

Physiological processes, such as ion channel activation and vesicle fusion, are affected by temperature. Therefore, recordings were performed near body temperature (35-37 °C). This was achieved using a custom made heating element below the recording chamber; six resistors were connected in series below a central disc of the rotating stage, which was isolated from the rest of the stage by a Teflon ring. The heating element was controlled using a potentiometer mounted on the equipment rack. A thermal probe was positioned in the recording chamber to provide a continuous read-out of the temperature around the tissue; this feedback was used by the potentiometer to maintain a constant temperature throughout the experiment. The potentiometer was calibrated using a separate thermocouple (Fluke, Washington, US) prior to experiments.

Accessing an IHC.

To access the basolateral membrane of an IHC, surrounding supporting cells were removed using a borosilicate glass cleaning pipette with a tip diameter of 3-4 µm. The cleaning pipette was connected to a syringe via plastic tubing, all of which was filled with normal ECS. The syringe was used to apply positive and negative pressure to the tip of the cleaning pipette (Figure 2.2).

Figure 2.2: Electrophysiological setup for recording from auditory hair cells.

A) Photo of the electrophysiology setup used to record electrical properties of cochlear IHCs.
B) Close up of the rotating stage of the microscope and recording chamber.

A) +B) Components of the setup: i=Olympus BX51 water immersion microscope, ii=custom made rotating stage and mount, iii=TMC anti-vibration table, iv=headstage holder of scientifica patchstar micromanipulator, v=headstage of cairn optopatch amplifier, mounted in a custom made holder, vi=electrode holder and patch electrode, vii= ground electrode, viii=arm of thermocouple probe, ix=solution changer, x= 10ml reservoirs for solution changer, xi=electrode holder for cleaning pipette, xii= Intracel micromanipulator for the cleaning pipette, xiii= Marzhauser manipulators, xiv=control for patchstar micromanipulator, xv=recording chamber, xvi=inflow from peristaltic pump, xvii=outflow to peristaltic pump, xviii=10ml syringe for applying positive and negative pressure to the cleaning pipette, xix=tubing for applying pressure to the patch electrode.

A)

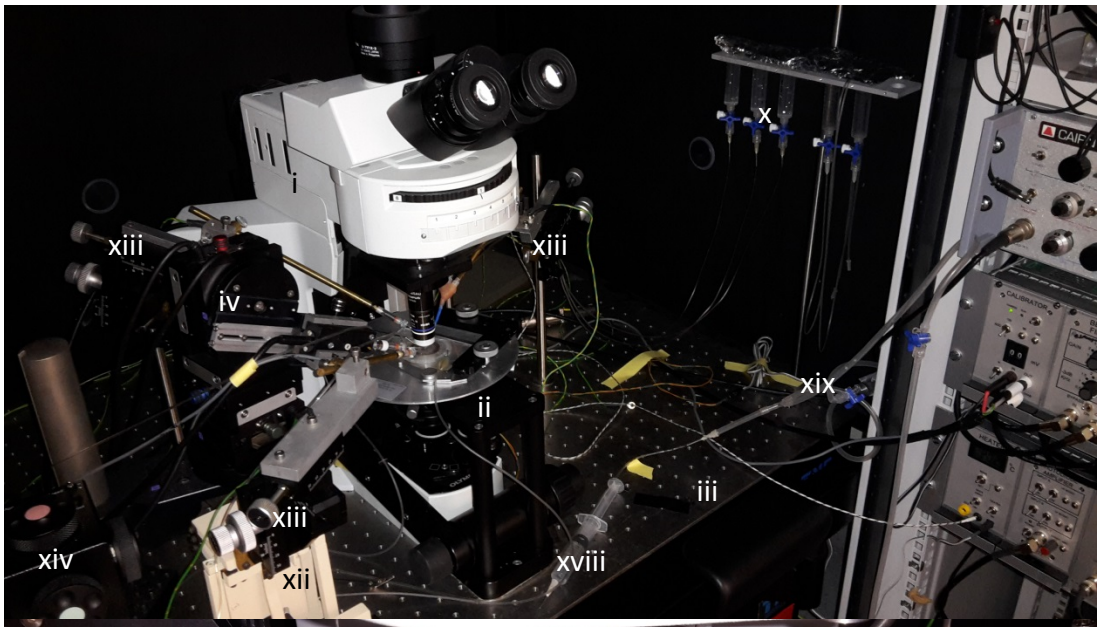
i
x
xiii
xiii
iv
xix
ii
iii
xiii
xiv
xii
xviii

B)

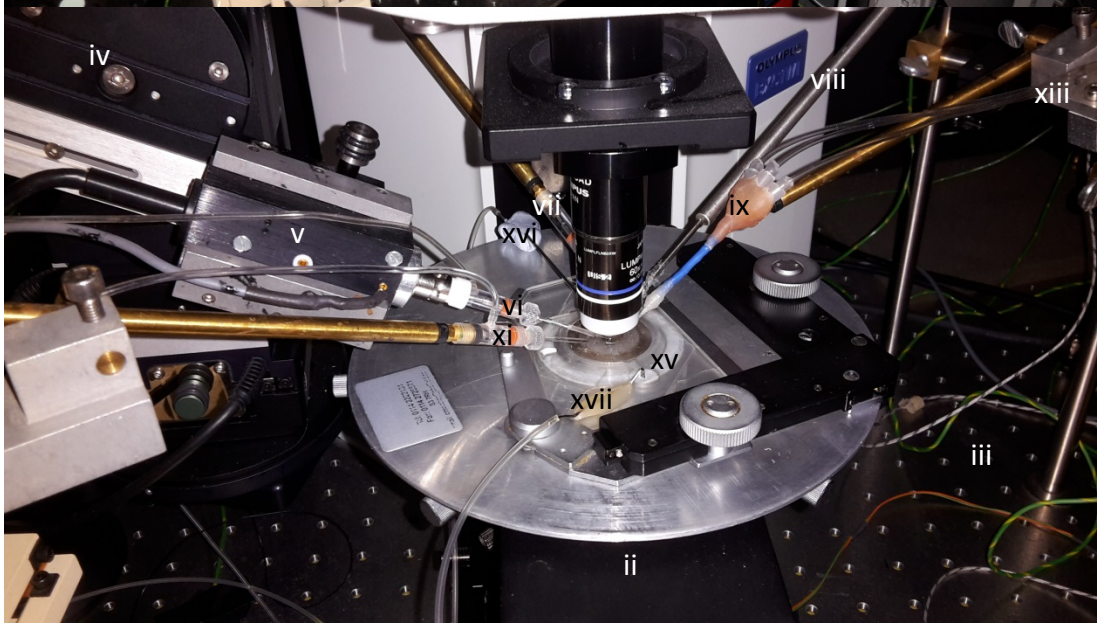
iv
viii
xiii
vii
ix
xvi
v
vi
xi
xv
xvii
iii
ii

Patch pipettes.

Patch pipettes with a resistance of 2-4 MΩ were pulled from soda glass capillaries using a vertical puller (PP-13 Narishigi instruments, Japan). To minimise fast capacitive transients, patch pipette shanks were coated with wax (Mr. Zoggs Sex Wax, USA) up to ≈100 µm from the tip of the pipette. Patch pipettes were back filled with a cesium glutamate based intracellular solution (Cs-ICS), to block potassium channels with cesium ions, further isolating I_{Ca}. Patch pipettes were attached to the headstage of an optopatch amplifier mounted on a patchstar micromanipulator (Figure 2.2) (Scientifica instruments, UK).

Establishing the patch-clamp configuration.

During approach to the IHC, positive pressure was applied to the patch pipette to create a flow of ICS from the tip of the patch pipette, which prevented dilution of ICS in the patch pipette by ECS. The outward flow of ICS from the patch pipette also prevented debris from contaminating the tip of the patch pipette, which may have interfered with the formation of a seal between the patch pipette and cell membrane. On reaching the IHC, an indent in the clean IHC membrane became visible, at which point gentle negative pressure was applied to assist formation of a high resistance (>1 GΩ) electrical seal between the tip of the patch pipette and the IHC, the “gigaseal”. After formation of the gigaseal, the holding potential was set at -81 mV (taking account of the liquid junction potential of -11 mV). At this point, fast capacitive transients during a +10 mV voltage step, were cancelled out using the fast capacitance circuitry of the optopatch amplifier.

After compensating for fast capacitance, negative pressure was briefly applied to the patch pipette, which ruptured the membrane of the IHC and established the whole-cell patch-clamp configuration. This was confirmed by the appearance of slow membrane transients during a +10 mV voltage step. These transients were minimised using the slow capacitance cancelling circuitry of the optopatch amplifier, which also allowed the measurement of cell membrane capacitance and the series resistance of the patch-clamp configuration.

Measuring changes in membrane capacitance.

Capacitance measurements were carried out using the "track-in" method for membrane capacitance measurements with an optopatch amplifier (Johnson, 2002). The track-in method is a modification of the "lock-in" technique for measuring cell membrane properties. Briefly, the "lock-in" technique utilises a phase-sensitive lock-in amplifier to measure the passive properties of cell membranes (Lindau and Neher, 1988).

Due to the charging and discharging properties of capacitors, the current across a capacitor is a function of the change in voltage over the change in time:

$$Ic(t) = C.dV/dT$$

where *Ic(t)* is the instantaneous current through the capacitor (in amps), C is the capacitance of the capacitor (in farads) and *dV/dT* is the instantaneous rate of change in the voltage (Vs^{-1}) (Horowitz and Hill, 1980). This means that when a sinusoidal voltage is applied to the capacitor, the phase of the current signal is shifted by 90^{o}.

A sinusoidal command voltage (37 mV peak to peak at 4 kHz) is applied to the cell around the holding potential and the returning current signal is separated by phase into two outputs (commonly known as real and imaginary), which are used to calculate membrane capacitance, membrane conductance and series resistance. If the detection-phase of the lock in amplifier is set to 90^{o}, changes in the real and imaginary outputs of the lock-in amplifier reflect changes in series resistance and membrane capacitance respectively (Johnson et al., 2002).

The track-in technique is a modification of the lock-in technique, utilising an integrated lock-in amplifier in the optopatch patch-clamp amplifier. The main advantage of this technique is the ability for compensatory circuitry within the amplifier to allow the real and imaginary outputs of the lock-in amplifier to provide negative feedback to the series resistance and membrane capacitance compensatory circuits of the amplifier. Therefore, both outputs are maintained at 0mV, preventing the build-up of signals at the outputs of the lock-in amplifier,

which can lead to phase errors interfering with the measurement of Rs and Cm in conventional lock in amplifiers (Lindau and Neher, 1988).

Changes in the series resistance of the patch-clamp configuration lead to changes in the time constant of the charging and discharging of the capacitor. While these changes are normally separated by the real output of conventional lock-in and the optopatch track-in amplifiers (Lindau and Neher, 1988; Johnson et al., 2002), large changes (>0.5 MΩ) – particularly increases – in Rs prevent accurate recordings of membrane currents, limiting the amplifiers capability to monitor changes in membrane capacitance.

The holding current, membrane resistance and leak conductance.

Other properties of the whole-cell patch clamp configuration were calculated offline including, the holding current (*I*h), the membrane resistance (Rm) and the leak conductance (gL). These properties were used to assess the overall condition of the cell and recording configuration.

*I*h is the current recorded while holding the cell at a given potential (-81 mV), expressed in pA. Rm is the resistance of the membrane of a cell, expressed in MΩ; it is determined by measuring the difference in the current recorded at the holding potential and the current recorded during a small voltage step (10 mV) and calculated using Ohm's law:

$$V = IR$$

where *V* = voltage, *I* = current and *R* = resistance.

This can be rearranged to calculate Rm:

$$Rm = 10\ mV \div Im\ pA$$

Where *Rm* = membrane resistance and *Im* = the change in recorded membrane currents during a +10 mV voltage step.

The +10 mV voltage step used to does not significantly change the open probability of voltage-gated channels in IHCs (Zampini et al., 2010); therefore the vast majority of the change in current will be "leak-current", due to the conductance of ions

through non-gated channels/pores in the cells membrane. This is the leak conductance, gL, which can be calculated as the reciprocal of Rm:

$$gL = 1 \div Rm$$

where *gL* is the conductance in nS and *Rm* is the resistance in GΩ.

2.4 Electrophysiological recordings of voltage responses and potassium currents IHCs:

A small number of experiments carried out in this study have used different experimental conditions to measure potassium currents and voltage responses in IHCs. These experiments have been used to test for differences in the overall physiology of IHCs from control mice, compared to IHCs from mice deficient for a particular protein (KO).

Current clamp electrophysiology was used to measure the resting membrane potential of IHCs and assess their voltage responses to current injections. Voltage clamp protocols were used to assess the current profiles of IHCs, notably; the large conductance calcium activated potassium current $I_{K,f}$, the slow delayed rectifier current $I_{K,s}$ and the negatively activating inward rectifier current $I_{K,n}$.

The procedures used for recording voltage responses and potassium currents were very similar to those used for recording calcium currents and changes in membrane capacitance. The main differences were in the conditions used during the recordings:

1) The intracellular solution loaded into the patch pipette was potassium based intracellular solution (K-ICS) rather than Cs-ICS. This is because cesium is a potassium channel blocker.
2) IHCs were maintained throughout the recordings by perfusion of normal ECS, as pharmacological channel blockers are not required to measure the potassium currents in IHCs.
3) The organ of Corti was maintained at room temperature (20-22˚C) rather than body temperature, which allows the preparation to be maintained in vitro for longer, allowing more results to be obtained from each preparation.

2.5 Animal care:

All studies were carried out on acutely isolated tissue from animals culled by a schedule 1 method outlined in the animals for scientific procedures act, 1986; therefore, no licence was required for these experiments. In accordance with internal guidelines, schedule 1 was carried out at the University of Sheffield by the author, after completion of modules 1, 2 and 3 of the home office animal handling course and registration as a schedule 1 practitioner.

Animals were housed at the University of Sheffield in accordance with UK home office guidelines. Genetically modified mice were bred under a dedicated project licence. Monogamous breeding pairs of each strain of animals were selected after genotyping by PCR. Breeding pairs were set as either; homozygous (-/-), heterozygous (+/-) crosses, or heterozygous, heterozygous crosses in order to produce pups with mixed genotypes in Mendelian ratios. This allows recordings of IHCs from knockout animals (-/-) to be compared to those from littermate controls (+/+, or +/-). In all cases, results from IHCs of heterozygous mice were compared to those from wild-type mice before pooling data.

Genotyping.

Mice were genotyped by PCR amplification of genomic DNA. For breeding stock and experiments carried out using IHCs from adult mice, DNA was isolated from ear-clips taken at, or after postnatal day 14. The tail was kept after experiments to confirm the genotype if necessary. For experiments performed using IHCs from immature mice, the tail was kept after the experiments and DNA was isolated from approximately 2 mm of tail.

DNA was isolated using proteinase K digestion. The DNA was then amplified by PCR using the primers outlined in table 2.2.

Ethical approval:

All experiments carried out in this study were approved by the University of Sheffield Ethical Review Committee.

2.6 Data handling, presentation and analysis:

Data was collected from the optopatch amplifier using Clampex 10.3 software (Molecular Devices, CA, USA) and a Digidata 1440A, analogue-digital converter (Molecular Devices, CA, USA). The current signal of IHCs was filtered at 2.5 kHz using a Bessel filter and amplified at 5 mV pA^{-1}.

Offline analysis was carried out using Clampfit software (Molecular Devices) to quantify and subtract *I*h (at -81 mV) and calculate Rm and gL, which was subtracted for each recording. This facilitated the measurement of the real amplitudes of the calcium currents recorded from IHCs. Current recordings were exported to OriginPro 8.5 analysis software (OriginLab, MA, USA), where the command voltage of each voltage step (set in Clampex 10.3) was corrected for the voltage drop due to Rs of the whole-cell configuration.

Calcium currents for each IHC were measured as the peak amplitude of the current recorded during a voltage step using Clampfit software. Changes in membrane capacitance were determined by averaging the recording of changes in membrane capacitance over a period of 100 ms shortly after each voltage step using Clampfit software. Linear and exponential fits of changes in membrane capacitance recordings were carried out using OriginPro software. Potassium currents were quantified using OriginPro; steady state currents are measured by averaging the amplitude of each recording over the last 20 ms of a voltage step and onset currents are measured as the amplitude of the current 2 ms after the start of the voltage step.

Statistical analysis of means was carried out in OriginPro software and average results are presented as mean ± S.E.M. To compare single data points, a two-tailed Student's T-test was used. To compare data sets with multiple points, two-way ANOVA with a Bonferroni post-test was used, as data sets had at least two independent variables, e.g. genotype and step duration. A P-value of < 0.05 was used as the benchmark criterion for statistical significance.

Table 2.4: Genotyping by PCR.

Strain	Primer	Primer sequence (5'-3')	Expected band sizes (bp)
DOC2B	RZ318	CGCTTGGTGGTCGAATGGGCAGGTAGC	WT: 660 KO: 1250
	Mav206	CGGCTACGAGTCAGACGACTG	
	Rz335R	CCTCAGGGACCACACAAGCCACCAGGAGAGG	
SynJ2	SynJ2 F	GGGGAGGGGTCCATGTTAAG	WT: 385 KO: 150
	SynJ2 R	CCGCAGAACACACTCTAGC	
	Cas_R1	TCGTGGTATCGTTATGCGCC	
Cx30	Cx30USP	GGTACCTTCTACTAATTAGCTTGG	WT: 544 KO: 460
	Cx30 DSP	AGGTGGTACCCATTGTAGAGGAAG	
	Cx30lacZ	AGCGAGTAACAACCCGTCGGATTC	
Wbp2	WBPT F	GCCCAATGGAGAGGAACAAG	WT: 642 KO: 380
	WBPT R	GTAACTCCAGCATCAGGGGG	
	Cas_R1	TCGTGGTATCGTTATGCGCC	

Chapter 3 - Is DOC2B a Calcium Sensor for Vesicle Priming, or Pool Replenishment at the Auditory Ribbon Synapse?

3.1 Introduction:

The presynaptic machinery for exocytosis at the auditory ribbon synapse is capable of sustaining high rates of vesicle fusion over sustained periods due to rapid replenishment of the vesicle pools (Griesinger et al., 2005). The calcium sensor otoferlin has been implicated in vesicle replenishment (Pangrsic et al., 2010); however it is likely that other calcium sensors regulate distinct steps in the vesicle cycle, such as vesicle priming. We have identified the double C2 domain protein DOC2B as a possible calcium sensor for vesicle priming at the presynaptic active zone of IHCs.

DOC2B as a regulator of the vesicle cycle

DOC2B is a soluble, ubiquitously expressed calcium sensor that binds phospholipids in a calcium-dependent manner (Orita et al., 1995; Kojima et al., 1996). In overexpression systems and neurons, cytosolic DOC2B translocates to the plasma membrane in response to calcium influx, as well as enhancing calcium dependent exocytosis in PC12 cells (Orita et al., 1996; Groffen et al., 2004; Groffen et al., 2006). DOC2 proteins bind a number of regulatory molecules for exocytosis, such as MUNC 18 and MUNC13 (Verhage et al., 1997; Hori et al., 1999), as well as competing with syntaxin-4 for MUNC18C binding (Ke et al., 2007) and binding to complexes of syntaxin-1 and SNAP-25, but not the individual proteins (Friedrich et al., 2008). Recent studies have shown that DOC2B can form complexes with both MUNC18-1 and MUNC18C in pancreatic islet cells, leading to the suggestion that DOC2B acts as a molecular scaffold for secretory proteins (Ramalingam et al., 2014). DOC2B has also been suggested to act as a calcium switch, enhancing the number of vesicles that are “fusion competent”, without affecting the number of morphologically docked vesicles (Friedrich et al., 2008). More recently, it has been shown that the sustained/asynchronous component of exocytosis is augmented in chromaffin cells lacking DOC2B, suggesting that DOC2B inhibits the sustained/asynchronous component of exocytosis in chromaffin cells, increasing fast/synchronous exocytosis. It was also found that in the absence of DOC2B the refilling of the RRP was faster but incomplete; suggesting the main role for DOC2B is controlling the

availability of vesicles for release (Pinheiro et al., 2013). Finally DOC2B has recently been shown to enhance SNARE-mediated membrane fusion by bending the plasma membrane (Yu et al., 2013), similar to the finding that membrane bending by synaptotagmin 1 is important for calcium regulated fusion (Hui et al., 2009). It seems likely that DOC2B is involved in regulating the transition of vesicles from the SRP to the RRP, promoting vesicle priming prior to fusion. The molecules regulating vesicle priming at the auditory ribbon synapse are currently unknown and the ubiquitous expression of DOC2B suggests it has roles in a wide variety of cell types; therefore, it is a good candidate for a novel regulator of exocytosis in IHCs.

Preliminary hearing tests using a “click box” to test the pinna reflex suggested mice deficient for DOC2B (DOC2B KO) were less sensitive to noise than littermate controls, suggesting they had a hearing impairment. Unfortunately further trials were unable to confirm this. Due to DOC2Bs reported role in replenishment of the RRP (Pinheiro et al., 2013), it seems unlikely that DOC2B deletion would abolish glutamate release at the auditory ribbon synapse and is unlikely to affect auditory thresholds. Therefore, I have investigated vesicle fusion in IHCs from DOC2B KO mice to determine if DOC2B has a role in regulating the supply, docking, or priming of synaptic vesicles at the auditory ribbon synapse. I have carried out electrophysiological measurements of calcium currents and changes in membrane capacitance in IHCs from DOC2B KO mice as a highly sensitive measure of exocytotic responses of IHCs to determine if DOC2B has a functional role in calcium-regulated exocytosis at the auditory ribbon synapse.

Research into the exact role of DOC2B in exocytosis has been hindered by a lack of suitable antibodies for immunostaining, preventing its localisation within neurons and secretory cells. Therefore we have been unable to confirm the expression of DOC2B within IHCs.

DOC2B KO mice were received from Sander Groffen (Groffen et al., 2010), and maintained on a C57Bl/6 background. Apical coil IHCs from control (DOC2B+/+ and DOC2B+/-) and knockout (KO) (DOC2B-/-) were studied in the acutely isolated organ of Corti from young (P5-8) and adult (P17-29) mice. No differences have been

observed between DOC2B+/- and DOC2B+/+ mice previously (Groffen et al., 2010; Pinheiro et al., 2013) and recordings of IHCs from DOC2B+/- mice were compared to those from DOC2B+/+ mice before pooling data.

3.2 Results:

3.2.1 Electrical properties of IHCs from control and DOC2B KO mice:

IHCs from control and DOC2B KO mice were held in the patch-clamp configuration in near physiological conditions (1.3 mM Ca^{2+} at 37˚C), at a potential of -81 mV. Significant differences were observed in some of the electrical properties between the IHCs from adult control and DOC2B KO mice (Table 3.1), for example, IHCs from control mice had a significantly ($P < 0.01$, Students T-test) lower series resistance (5.27 ± 0.2 MΩ, n = 20) and higher membrane capacitance (10.40 ± 0.2 pF, n = 20) than IHCs from DOC2B KO mice (Rs = 6.34 ± 0.3 MΩ; Cm = 7.50 ± 0.2 pF, n = 16). IHCs from control mice also had significantly larger holding currents and leak conductances (*I*h = -47.4 ± 5.7 pA and gL = 1.58 ± 0.16 nS, n = 20) than those from DOC2B KO mice (*I*h = -12.9 ± 1.1 pA and gL = 0.62 ± 0.02 nS, n = 16). This suggests that there are more non-gated ion channels expressed in the plasma membrane of IHCs from control mice than DOC2B KO mice. However, as I was able to record calcium currents and changes in membrane capacitance from control and DOC2B KO IHCs, this was not followed up on and falls outside of the scope of this study.

In contrast, no significant differences were observed between the electrical properties of IHCs from prehearing (P5 – P8) control and DOC2B KO mice, suggesting that the membrane properties of IHCs from DOC2B KO mice are normal at this age.

Table 3.1: Electrical properties of IHCs from control and DOC2B KO mice.

Genotype (age)	Rs (MΩ)	Cm (pF)	*I*h at -81 mV (pA)	Rm (MΩ)	gL (nS)	n
Control (P17-P29)	5.27 ± 0.2	10.40 ± 0.2	-47.4 ± 5.7	769 ± 82	1.58 ± 0.16	20
KO (P17-P29)	6.34 ± 0.3	7.50 ± 0.2	-12.9 ± 1.1	1643 ± 45	0.62 ± 0.02	16
Control (P5-P8)	6.2 ± 0.7	9.15 ± 0.7	-132.5 ± 27.7	405 ± 95	3.9 ± 1.3	6
KO (P5-P8)	6.9 ± 0.8	9.34 ± 0.5	-95.8 ± 9.4	359 ± 28	2.0 ± 0.3	8

3.2.2 Exocytosis from the ribbon synapse of IHCs from DOC2B KO mice:

To investigate the function of the ribbon synapse in IHCs from adult (P17 – P29) DOC2B KO mice, a series of voltage steps in 10 mV increments were applied to the cell. Voltage steps were applied for 100 ms to trigger a robust increase in membrane capacitance. Pharmacological blockers of potassium currents were used to isolate calcium currents as described previously (section 2.2). For clarity, a single stimulus protocol has been illustrated (Figure 3.1A), showing a holding potential of -81 mV, the sinusoidal voltage command around the holding potential and a depolarising step to -11 mV. The maximal calcium current and corresponding change in membrane capacitance is observed at -11 mV and the responses of single IHCs from a control (black) and a DOC2B KO (grey) mouse are illustrated (Figure 3.1B). The peak of the calcium current was measured for steps to different command voltages and averaged to generate an I-V curve for IHCs from control (black) and DOC2B KO (grey) mice (Figure 3.1C). The corresponding changes in membrane capacitance were measured by averaging 100 ms of the ΔCm response shortly after the end of the voltage step and averaged to generate a mean change in membrane capacitance for each of the command voltages (Figure 3.1D). There was no significant difference in either the maximal calcium current elicited by a depolarising voltage step to -11 mV, or the corresponding change in membrane capacitance between IHCs from control (I_{Ca} = -162.7 ± 21.7 pA; ΔCm = 25.5 ± 2.4 fF, n = 9) and DOC2B KO mice (I_{Ca} = -146.5 ± 7.1 pA; ΔCm = 26.9 ± 2.8 fF, n = 6), nor was a significant difference found in the I-V curves, or the corresponding changes in membrane capacitance using two-way ANOVA.

3.2.3 Kinetics of exocytosis at the ribbon synapses of DOC2B KO mice:

I have investigated the kinetics of exocytosis in IHCs from DOC2B KO mice to determine if DOC2B deletion affects the availability of vesicles for release at IHC ribbon synapses. IHCs held at -81 mV were depolarised with voltage steps to -11 mV for increasing durations (2 - 1500 ms).

Figure 3.1: Calcium currents and changes in membrane capacitance of IHCs from control and DOC2B KO mice in response to voltage steps.

A) Example of the step protocol applied to IHCs. A sinusoidal stimulus (37 mV peak to peak at 4 kHz) was applied to cells at a holding potential of -81 mV, which was interrupted for 100 ms voltage steps in 10 mV increments (-11 mV in the example).
B) Example of the inward calcium current (top) and corresponding change in membrane capacitance (bottom) of an IHC from a control (black) and a DOC2B KO (grey) mouse in response to a 50 ms depolarising voltage step (to -11 mV). The recordings of IHCs from both control and DOC2B KO mice are produced by averaging two recordings from an individual IHC.
C) Average peak of the calcium current elicited by applying 100ms voltage steps, in 10 mV increments, to IHCs from control (black, n = 9) and DOC2B KO (grey, n = 6) mice (P17 – P29).
D) Average change in membrane capacitance of IHCs from control (black, n = 9) and DOC2B KO (grey, n = 6) mice (P17 – P29) in response to 100 ms voltage steps in 10 mV increments.

No significant differences were observed in either the amplitude of the calcium current, or the change in membrane capacitance in response to voltage steps, of IHCs from control and DOC2B KO mice.

N.B The command voltage for each voltage step was corrected for the voltage drop across the series resistance, and each point has a voltage ± SEM, however the error bars are too small to be seen.

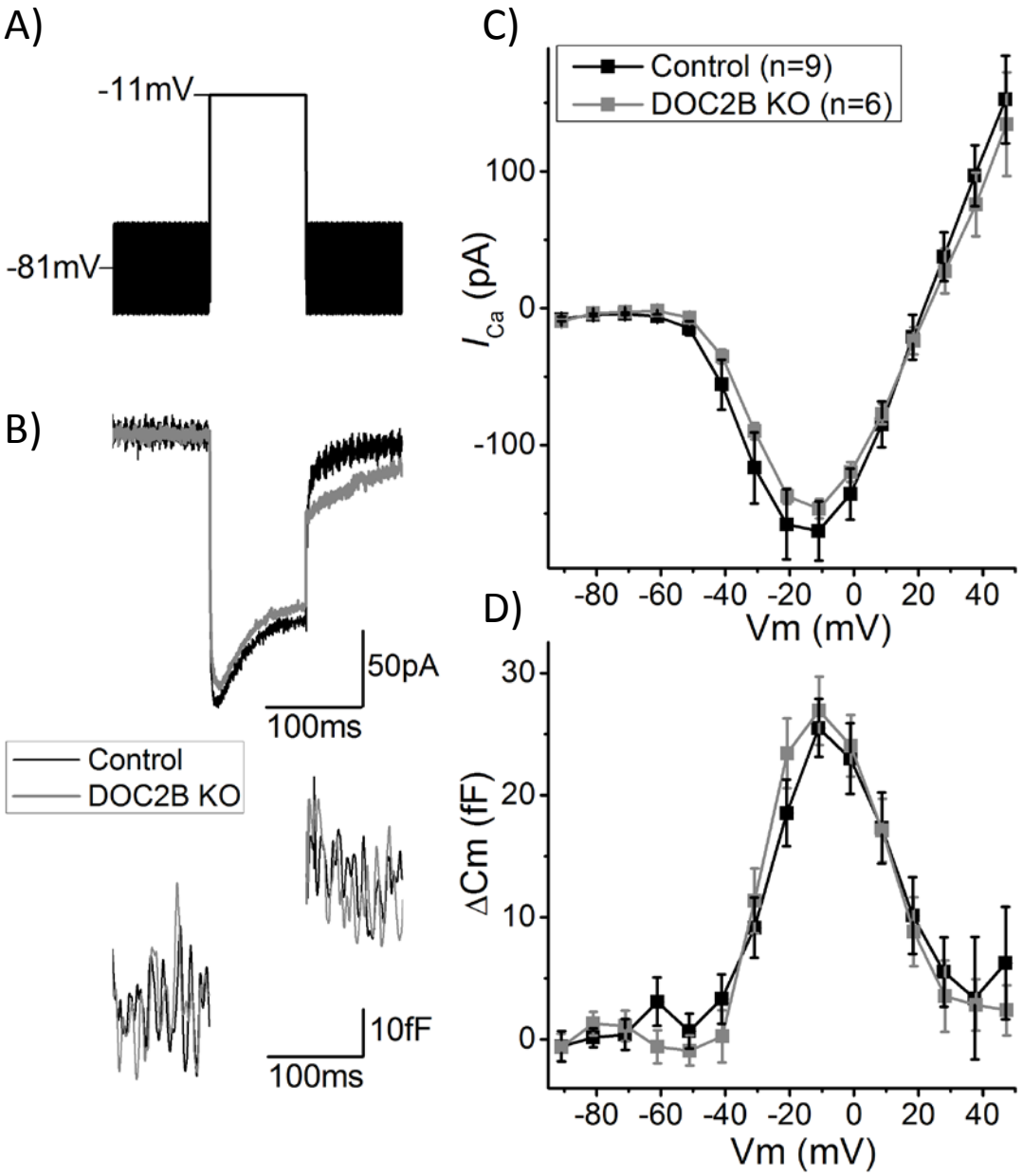
A)
-11mV
-81mV
B)
50pA
100ms
Control
DOC2B KO
10fF
100ms
C)
Control (n=9)
DOC2B KO (n=6)
100
0
-100
I_{Ca} (pA)
-80 -60 -40 -20 0 20 40
Vm (mV)
D)
30
20
10
0
ΔCm (fF)
-80 -60 -40 -20 0 20 40
Vm (mV)

In order to investigate possible differences in the availability of vesicles for release, the kinetics of exocytosis were tested by depolarising IHCs to -11 mV for increasing lengths of time. Short (2 – 100 ms) depolarising voltage steps were used to assess the release of the RRP of synaptic vesicles (Figure 3.2A), which are likely to be docked in the presynaptic active zone. Longer depolarising steps (100 – 1500 ms) were used to assess the availability of vesicles in the secondary releasable pool (SRP) for release (Figure 3.2).

Short depolarising voltage steps elicit similar changes in membrane capacitance in IHCs from control and DOC2B KO mice (ΔCm = 19.1 ± 1.9 fF, n = 6; ΔCm = 16.7 ± 0.9 fF, n = 7, respectively for 50 ms voltage steps) (Figure 3.2). No significant differences were identified between the responses by two-way ANOVA, suggesting normal numbers of synaptic vesicles are available for release from the RRP at auditory ribbon synapses of DOC2B KO mice.

In response to longer depolarising voltage steps, IHCs from control mice show similar increases in membrane capacitance to IHCs from DOC2B KO mice (ΔCm = 0.519 ± 0.240 pF, n = 6; ΔCm = 0.519 ± 0.351 pF, n = 6 respectively for 1 s voltage steps) (Figure 3.2). Two-way ANOVA revealed that there were no significant differences between the responses to longer depolarising steps, suggesting that recruitment, docking and priming of vesicles in the SRP is not affected by deletion of DOC2B.

This suggests that DOC2B is not important for regulating the availability of vesicles for release at the presynaptic active zone of the auditory ribbon synapse.

3.2.4 Vesicle pool replenishment in IHCs from DOC2B KO mice:

It is possible that DOC2B is required for replenishment of vesicle pools during prolonged periods of stimulation. To test this; changes in membrane capacitance were monitored in IHCs held at -81 mV. Repetitive depolarising voltage steps to -11 mV were applied to deplete the vesicle pools and the cumulative increase in membrane capacitance was assessed by averaging the change in membrane capacitance during the inter-step intervals.

Figure 3.2: Kinetics of exocytosis in IHCs from DOC2B KO mice.

A) Average change in membrane capacitance of IHCs from control (black, n = 6) and DOC2B KO (grey, n = 7) mice (P17 – P29) in response to short (2 – 100 ms) depolarising voltage steps to -11 mV from a holding potential of -81 mV.
B) Average change in membrane capacitance of IHCs from control (black, n = 7) and DOC2B KO (grey, n = 6) mice (P17 – P29) in response to long (0.1 - 1.5 s) depolarising voltage steps to -11 mV from a holding potential of -81 mV.

No significant differences were observed between the responses of IHCs from control and DOC2B KO mice to either short, or long depolarising steps.

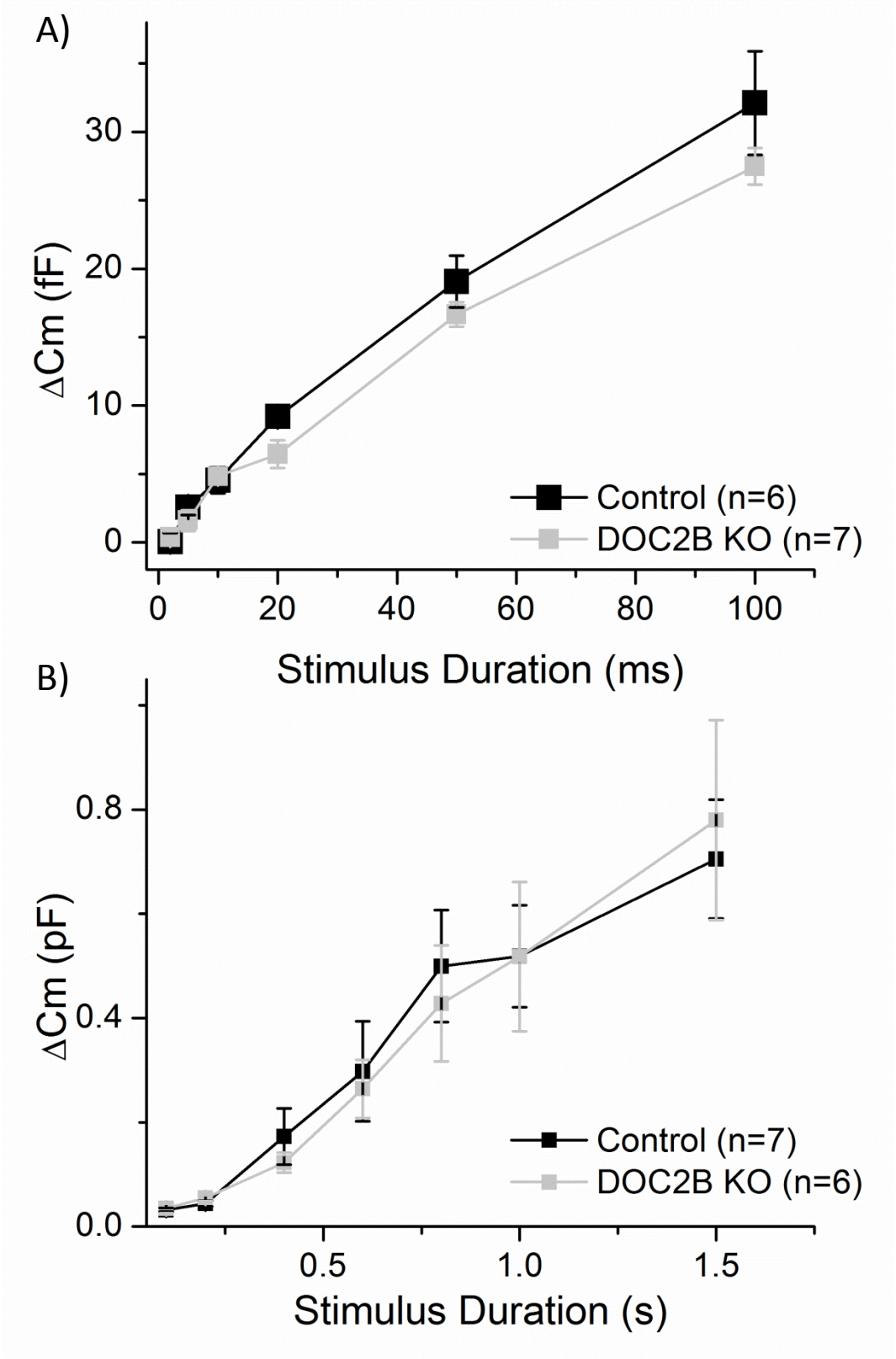
A)
30
20
10
0
ΔCm (fF)
0
20
40
60
80
100
Stimulus Duration (ms)
Control (n=6)
DOC2B KO (n=7)
B)
0.8
0.4
0.0
ΔCm (pF)
0.5
1.0
1.5
Stimulus Duration (s)
Control (n=7)
DOC2B KO (n=6)

Figure 3.3: Vesicle replenishment during repetitive depolarising voltage steps.

A) Example of the first 0.5 s recording of a protocol used to test replenishment of the readily releasable pool of synaptic vesicles. Change in membrane capacitance (top) of an IHC from a control (black) and DOC2B KO (grey) mouse in response to repetitive 50 ms voltage steps to -11 mV with a 50 ms inter-step interval (bottom). A sinusoidal voltage command (37 mv peak to peak at 4 kHz) was applied to IHCs held at -81 mV and interrupted for voltage steps. The recordings displayed are individual recordings from a single IHC.

B) Average cumulative increase in membrane capacitance of IHCs from control (black, n = 7) and DOC2B KO (grey, n = 10) mice (P17 – P29) in response to repetitive 50 ms depolarising voltage steps.

C) Example of the first 6 s recording of a protocol used to test the replenishment of the secondary releasable pool of synaptic vesicles. Change in membrane capacitance (top) of an IHC from a control (black) and DOC2B KO (grey) mouse in response to repetitive 1 s voltage steps to -11 mV with a 200 ms inter-step interval (bottom). A sinusoidal voltage command (37 mv peak to peak at 4 kHz) was applied to IHCs held at -81 mV and interrupted for voltage steps. The recordings displayed are individual recordings from a single IHC.

D) Average cumulative increase in membrane capacitance of IHCs from control (black, n = 6) and DOC2B KO (grey, n = 8) mice (P17 – P29) in response to repetitive 1 s depolarising voltage steps.

No significant differences were observed between the responses of IHCs from control and DOC2B KO mice to repetitive depolarisations, either for short (50 ms), or long (1 s) voltage steps.

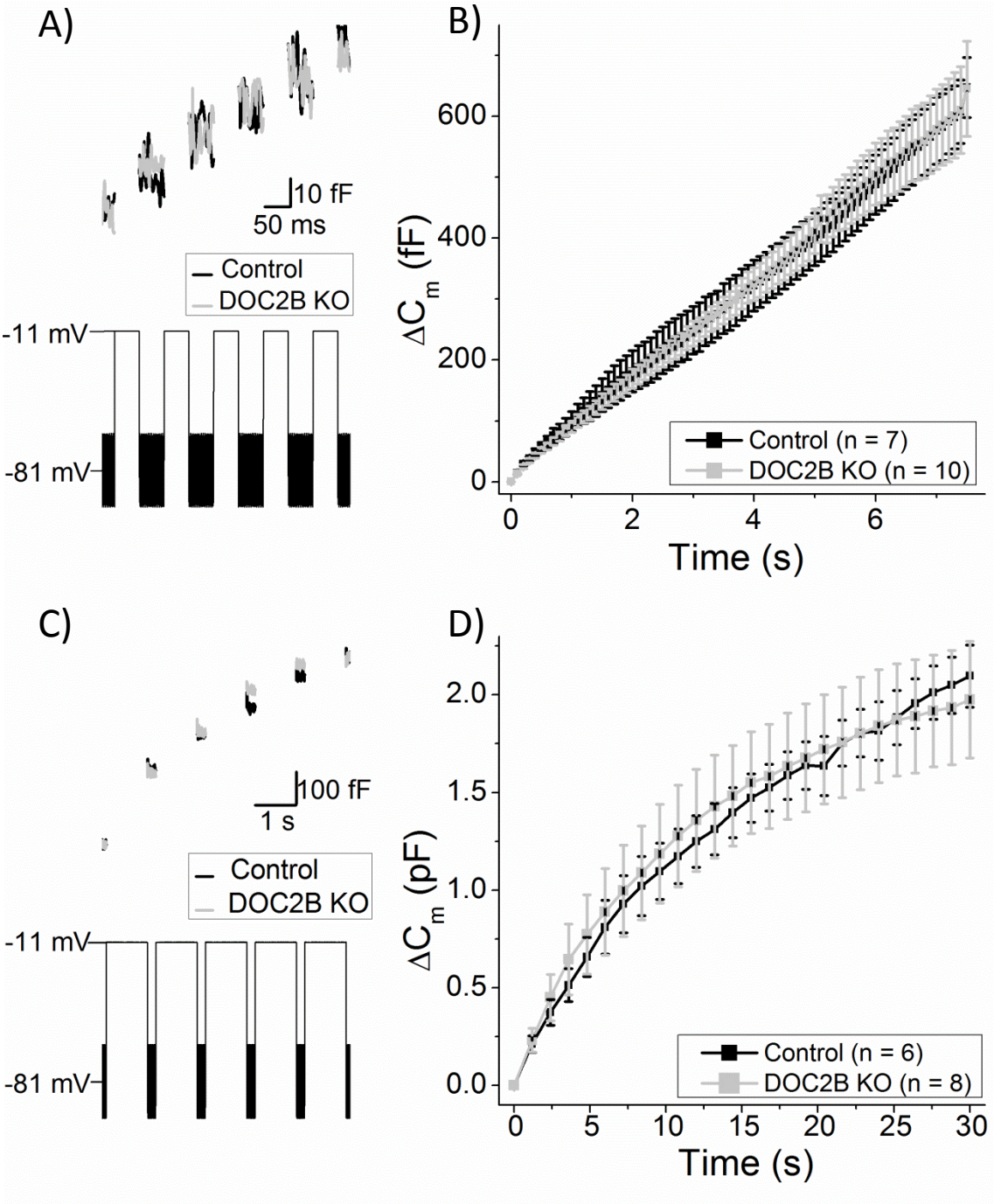
A)
10 fF
50 ms
Control
DOC2B KO
-11 mV
-81 mV
B)
600
400
200
0
ΔC_m (fF)
Control (n = 7)
DOC2B KO (n = 10)
0
2
4
6
Time (s)
C)
100 fF
1 s
Control
DOC2B KO
-11 mV
-81 mV
D)
2.0
1.5
1.0
0.5
0.0
ΔC_m (pF)
Control (n = 6)
DOC2B KO (n = 8)
0
5
10
15
20
25
30
Time (s)

To test the replenishment of the RRP, 50 ms depolarising steps with a 50 ms inter-step interval were applied to IHCs from control and DOC2B KO mice. The cumulative change in membrane capacitance was measured after each depolarisation (Figure 3.3A). The cumulative increase in membrane capacitance was the same between IHCs from control and DOC2B KO mice (ΔCm = 647.4 ± 49.3 fF, n = 6; ΔCm = 645.4 ± 78.3 fF, n = 10 after 7.5 s, or 75 steps). This suggests that DOC2B is not required for refilling of the RRP during prolonged stimulation in IHCs from DOC2B KO mice.

To determine if DOC2B is involved in replenishment of the SRP in IHCs, 1 s depolarising voltage steps were applied with a 200 ms inter-step interval. No significant differences were observed in the cumulative increase in membrane capacitance of IHCs from control and DOC2B KO mice (ΔCm = 1.64 ± 0.37 pF, n = 6; ΔCm = 1.72 ± 0.28 pF, n = 8 after 20.4 s, or 18 steps) (Figure 3.3), demonstrating that DOC2B is not required for replenishment of the SRP after repetitive depletions in IHCs.

Taken together, these results demonstrate that DOC2B is not required for refilling of either the RRP or SRP at the auditory ribbon synapse, suggesting that DOC2B does not regulate the vesicle cycle in IHCs.

3.2.5 Exocytosis from the ribbon synapse of immature IHCs:

To explore a possible role for DOC2B in developing IHCs, we measured the peak calcium current and corresponding capacitance changes of IHCs from immature (P5 – P8) DOC2B KO mice and littermate controls in response to 100 ms voltage steps in 10mV increments. An example stimulus protocol of a depolarising voltage step to -11 mV, whole cell membrane current and membrane capacitance recording is shown (Figure 3.4A+B). The peak calcium current responses and corresponding changes in membrane capacitance of eight IHCs from DOC2B KO mice and five littermate controls have been averaged and plotted against the command voltage (Figure 3.4C+D). IHCs from DOC2B KO mice have normal maximal calcium currents (I_{Ca} = -620.6 ± 55.2 pA n = 8) and corresponding capacitance changes (ΔCm = 40.0 ± 3.3 fF, n = 8), compared to littermate controls (I_{Ca} = -608.6 ± 52.1 pA; ΔCm = 41.6 ±

Figure 3.4: Calcium currents and changes in membrane capacitance of IHCs from prehearing control and DOC2B KO mice in response to voltage steps.

A) Example of the step protocol applied to IHCs. A sinusoidal stimulus (37 mV peak to peak at 4 kHz) was applied to cells at a holding potential of -81 mV, which was interrupted for 100 ms voltage steps in 10 mV increments (-11 mV in the example).
B) Example of a single recording of the inward calcium current (top) and corresponding change in membrane capacitance (bottom) from a single IHC from a control (black) and a DOC2B KO (grey) mouse in response to a 100 ms depolarising voltage step (to -11 mV).
C) Average peak of the calcium current elicited by applying 100 ms voltage steps, in 10 mV increments, to IHCs from prehearing control (black, n = 5) and DOC2B KO (grey, n = 8) mice (P5 – P7).
D) Average change in membrane capacitance of IHCs from control (black, n = 5) and DOC2B KO (grey, n = 8) mice (P5 – P7) in response to 100 ms voltage steps in 10 mV increments.

No significant differences were observed in either the amplitude of the calcium current, or the change in membrane capacitance in response to 100 ms voltage steps.

N.B The command voltage for each voltage step was corrected for the voltage drop across the series resistance, and each point has a voltage ± SEM, however the error bars are too small to be seen.

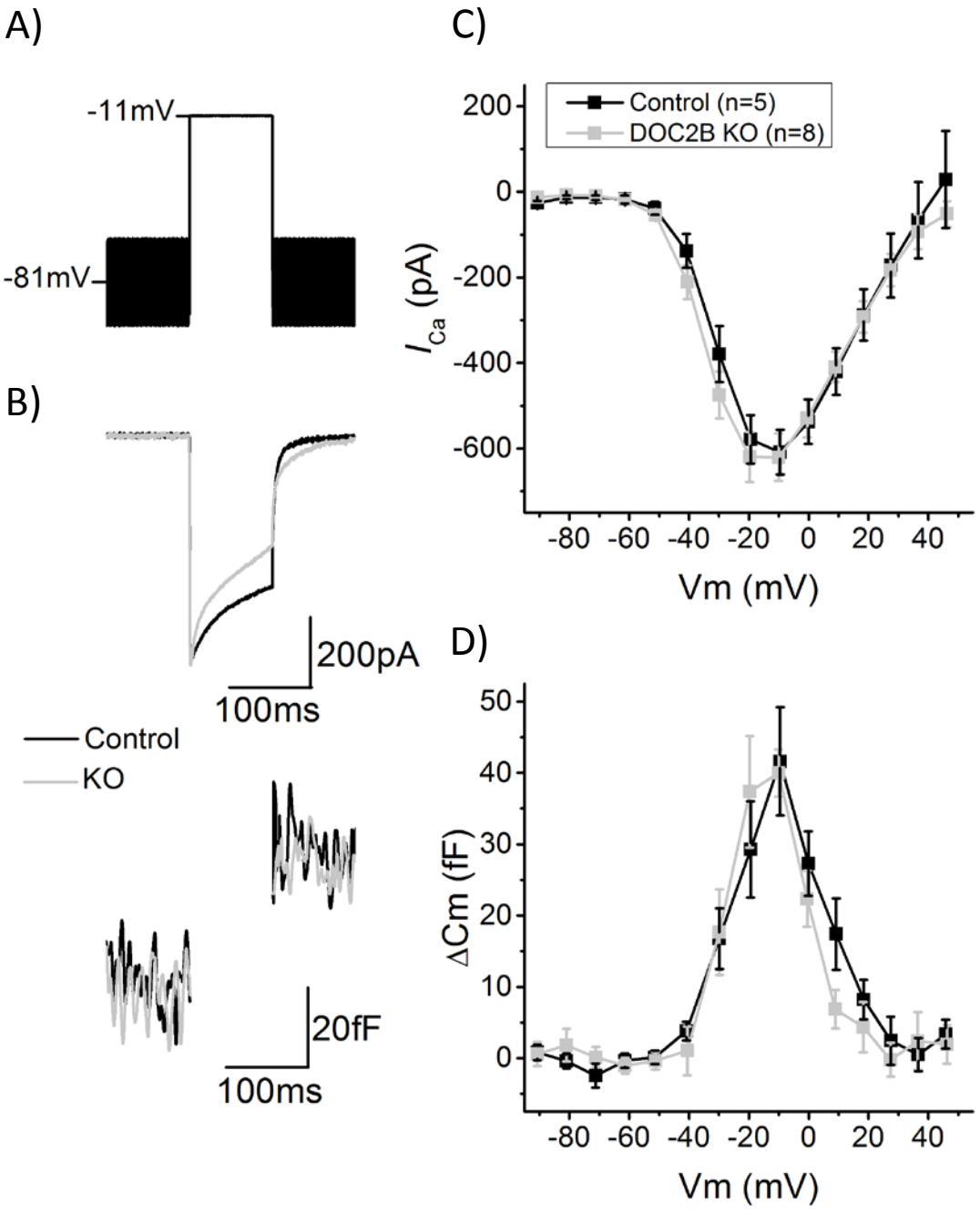
A)
-11mV
-81mV
B)
200pA
100ms
Control
KO
20fF
100ms
C)
Control (n=5)
DOC2B KO (n=8)
I_{Ca} (pA)
200
0
-200
-400
-600
-80 -60 -40 -20 0 20 40
Vm (mV)
D)
ΔCm (fF)
50
40
30
20
10
0
-80 -60 -40 -20 0 20 40
Vm (mV)

7.6 fF, n = 5). Two way ANOVA was used to compare the overall responses of the IHCs from DOC2B KO mice and littermate controls and revealed no significant differences in either the IV curve, or corresponding changes in membrane capacitance.

In the example shown, the kinetics of the calcium current appear different, specifically, the current in the recording from the IHC of a DOC2B KO mouse appears to inactivate faster. This difference is not consistent and is likely to be due to differences in the blockade of potassium channels leading to some contamination of the current recorded by potassium currents.

3.3 Discussion:

To understand how auditory stimuli can be conveyed to the CNS with such temporal precision and fidelity, it is vital to determine the molecules expressed at the ribbon synapse and their roles in regulating synaptic function, particularly with regard to calcium sensors that may regulate the vesicle cycle. The apparent ubiquitous expression of DOC2B (Kojima et al., 1996) and the high-affinity for calcium of double-C2 domain proteins (Ubach et al., 1999) made DOC2B an exciting candidate for a novel regulator of vesicle dynamics at the auditory ribbon synapse.

I have shown that DOC2B is not required for exocytosis in IHCs. It is possible that other calcium sensing proteins expressed in IHCs mask any effects of DOC2B deletion on exocytosis. For example, it has been suggested that different ribbon synapses within an IHC have different calcium-sensitivities for exocytosis (Heil and Neubauer, 2010). If this is the case, different calcium-sensitive molecules may regulate the exocytotic process at each synapse, providing redundancy in the exocytotic machinery at the cellular level.

While the above experiments do not rule out a role for DOC2B at IHC ribbon synapses, they strongly suggest that DOC2B is not involved in fast, synchronous exocytosis of synaptic vesicles, or replenishment of synaptic vesicle pools. However, it is possible that DOC2B is involved in other processes at the ribbon synapse, e.g. DOC2B has been suggested to be a calcium sensor for spontaneous vesicle fusion in purkinje cells (Groffen et al., 2010). At the ribbon synapse, spontaneous glutamate

release is likely to drive spontaneous activity in type I afferent fibres and DOC2B may mediate spontaneous fusion events at ribbon synapses. However there is limited evidence to suggest that DOC2B is a calcium sensor for vesicle fusion and ultimately neurotransmitter release. The bulk of the evidence for DOC2B's role in exocytosis supports a role in vesicle replenishment and priming by other factors such as Munc13 (Pinheiro et al., 2013; Ramalingam et al., 2014).

A recent investigation into vesicle priming at the ribbon synapse of auditory hair cells failed to detect all 4 known isoforms of Munc 13 (1-4) at the ribbon synapse of mature IHCs. Also, IHCs in organotypic cultures of the organ of Corti from mice lacking Munc13-1 and Munc13-2 displayed a normal exocytotic response to depolarising stimulus, suggesting vesicles at the ribbon synapse of IHCs do not undergo conventional Munc13 dependent priming (Vogl et al., 2015). These findings support our results that DOC2B is not required for normal function of the ribbon synapse of IHCs, as synapses lacking Munc13 are unlikely to require its scaffold protein DOC2B. The ability of IHCs lacking DOC2B to maintain a rapid supply of synaptic vesicles to replenish the vesicle pools during repetitive depolarisations further suggests that DOC2B does not regulate the vesicle cycle in IHCs.

Chapter 4 - The Inositol-5-phosphatase Family Member Synaptojanin-2 may Regulate Endocytosis at the Auditory Ribbon Synapse.

4.1 Introduction:

4.1.1 Endocytosis at the auditory ribbon synapse.

Endocytosis is an essential cellular process that allows the internalisation of membrane proteins and external molecules. This is particularly true at synapses, where vesicular membranes and exocytotic machinery needs to be retrieved for synaptic vesicle recycling (Kononenko and Haucke, 2015). In IHCs, endocytosis has received little attention compared to exocytosis; however recent studies are beginning to shed light on the regulation of endocytosis at the auditory ribbon synapse.

Two forms of endocytosis have been identified in IHCs maintained in-vitro (Neef et al., 2014): a slow linear endocytosis that occurs in response to short stimulations that trigger the release of relatively small numbers of synaptic vesicles, and rapid exponential endocytosis after longer stimulations that trigger the release of greater numbers of synaptic vesicles. After the rapid exponential endocytic response to large exocytotic events, a slow linear decline in membrane capacitance persists, likely to represent continuing CME. The slow linear component of endocytosis has been linked to clathrin-mediated endocytosis (CME) as inhibitors of dynamin and clathrin impair this component of the endocytic response (Neef et al., 2014). Dynamin inhibitors also reduce the rate of vesicle release in response to trains of 1 s depolarising voltage steps, suggesting that CME is important for the replenishment of synaptic vesicles at ribbon synapses (Duncker et al., 2013).

At central synapses, CME is regulated by the synaptojanin family of proteins; particularly synaptojanin 1 (SynJ1) (Cremona et al., 1999) and possibly synaptojanin 2 (SynJ2) (Rusk et al., 2003), which appear to regulate the internalisation and uncoating of clathrin coated vesicles (discussed below). SynJ2 is expressed in mammalian auditory hair cells, while SynJ1 is expressed in SGNs (Manji et al., 2011); suggesting SynJ2 may be a regulator of CME at the ribbon synapses of auditory hair cells. Furthermore, *mozart* mice which are homozygous carriers of a point mutation in SynJ2 (N538K) show progressive hearing loss and hair cell death (Manji et al., 2011), demonstrating a role for SynJ2 in maintenance of auditory hair cells.

4.1.2 Synaptojanins and their role in endocytosis.

SynJ1 and SynJ2 are members of the inositol-5-phosphatase family of proteins, which remove phosphate groups from the 5' position of phosphoinositides (McPherson et al., 1994; McPherson et al., 1996; Nemoto et al., 1997). SynJ1 and SynJ2 contain an N-terminal Sac1 and 5'phosphatase domain, with a proline-rich C-terminus. While the Sac1 domain and 5'-phosphatase domains share 57.2% and 53.8% homology, there is little homology in the proline-rich region, which may affect intracellular targeting. When SynJ1 and SynJ2 are expressed in Chinese hamster ovary cells, they can be separated into different fractions by centrifugation (Nemoto et al., 1997), supporting the idea that differences in the proline-rich region lead to differences in intracellular targeting. The Sac1-like domain is capable of directly hydrolysing phosphatidylinositol-phosphates into phosphatidylinositol (PI) (Guo et al., 1999).

Phosphoinositides are lipid membrane molecules produced by phosphorylation of the inositol head group of phosphatidylinositol (PI) (Figure 4.1). PI's have diverse roles in membrane identity, membrane trafficking and intracellular signalling (Di Paolo and De Camilli, 2006; Balla, 2013; Billcliff and Lowe, 2014). The 5' phosphatase domains of SynJ1 and SynJ2 show selective activity towards certain phosphoinositides, dependent on the phosphorylation state of the inositol ring. For example, the 5'-phosphatase domains of SynJ1 and SynJ2 show stronger activity towards phosphatidylinositol-4,5-bisphosphate (PI(4,5)P2) than phosphatidylinositol-3,4,5-trisphosphate PI(3,4,5)P3. There are also differences in their activity; the 5'phosphatase domain of SynJ1 is capable of dephosphorylating the soluble inositol-phosphates, while that of SynJ2 is not (Schmid et al., 2004).

SynJ1 has been localised to clathrin-coated synaptic vesicles (Haffner et al., 1997) and SynJ1 deficient mice die shortly after birth with an accumulation of clathrin-coated vesicles in nerve terminals (Cremona et al., 1999). Although these findings suggest that SynJ1 is involved in the uncoating of clathrin-coated vesicles, later work has shown that SynJ1 activity is also required for the fission of clathrin coated vesicles at the plasma membrane (Mani et al., 2007). SynJ2 has been shown

Figure 4.1: Structure of phosphatidylinositol and phosphatidylinositol-phosphates.

A) The basic structure of phosphatidylinositol; an inositol ring (Arrow), connected to a lipid chain by a phosphate group at position 1 on the inositol ring (Thuronyi, 2010).

B) Phosphorylation of the inositol ring (left) on phosphatidyl produces a phosphatidyl-inositol-phosphate. The number of phosphate groups and their positions on the inositol rings is used to name the molecule (i.e. phosphatidylinositol-4,5-bisphosphate has two additional phosphate groups on the 4^{th} and 5^{th} positions of the inositol ring)(Yikrazuul, 2010).

A)

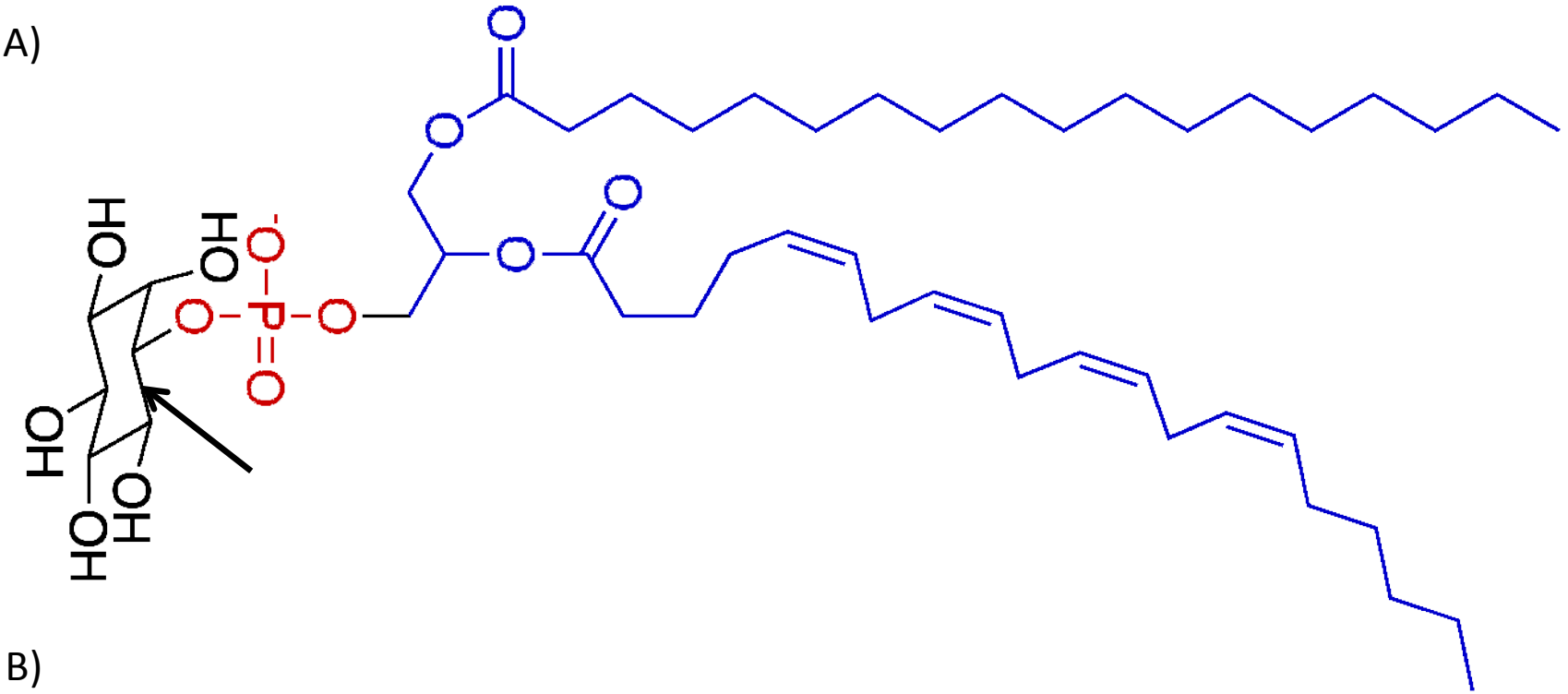

B)

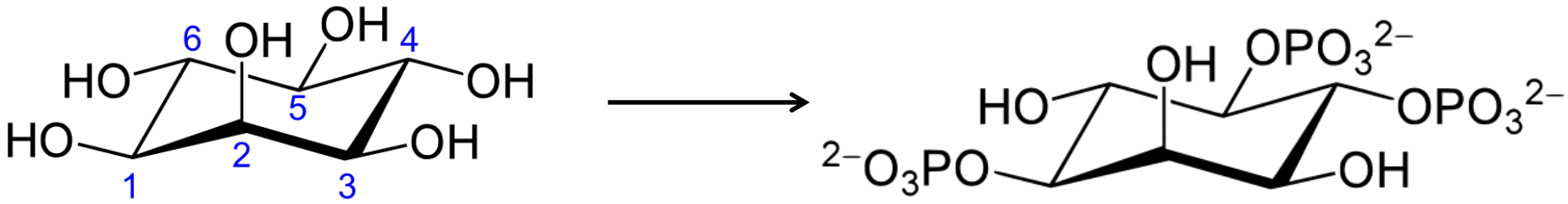

to function at an early stage of endocytosis in a lung carcinoma cell-line, where SiRNA knockdown of SynJ2 reduces the number of clathrin-coated pits and vesicles, an effect that could be rescued by expression of SynJ2, but not SynJ1 (Rusk et al., 2003).

Regulation of the phosphorylation state of phosphoinositides by phosphatidyl-inositol kinases and synaptojanins appears to be a key signalling factor in CME, possibly starting with accumulation of PI(4,5)P2 leading to clathrin-coated pit formation and invagination of the plasma membrane. Membrane curvature or clathrin adaptor molecules may be important for recruitment of endophilin and synaptojanins. Subsequently, the hydrolysis PI(4,5)P2 to PI(4)P by synaptojanin, appears to be crucial for membrane fission and the budding of clathrin-coated vesicles. SynJ1 also appears to have a secondary role in removal of the clathrin coat from internalised vesicles. As most of the studies on synaptojanins role in CME have focused on SynJ1, it is currently unclear if SynJ2 plays the same roles in membrane fission and vesicle uncoating as SynJ1.

4.1.3 Synaptojanins at ribbon synapses.

Photoreceptor ribbon synapses.

The importance of SynJ1 in endocytosis at ribbon synapses was first identified in zebrafish photoreceptors. The *nrc* mutant zebrafish shows a loss of ribbon anchoring and impaired synaptic transmission at photoreceptor ribbon synapses (Allwardt et al., 2001; Van Epps et al., 2001). This is due to a premature stop codon in the SynJ1 gene and knockdown of SynJ1 phenocopies the *nrc* mutant (Van Epps et al., 2004).

At ribbon synapses of photoreceptors in the mouse retina, two forms of endocytosis have been described by their appearance in electron micrographs. In both light adapted (low activity) and dark adapted (high activity) retina, clathrin coated pits and vesicles are present, while in the dark adapted retina, a second type of structure becomes apparent, consisting of large interconnected electron-dense vesicles (Fuchs et al., 2014). This was suggested to be a compensatory mechanism for reclaiming vesicular components after prolonged periods of synaptic activity,

reminiscent of the formation of bulk endosomes described at IHC ribbon synapses (Neef et al., 2014). These larger structures were shown to be devoid of clathrin, but co-localised with SynJ1, endophilin and dynamin3 (Fuchs et al., 2014). The presence of SynJ1 in these endosomal-like structures at photoreceptor ribbon synapses suggests a requirement for inositol-phosphatase activity in the formation of bulk endosomes at photoreceptor ribbon synapses.

Hair cell ribbon synapses.

The *comet* mutant zebrafish carries a premature stop codon in SynJ1 and was identified by ENU-mutagenesis screens for balance defects that indicate vestibular dysfunction. SynJ1 was localised to hair cells of the lateral line and inner ear of the zebrafish. Increased numbers of coated vesicles were observed near the ribbon synapses of hair cells in the *comet* mutant zebrafish, (Trapani et al., 2009). This suggests that SynJ1 is important for CME in zebrafish hair cells.

There is limited evidence for the role of synaptojanins in mammalian auditory hair cells, however it has been shown that SynJ2 is expressed in the sensory epithelium of the organ of Corti, while SynJ1 is expressed in the spiral ganglion neurons. This combined with progressive hearing loss and hair cell degeneration in the *mozart* mutant mouse suggesting that SynJ2 could be responsible for regulating endocytosis in IHCs (Manji et al., 2011).

4.1.4 Investigating the role of SynJ2 at the ribbon synapse of mouse auditory hair cells.

I have investigated the role of SynJ2 at IHC ribbon synapses using electrophysiology. Mice deficient for SynJ2 were created at the Wellcome Trust Sanger institute by Professor Karen Steel; these mice show progressive high frequency hearing loss starting at 4 weeks old (unpublished data). Changes in membrane capacitance have been monitored to investigate exocytosis, endocytosis and vesicle replenishment in IHCs from SynJ2 KO mice. To further investigate the membrane physiology of IHCs from SynJ2 KO mice, measurements of membrane potential, voltage responses and membrane currents have also been carried out.

All experiments have been carried out on mature (P16-P45) IHCs in the mid-high frequency region (approximately 20-40 kHz) of the cochleae from control (SynJ2+/+ and SynJ2+/-) and SynJ2 KO (SynJ2 -/-) mice. The results of hearing tests from SynJ2 +/- mice show no significant differences to those from wild-type mice (unpublished data) and electrophysiological recordings of IHCs from SynJ2+/- mice were compared to recordings from wild-type mice before pooling results.

4.2 Results:

4.2.1 Electrical properties of IHCs from control SynJ2 KO mice.

IHCs from control and SynJ2 KO mice were held in the patch-clamp configuration for recording changes in membrane capacitance in near physiological conditions (1.3 mM Ca^{2+} at 37˚C), at a potential of -81 mV. In these conditions, no significant differences were observed between the electrical properties of the membranes of IHCs from control and SynJ2 KO mice (Table 4.1).

Table 4.1: The electrical properties of IHCs from control and SynJ2 KO mice in the whole-cell patch-clamp configuration for recording calcium currents and changes in membrane capacitance.

Genotype	Rs (MΩ)	Cm (pF)	*I*h at -81 mV (pA)	Rm (MΩ)	gL (nS)	N
control	5.8 ± 0.2	7.7 ± 0.3	-20.3 ± 6.7	1628 ± 132	0.7 ± 0.1	22
KO	6.1 ± 0.2	7.4 ± 0.2	-11.5 ± 1.3	1603 ± 42	0.6 ± 0.0	27

In a subset of experiments presented later in this chapter (section 4.2.6), IHCs from control and SynJ2 KO mice were held in the patch-clamp configuration for recording voltage responses and potassium currents (described in section 4.2), notably they were maintained at room temperature (20 – 22˚C) and a potassium based intracellular solution (K-ICS, section 2.2) was used. No significant differences were observed between the electrical properties of IHCs from control and SynJ2 KO mice were observed in these conditions (Table 4.2).

Table 4.2: Electrical properties of IHCs from control and SynJ2 KO mice in the whole-cell patch-clamp configuration for recording potassium currents and voltage responses.

Genotype	Rs (MΩ)	Rs after 80% compensation (MΩ)	Cm (pF)	*I*h at-84 mV (pA)	Rm (MΩ)	gL (nS)	n
control	6.4 ± 0.2	1.29 ± 0.05	7.5 ± 0.5	-43.3 ± 5.2	1293 ± 90	0.8 ± 0.1	8
KO	7.2 ± 0.4	1.43 ± 0.07	8.4 ± 0.7	-61.3 ± 11.5	1969 ± 666	0.9 ± 0.2	8

4.2.2 Vesicle release at the ribbon synapse of IHCs from SynJ2 KO mice.

Presynaptic function in IHCs from adult (P18 – 23) SynJ2 KO mice was investigated using a series of 50 ms voltage steps to depolarizing command voltages. Calcium currents and corresponding capacitance changes were recorded as described previously (Section 2.3). The maximal amplitude of the calcium current elicited by a voltage step which depolarised IHCs to -11 mV was similar between IHCs from control (I_{Ca} = -150.6 ± 4.6 pA, n = 6) and those from SynJ2 KO (I_{Ca} = -140.8 ± 7.6 pA, n = 11) mice. The corresponding change in membrane capacitance was also not significantly different between IHCs from control (ΔCm = 14.9 ± 1.4 fF, n = 9) and SynJ2 KO (ΔCm = 17.2 ± 1.5 fF, n = 11) mice (Figure 4.2). This shows that exocytosis is normal in IHCs from SynJ2 KO mice, demonstrating that SynJ2 is not required for normal function of the exocytotic machinery at auditory ribbon synapses. This supports evidence from hippocampal neurons of SynJ1 KO mice that shows synaptic activity is only impaired during prolonged periods of high-frequency stimulation (Cremona et al., 1999).

4.2.3 Clathrin-mediated endocytosis in SynJ2 deficient IHCs.

To monitor slow CME, a 100 ms depolarising voltage step to -11mV was applied to the IHCs from P17 – P27 mice to generate a robust exocytotic response (Control = 38.5 ± 7.6 fF, n = 6; KO = 36.6 ± 8.8 fF, n = 7). Following the voltage step, changes in membrane capacitance were recorded for 30 s to monitor the reuptake of vesicular membranes from the presynaptic membranes.

Figure 4.2: Calcium currents and changes in membrane capacitance of IHCs from control and SynJ2 KO mice in response to voltage steps.

A) Example of the step protocol applied to IHCs. A sinusoidal stimulus (37 mV peak to peak at 4 kHz) was applied to cells at a holding potential of -81 mV, which was interrupted for 50 ms voltage steps in 10 mV increments (-11 mV in the example).
B) Example of the inward calcium current (top) and corresponding change in membrane capacitance (bottom) of an IHC from a control (black) and a SynJ2 KO (grey) mouse in response to a 50 ms depolarising voltage step (to -11 mV). The recording of an IHC from a control mouse is a single recording from an individual cell and the recordings from the IHC from a SynJ2 KO mouse is the averaged trace from two recordings of an individual cell.
C) Average peak of the calcium current elicited by applying 50 ms voltage steps, in 10 mV increments, to IHCs from control (black, n = 11) and SynJ2 KO (grey, n = 9) mice (P17 – P27).
D) Average change in membrane capacitance of IHCs from control (black, n = 11) and SynJ2 KO (grey, n = 9) mice (P17 – P27) in response to 50 ms voltage steps in 10 mV increments.

No significant differences were observed in either the amplitude of the calcium current, or the change in membrane capacitance in response to voltage steps, of IHCs from control and SynJ2 KO mice.

N.B The command voltage for each voltage step was corrected for the voltage drop across the series resistance, and each point has a voltage ± SEM, however the error bars are too small to be seen.

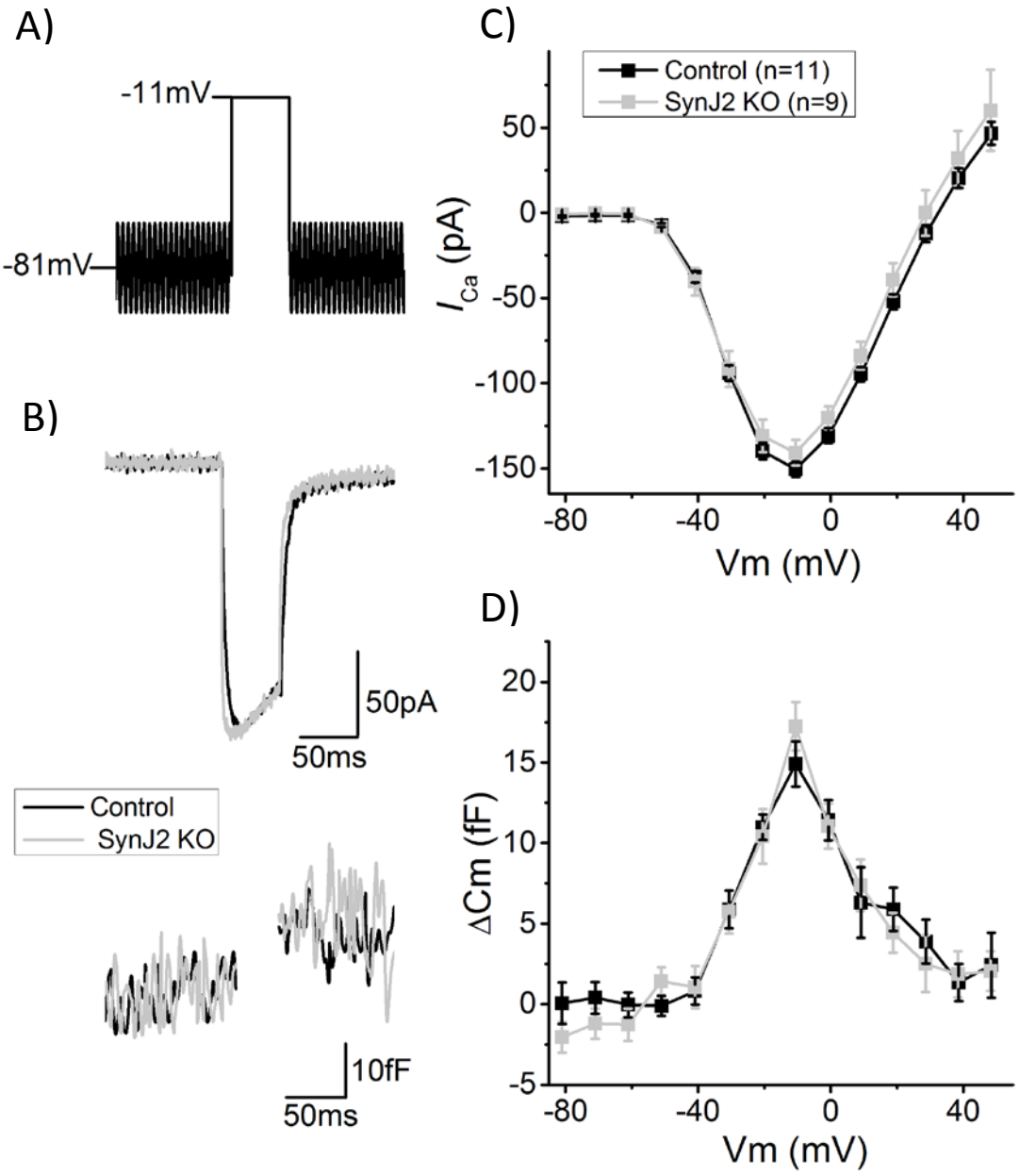
A)
-11mV
-81mV
B)
50pA
50ms
Control
SynJ2 KO
10fF
50ms
C)
Control (n=11)
SynJ2 KO (n=9)
I_{Ca} (pA)
50
0
-50
-100
-150
-80
-40
0
40
Vm (mV)
D)
ΔCm (fF)
20
15
10
5
0
-5
-80
-40
0
40
Vm (mV)

In control IHCs and those from DOC2B KO mice, a slow decrease in membrane capacitance could be recorded (Figure 4.3). This appeared similar to the previous studies on endocytosis (Moser and Beutner, 2000; Neef et al., 2014) and could be approximated with a linear fit, using a linear equation:

$$y = - ax + b$$

where a = the slope of the membrane capacitance recording and b = the y intercept. The linear fit was applied to the data between the start of the decrease in membrane capacitance and the time that the capacitance trace returned to baseline.

After returning to baseline capacitance levels, the decline in Cm continued below prestimulus levels, (Figure 4.3B). A similar "overshoot" can be seen in the published studies of endocytosis in IHCs (Neef et al., 2014), however no explanation has been proposed. It is possibly an artefact of holding the IHC at a hyperpolarised potential, preventing the fusion of further vesicles and addition of their membranes to the IHC membrane to maintain a balance. In-vivo, it is likely that spontaneous fusion of synaptic vesicles and CME would be balanced to allow efficient recycling of vesicle membranes, a balance that may be disrupted in-vitro.

While the results presented here show a similar decline in membrane capacitance as the previously published data, there is one major difference, I observed a higher rate of membrane uptake 5.2 ± 1.0 fF s^{-1} than the published 1.3 ± 0.2 fF s^{-1} (Neef et al., 2014). However, we have carried out our recordings at a physiological temperature (35 – 37 ^{o}C), rather than room temperature and it seems likely that this has accelerated the process of membrane reuptake.

The rate of decline in membrane capacitance and the time taken to return to baseline was quantified for IHCs from control (5.15 ± 1.03 fF s^{-1}; 8.56 ± 1.17 s, respectively, n = 6) and SynJ2 KO (5.42 ± 0.77 fF s^{-1}; 7.68 ± 0.81 s, respectively, n = 7) mice. No significant differences in the endocytic response to small exocytotic events were revealed between control IHCs and those from SynJ2 KO mice. This result suggests that SynJ2 is not required for the reuptake of presynaptic membranes by CME in IHCs.

Figure 4.3: IHCs from SynJ2 KO mice display normal, slow linear reuptake of plasma membrane in response to small exocytotic events elicited by short depolarising voltage steps.

A) Stimulus protocol for monitoring endocytosis following small exocytotic events. A sinusoidal voltage command (37 mV peak to peak at 4 kHz) was applied around a holding potential of -81 mV. This was interrupted for a 100 ms voltage step to -11 mV, before monitoring changes in membrane capacitance for 12 s following the step.

B) Averaged recordings of membrane capacitance changes of IHCs from control (black, n = 6) and SynJ2 KO (grey, n = 7) to the stimulus outlined in A). A linear fit (white line) has been applied to the averaged responses of control IHCs as an example of the fit carried out on individual IHCs. The start of the capacitance response following the voltage step (arrow) was used to determine the time taken for the capacitance of the IHC to return to prestimulus levels.

C) The average rate of decline in membrane capacitance of IHCs from control (black, n = 6) and SynJ2 KO (grey, n = 7) mice (P17 – P27), determined from the linear fit.

D) The average time taken for the membrane capacitance of IHCs from control (black, n = 6) and SynJ2 KO (grey, n = 7) to return to prestimulus levels.

No significant differences were observed in either the rate of membrane reuptake, or the time taken for the membrane capacitance to return to prestimulus levels

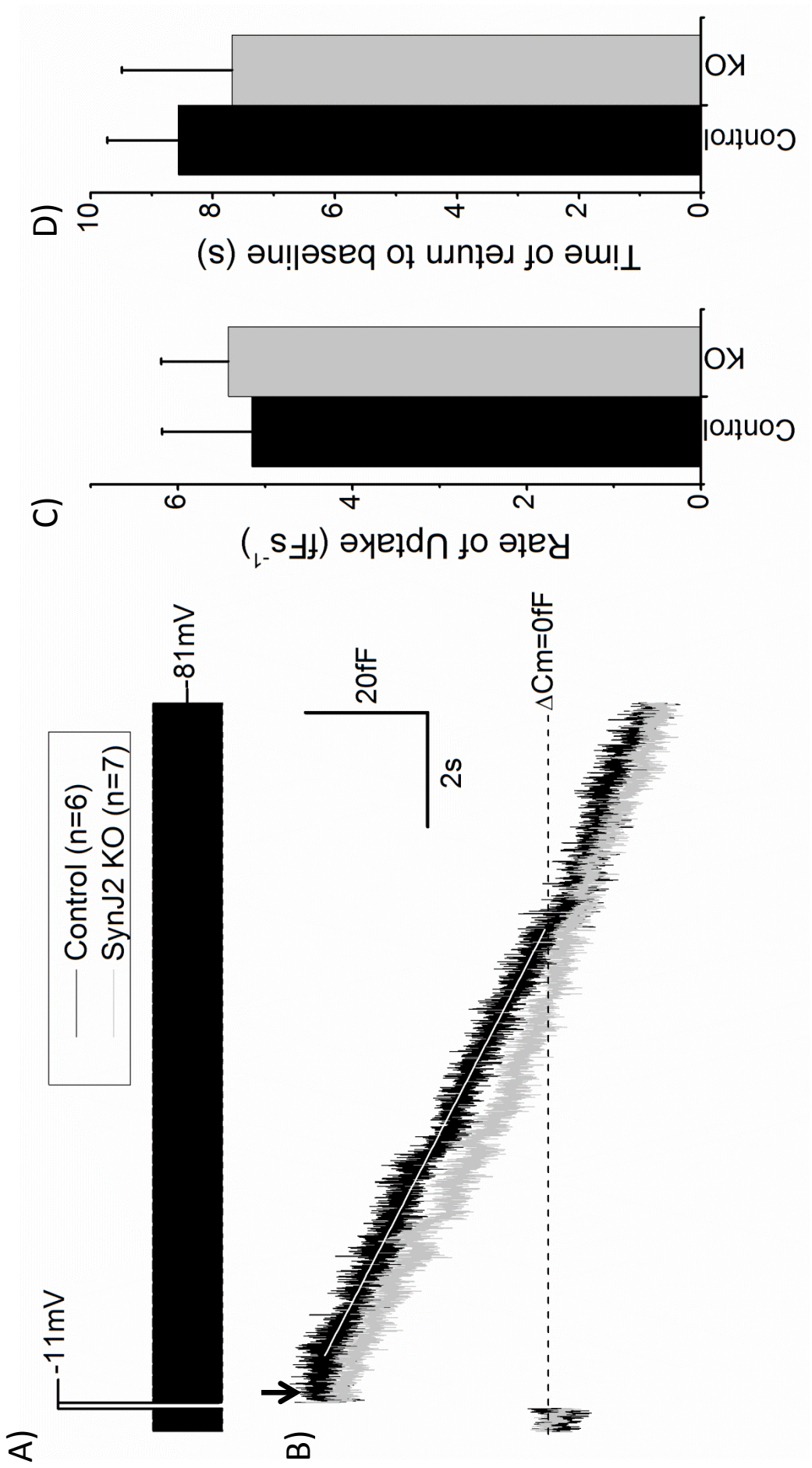
A)
-11mV
81mV
Control (n=6)
SynJ2 KO (n=7)
B)
20fF
2s
ΔCm=0fF
C)
Rate of Uptake (fFs-1)
0
2
4
6
Control
KO
D)
Time of return to baseline (s)
0
2
4
6
8
10
Control
KO

4.2.4 The endocytic response to large exocytotic events.

Exponential endocytosis.

To monitor the fast, exponential component of endocytosis, IHCs were depolarised to -11 mV for 1 s to trigger the fusion of large numbers of synaptic vesicles and a large increase in the membrane capacitance (100's fF). Following this, a rapid, exponential decrease in membrane capacitance was observed in IHCs from control and SynJ2 KO mice (Figure 4.4). After 1 second depolarising voltage steps, the increase in membrane capacitance was similar between IHCs from adult (P17 – 27) control (ΔCm = 282.5 ± 41.4 fF, n = 5) and SynJ2 KO (ΔCm = 329.1 ± 68.7 fF, n = 6) mice. To quantify both portions of the endocytic response to large exocytotic events, each recording was fitted with an equation comprised of an exponential equation and a linear equation:

$$y = ce^{-x/\tau} + d - ax$$

where c = the amplitude of the exponential component, τ = the time constant of the exponential decrease in membrane capacitance, d = the integration constant for the equation, and a = the rate of linear decrease in membrane capacitance.

No significant differences were observed in either the amplitude, or rate constant of the exponential component of endocytosis in endocytosis in IHCs from control (c = 171.8 ± 37.3 fF; τ = 0.48 ± 0.04 s; n = 5) and SynJ2 KO (c = 214.7 ± 42.9 fF; τ = 0.60 ± 0.27; n = 5) mice, suggesting SynJ2 is not required for bulk endocytosis in IHCs.

CME after exponential endocytic events.

Following the exponential component of the endocytic response to large exocytotic events, a slow linear decrease in membrane capacitance persists, which is likely to represent CME (Neef et al., 2014). To confirm this is the case, we compared the rates of decline in membrane capacitance in control IHCs. This revealed that the rate of membrane reuptake was similar during the linear portion of the endocytic response to large exocytotic events (6.71 ± 1.84 fF s^{-1}, n = 5) as the endocytic response to small exocytotic events (5.15 ± 1.03 fF s^{-1}, n = 6), suggesting the mechanism controlling the linear decline in membrane capacitance is the same.

Figure 4.4: IHCs from SynJ2 KO mice display normal endocytic responses to large exocytotic events stimulated by long depolarisations of the IHC.

A) Stimulus protocol for monitoring endocytosis following large exocytotic events. A sinusoidal voltage command (37 mV peak to peak at 4 kHz) was applied around a holding potential of -81 mV. This was interrupted for a 1 s voltage step to -11 mV, before monitoring changes in membrane capacitance for 30 s following the step (12 s shown in the example).

B) Averaged recordings of membrane capacitance changes of IHCs from control (black, n = 5) and SynJ2 KO (grey, n = 5) to the stimulus outlined in A). An example of the exponential + linear fit applied to each of the recordings has been carried out on the control trace (white line).

C) Average increase in membrane capacitance (ΔCm) stimulated by the depolarising step.

D) Amplitude of the exponential component of the endocytic response to large exocytotic events of IHCs from control (black, n = 5) and SynJ2 KO (grey, n = 5) mice, estimated using the equation described (Page 86)

E) The time constant of the exponential equation (Page 86) used to fit the initial rapid decrease in membrane capacitance of IHCs from control (black, n = 5) and SynJ2 KO (grey, n = 5) mice, following large exocytotic events.

F) The average rate of decrease in membrane capacitance of the linear portion of the endocytic response of IHCs from control (black, n = 5) and SynJ2 KO (grey, n = 5) mice.

No significant differences were observed in the endocytic responses observed after long depolarising voltage steps were used to stimulate large exocytotic events between IHCs from control and SynJ2 KO mice.

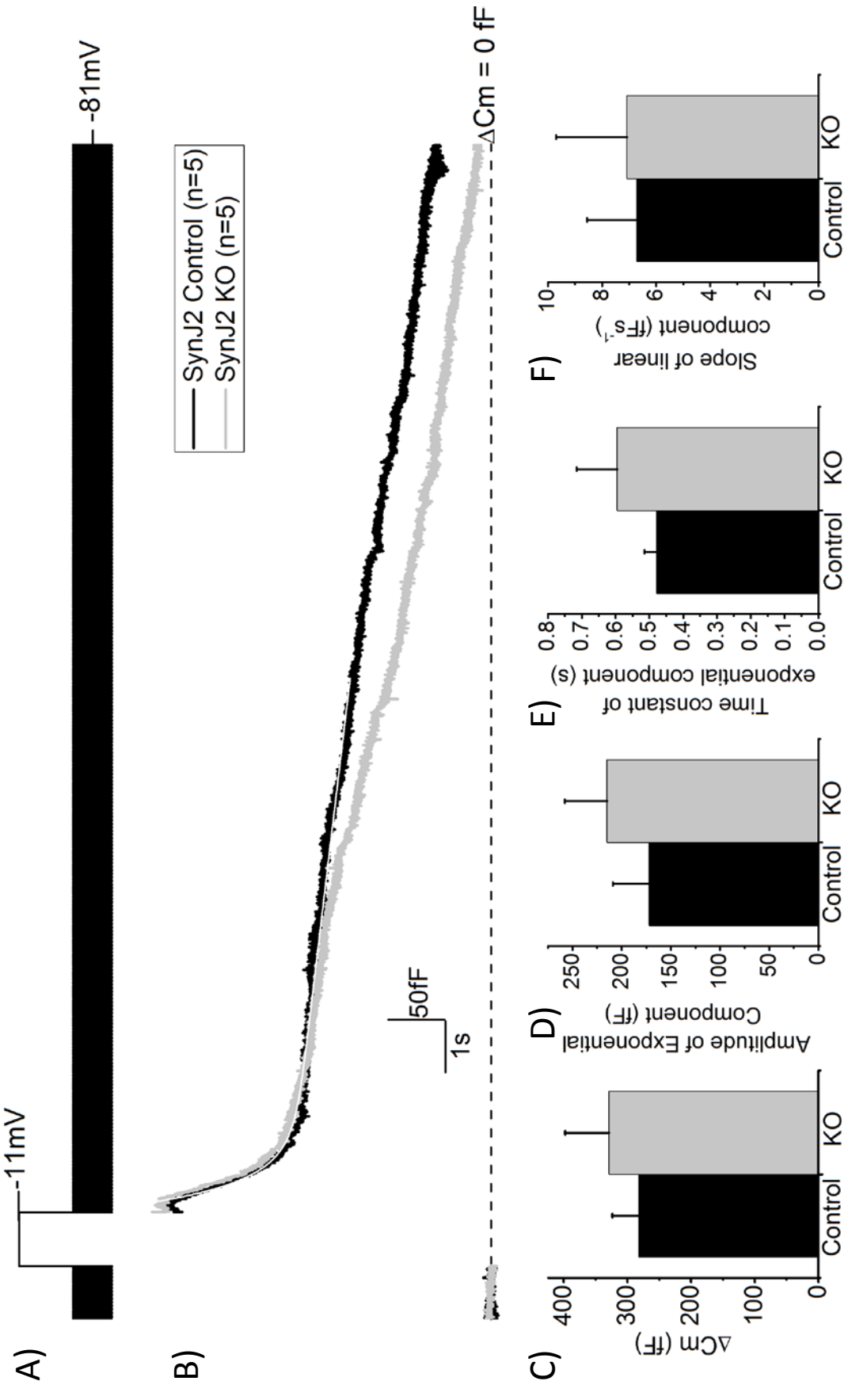
A)
-11mV
-81mV
B)
SynJ2 Control (n=5)
SynJ2 KO (n=5)
50fF
1s
ΔCm = 0 fF
C)
ΔCm (fF)
0
100
200
300
400
Control
KO
D)
Amplitude of Exponential Component (fF)
0
50
100
150
200
250
Control
KO
E)
Time constant of exponential component (s)
0.0
0.1
0.2
0.3
0.4
0.5
0.6
0.7
0.8
Control
KO
F)
Slope of linear component (fFs-1)
0
2
4
6
8
10
Control
KO

The linear rate of decline in Cm observed after the exponential component of the endocytic response to large exocytotic events was not significantly different between IHCs from control (6.71 ± 1.84 fF s^{-1}, n = 5) and those from SynJ2 KO (7.07 ± 2.63 fF s^{-1}, n = 5) mice.

Taken together, the results presented above suggest that SynJ2 is not required for the reuptake of vesicular membranes and components following exocytotic events at the ribbon synapse of IHCs.

4.2.5 Vesicle replenishment at the ribbon synapse of IHCs from SynJ2 KO mice.

Hippocampal neurons from SynJ1 KO mice show enhanced synaptic depression during high-frequency stimulation (Cremona et al., 1999). The loss of SynJ1 is thought to lead to impaired vesicle recycling and a failure to replenish the vesicle pools during high-frequency stimulation. As described previously (Duncker et al., 2013), dynamin inhibitors that prevent CME lead to a reduction in the exocytotic response to repetitive 1 s step depolarisations. To determine if SynJ2 is important for synaptic vesicle recycling in IHCs, repetitive depolarising voltage steps were used to deplete the vesicle pools.

To test the replenishment of the readily releasable pool of vesicles, a train of 50 ms depolarising voltage steps to -11 mV with an inter-step interval of 50 ms was applied to IHCs from adult (P18 – 25) control and SynJ2 KO mice. After 7.5 s (or 75 voltage steps), the cumulative increase in membrane capacitance was found to be similar for IHCs from control mice (830.8 ± 129.8 fF, n = 8) and those from SynJ2 KO mice (898.8 ± 76.6 fF, n = 11) (Figure 4.5A). This demonstrates that in the absence of SynJ2, IHCs are able to replenish the RRP effectively.

To determine if the lack of SynJ2 affects the ability of IHCs to replenish the SRP, IHCs were held at -81 mV and repetitively depolarised to -11 mV for 1 s voltage steps, with a 200 ms inter-step interval. The cumulative increase in membrane capacitance was monitored between steps and no significant differences were observed in the cumulative increase in membrane capacitance of IHCs from control (2.13 ± 0.10 pF, n = 6) and SynJ2 KO (2.17 ± 0.24 pF, n = 10) mice after 20.4 s, or 18 voltage steps (Figure 4.5B). Indicating normal replenishment of the SRP in IHCs from

Figure 4.5: Vesicle replenishment during repetitive depolarising voltage steps.

A) Example of the first 0.5 s recording of a protocol used to test replenishment of the readily releasable pool of synaptic vesicles. Change in membrane capacitance (top) of an IHC from a control (black) and SynJ2 KO (grey) mouse in response to repetitive 50 ms voltage steps to -11 mV with a 50 ms inter-step interval (bottom). A sinusoidal voltage command (37 mv peak to peak at 4 kHz) was applied to IHCs held at -81 mV and interrupted for voltage steps. The recordings displayed are individual recordings from a single IHC.

B) Average cumulative increase in membrane capacitance of IHCs from control (black, n = 8) and SynJ2 KO (grey, n = 11) in response to repetitive 50 ms depolarising voltage steps.

C) Example of the first 6 s recording of a protocol used to test the replenishment of the secondary releasable pool of synaptic vesicles. Change in membrane capacitance (top) of an IHC from a control (black) and SynJ2 KO (grey) mouse in response to repetitive 1 s voltage steps to -11 mV with a 200 ms inter-step interval (bottom). A sinusoidal voltage command (37 mv peak to peak at 4 kHz) was applied to IHCs held at -81 mV and interrupted for voltage steps. The recordings displayed are individual recordings from a single IHC.

D) Average cumulative increase in membrane capacitance of IHCs from control (black, n = 6) and SynJ2 KO (grey, n = 10) mice (P17 – P27) in response to repetitive 1 s depolarising voltage steps.

No significant differences were observed between the responses of IHCs from control and SynJ2 KO mice to repetitive depolarisations, either for short (50 ms), or long (1 s) voltage steps.

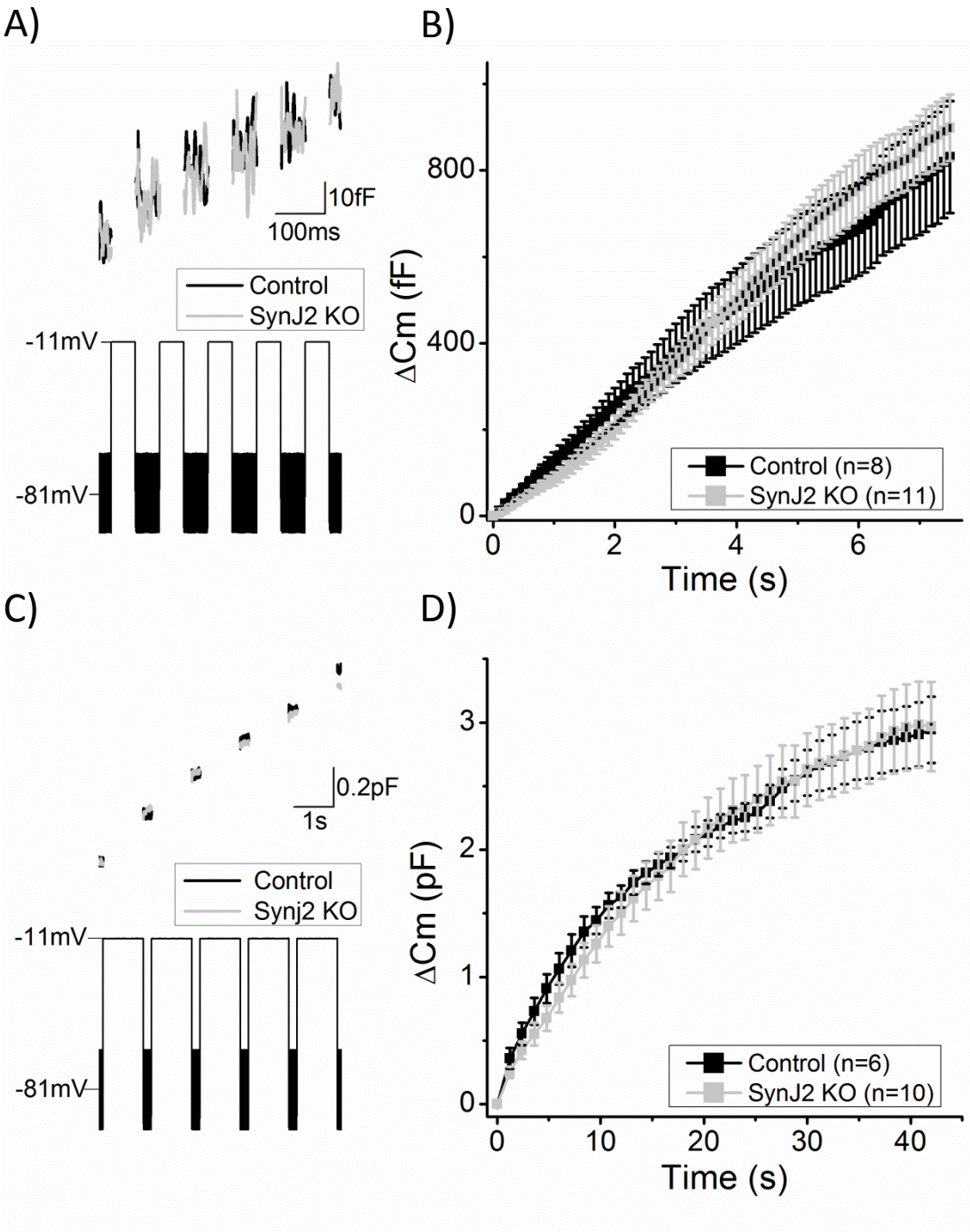
A)
B)
10fF
100ms
Control
SynJ2 KO
-11mV
-81mV
800
400
0
ΔCm (fF)
Control (n=8)
SynJ2 KO (n=11)
0
2
4
6
Time (s)
C)
D)
0.2pF
1s
Control
Synj2 KO
-11mV
-81mV
3
2
1
0
ΔCm (pF)
Control (n=6)
SynJ2 KO (n=10)
0
10
20
30
40
Time (s)

SynJ2 KO mice, this indirectly suggests that SynJ2 is not involved in synaptic vesicle recycling in IHCs, as recycling appears to be important for replenishment of the SRP (Duncker et al., 2013).

4.2.6 IHCs from SynJ2 KO mice exhibit normal responses to current injections and voltage steps.

To determine any possible role for SynJ2 in the general function and/or development of IHCs, current clamp and voltage clamp protocols were used to assess their voltage and current responses, respectively. These experiments were carried out at room temperature using a potassium chloride based intracellular solution, as described in section 2.4.

Current clamp was used to hold IHCs at the resting membrane potential and apply a series of current steps in 100 pA increments from -100 pA to +900 pA (Figure 4.6). The resting membrane potential of the IHCs was quantified by averaging the voltage of the IHC before current injection. The resting membrane potential of control IHCs (-76.1 ± 0.5, n = 6) is not different to the resting membrane potential of IHCs from SynJ2 KO mice (-74.0 ± 0.4 mV, n = 6). The average steady state voltage response was quantified as the mean voltage over the last 25 ms of each current injection. No significant differences were observed in the voltage responses of IHCs from control and SynJ2 KO mice to current injections.

To assess the current profiles of IHCs from SynJ2 KO mice, cells were held at -84 mV, before applying hyperpolarising and depolarising 170 ms voltage steps in 10 mV increments, starting from -124 mV. This stimulus protocol elicits small inward currents in response to hyperpolarising voltage steps and very large outward currents in response to depolarising steps. The outward current response to depolarising command voltages is a combination of two currents expressed in mature IHCs; the large conductance Ca^{2+} activated K^+ current $I_{k,f}$ and the slow delayed rectifier current $I_{K,s}$ (Marcotti et al., 2003a). To assess the overall current responses of IHCs to voltage steps, the current response was averaged over 20 ms at the end of the command voltage, the “steady state” current (Figure 4.7). No significant differences were observed in the steady state current responses of IHCs

Figure 4.6: Mature IHCs from SynJ2 KO mice show normal voltage responses to current injection.

A) Current clamp electrophysiology was used to monitor the voltage responses of IHCs from control and SynJ2 KO mice. IHCs were clamped at the resting membrane potential before application of 250 ms hyperpolarising and depolarising current injections in 100 pA increments

B) Voltage response of an IHC from control (black, top) and SynJ2 KO (grey, bottom) mice.

C) Average steady state voltage responses of IHCs from control (black, n = 6) and SynJ2 KO (grey, n = 6) mice (P18 – P45) to current injections in 100 pA increments. Measured as the mean voltage over the last 25 ms of the current injection

The average resting membrane potential of control IHCs (75.4 ± 0.66 mV, n = 6) was not different from IHCs from SynJ2 KO mice (-73.2 ± 1.11 mV, n = 6). No significant difference was detected between the voltage responses to current injections of IHCs from control or SynJ2 KO mice.

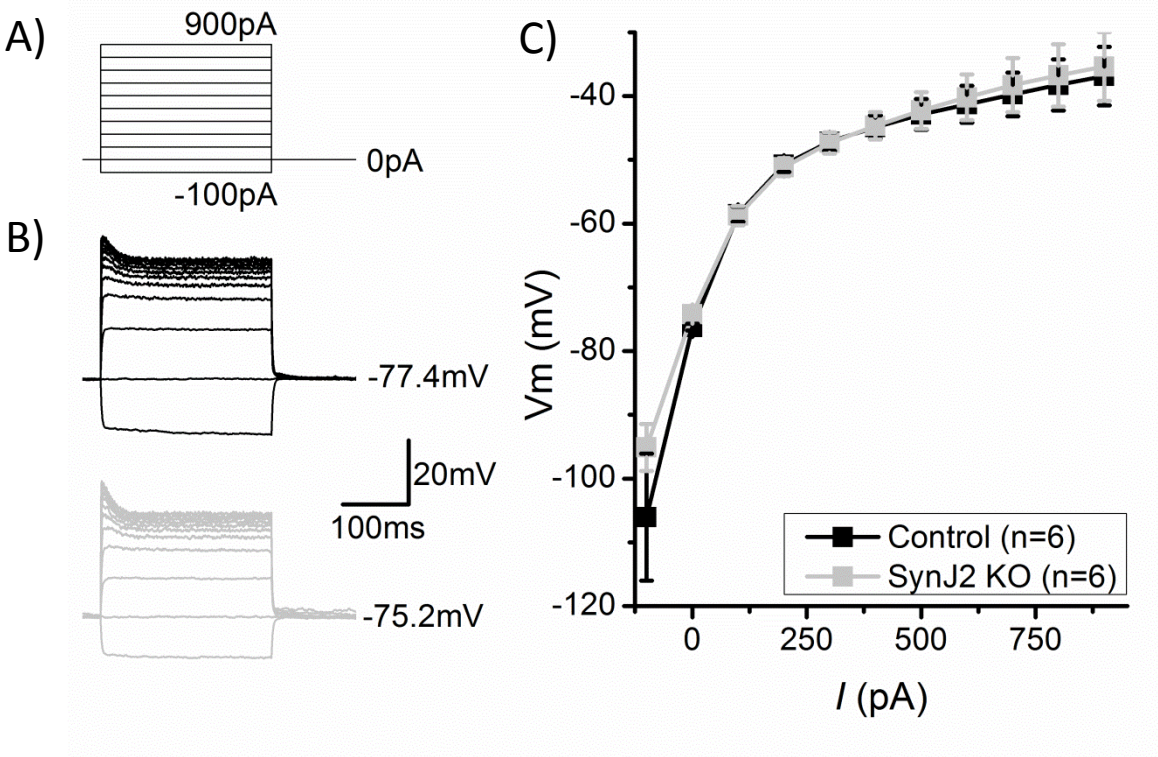

Figure 4.7: IHCs lacking SynJ2 show normal current profiles in response to voltage steps.

A) Stimulus protocol used to elicit current responses from IHCs of adult mice (P18 – P45). IHCs were held at -84 mV, hyperpolarising and depolarising voltage steps were applied in 10 mV increments for 170 ms (top panel).
B) Current responses of single IHCs from a control (black) and SynJ2 KO (grey) mouse to the stimulus protocol in A). The recordings displayed are the averaged traces from two recordings from an individual cell.
C) Average amplitude of the steady state current response to voltage steps of IHCs from control (black, n = 6) and SynJ2 KO (grey, n = 8) mice. The average current was measured over 20 ms at the end of the voltage step
D) Average current response of IHCs from control (black, n = 6) and SynJ2 KO (grey, n = 8) mice, measured 2 ms after the onset of the voltage step as a measure of the rapidly activating large-conductance Ca^{2+} activated potassium current, $I_{K,f}$.

No significant difference was observed in the amplitude of either the steady state current, or onset current responses between IHCs from control and SynJ2 KO mice.

N.B The command voltage for each voltage step was corrected for the voltage drop across the series resistance, and each point has a voltage ± SEM, however the error bars are too small to be seen.

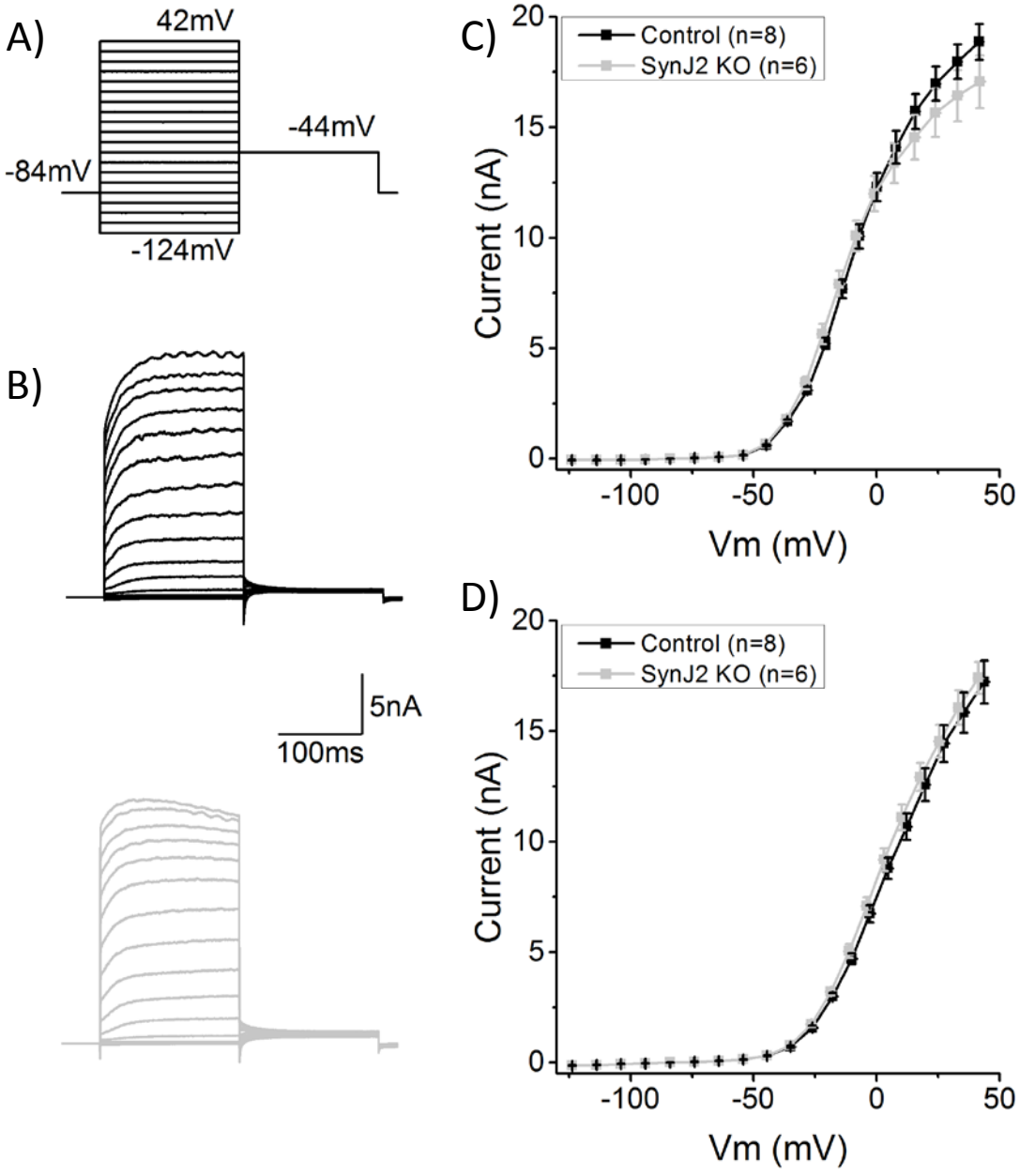
A)
42mV
-44mV
-84mV
-124mV
B)
5nA
100ms
C)
Control (n=8)
SynJ2 KO (n=6)
Current (nA)
Vm (mV)
D)
Control (n=8)
SynJ2 KO (n=6)
Current (nA)
Vm (mV)

from control and SynJ2 KO mice. The current response to depolarising voltage steps could be used to estimate $I_{K,f}$, as the BK channels that carry the current activate rapidly (Kros et al., 1998), before the $I_{K,s}$. To estimate the amplitude of $I_{K,f}$, the current response to the different voltage steps was measured 2 ms after the onset of the command voltage, the "onset" current (Figure 4.7). No significant differences were observed between the onset current responses of IHCs from control and SynJ2 KO mice.

Another potassium current expressed in mature IHCs is the negatively activating, delayed rectifier current ($I_{K,n}$) (Marcotti et al., 2003a). $I_{K,n}$ is carried by KCNQ4 channels, which are rapidly deactivating and have a high open probability near the resting membrane potential. To record $I_{K,n}$, IHCs were held at -64 mV to prevent deactivation of KCNQ4 channels at more negative potentials, then hyperpolarising voltage steps were applied in 10 mv decrements starting at -64 mV (Figure 4.8). This changed the driving force for potassium ions, leading to deactivating inward currents after the start of the voltage step $I_{K,n}$ (Figure 4.8). No significant differences were observed in the current responses of IHCs to hyperpolarising voltage steps in these conditions.

After the hyperpolarising voltage step, the holding potential was set to -124 mV for 170 ms to assess the activation of KCNQ4 channels. This provided a large inward driving force for potassium ions that lead to an inward current with amplitude proportional to the number of KCNQ4 channels open at the end of the preceding voltage step. The difference between the amplitude of the current at the start of the new holding potential (-124 mV) and the steady state current at the end of the preceding voltage step was calculated and used to generate an activation curve (Figure 4.8D). This shows that the maximal inward current was observed when the preceding voltage step was near the resting membrane potential and the open probability of KCNQ4 channels is high (Marcotti et al., 2003a). No significant differences were observed in the activation curves for $I_{K,n}$ of IHCs from control and SynJ2 KO mice.

Figure 4.8: IHCs lacking SynJ2 display normal current profiles of the mature delayed rectifier current $I_{K,n}$.

A) Stimulus protocol used to elicit the negatively activating inward rectifier current $I_{K,n}$ in IHCs from adult mice. IHCs were held at -64 mV and current elicited by applying a series of 170 ms hyperpolarising voltage steps in 10 mV decrements, before holding at -124 mV for 170 ms (P18 – P45).

B) Example response of individual IHCs from control (black, top), and SynJ2 KO (grey, bottom) mice. The $I_{K,n}$ current is the deactivating current visible at the start of hyperpolarising voltage steps. The recordings displayed are the averaged products of two recordings from an individual cell.

C) Average amplitude of the inward current measured immediately after the onset of the command voltage (solid arrowheads) in IHCs from control (black, n = 6) and SynJ2 KO (grey, n = 8) mice.

D) Activation curve for $I_{K,n}$ in IHCs from control (black, n = 6) and SynJ2 KO (grey, n = 8) mice. Values obtained by subtracting the holding current (control Ih = 147.4 pA; SynJ2 KO Ih = -133.0 pA) at -124 mV from the amplitude of the current immediately after hyperpolarising the IHC to -124 mV (hollow arrowheads).

No significant difference was observed between the amplitude, or activation of $I_{K,n}$ in IHCs from control and SynJ2 KO mice.

N.B The command voltage for each voltage step was corrected for the voltage drop across the series resistance, and each point has a voltage ± SEM, however the error bars are too small to be seen.

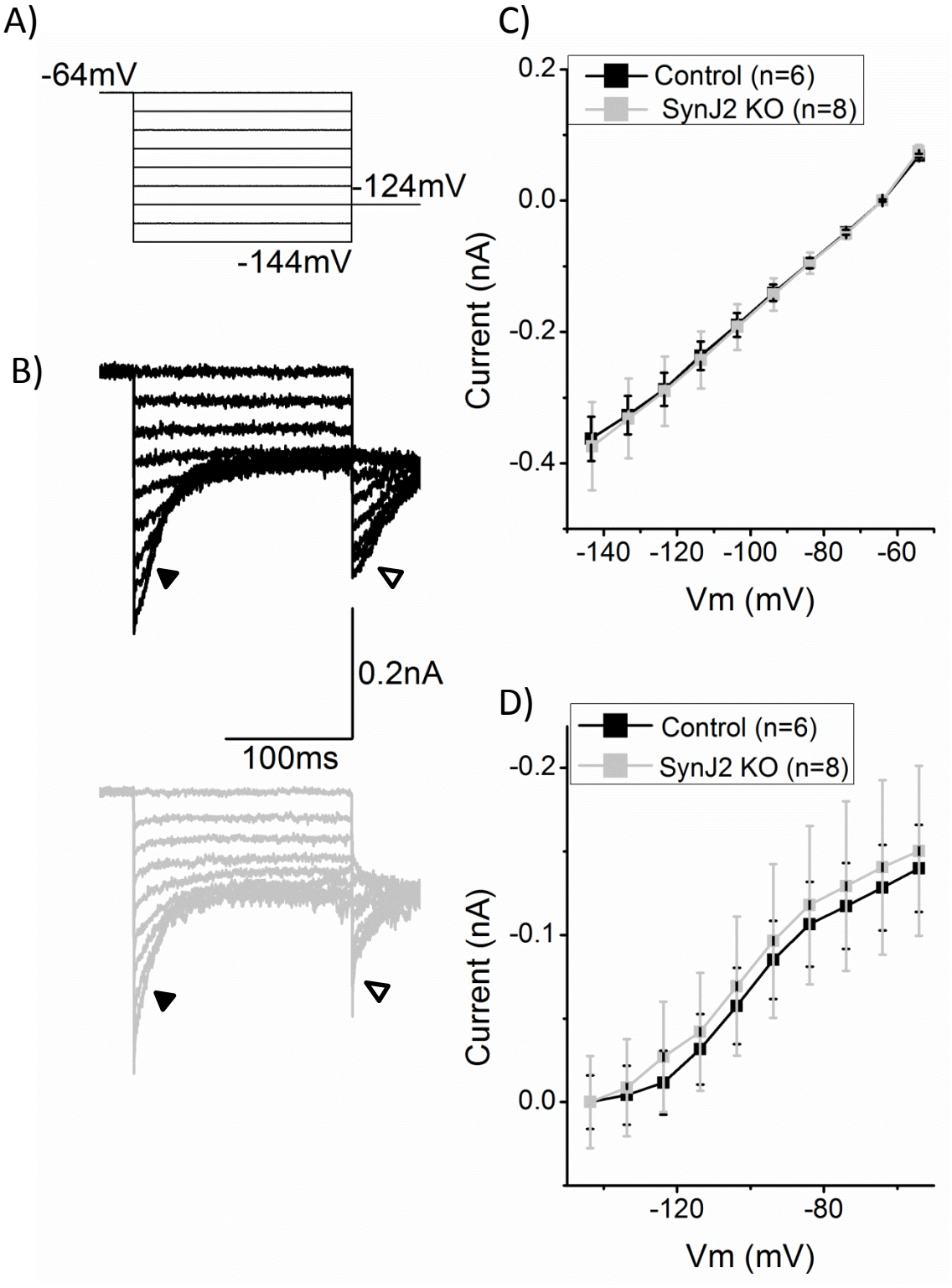
A)
-64mV
-124mV
-144mV
B)
0.2nA
100ms
C)
Control (n=6)
SynJ2 KO (n=8)
Current (nA)
Vm (mV)
D)
Control (n=6)
SynJ2 KO (n=8)
Current (nA)
Vm (mV)

The lack of a significant difference in either the voltage responses to current injections, or current responses to voltage commands, coupled with the normal I_{Ca} shown earlier indicates IHCs from SynJ2 KO mice express a normal cohort of ion channels in their plasma membrane.

4.3 Discussion:

SynJ2 has been shown to be expressed in IHCs and OHCs in the mouse cochlea and mice homozygous for the *mozart* mutation in SynJ2, show progressive hearing loss and hair cell death (Manji et al., 2011). This point mutation results in the substitution of an asparagine residue for a lysine residue in the 5'-phosphatase domain of SynJ2, which abolishes its 5'-phosphatase activity (Manji et al., 2011), suggesting that it is the loss of this activity that leads to hair cell death. SynJ2 has been shown to be important for the formation of clathrin-coated pits in a lung carcinoma cell-line (Rusk et al., 2003). Therefore SynJ2 was considered likely to be a novel regulator of CME and/or vesicle recycling at the presynaptic active zone of auditory hair cells.

SynJ2 is dispensable for endocytosis in neurones.

The importance of SynJ1 for CME and synaptic vesicle recycling at the synapses of central neurones is well established, notably the enhanced synaptic depression during high-frequency stimulation of hippocampal neurons from SynJ1 KO mice (Cremona et al., 1999), and maintaining temporal fidelity of synaptic transmission at the zebrafish hair cell ribbon synapse (Trapani et al., 2009). The role of SynJ2 is less well established, although similarities in the structure and activity of the 5'-phosphatase and Sac1 domains suggest they have similar roles in regulating the phosphorylation of phosphatidylinositols, despite differences in subcellular localisation (Nemoto, 1997).

SynJ2 has been shown to be important for an early stage of CME in a lung carcinoma cell-line, where SiRNA knockdown led to a reduction in the number of clathrin coated pits(Rusk et al., 2003). This implicates SynJ2 in CME and the authors suggest SynJ2 is important for a distinct step in CME, i.e. clathrin-coated pit formation, while SynJ1 is important for a later step in CME, such as clathrin

uncoating. However, SynJ1 appears to be expressed throughout the CNS, while SynJ2 expression seems to be restricted to certain structures in the brain, including the anterior olfactory cortex and the hippocampal CA1 and CA3 regions (Kudo et al., 1999). Therefore SynJ2 seems dispensable for endocytosis in some neurons.

SynJ2 does not regulate endocytosis at the auditory ribbon synapse.

We have shown that exocytosis and endocytosis is normal in IHCs from SynJ2 KO mice, demonstrating that SynJ2 is not a regulator of the vesicle cycle at the auditory ribbon synapse. It is possible that SynJ2 is a regulator of endocytosis in non-synaptic regions of IHCs, e.g. at the apical pole, where vesicle internalisation has been observed in bullfrog hair cells and mammalian IHCs (Kachar et al., 1997; Griesinger et al., 2002). However, apical pole endocytosis has been shown to contribute to the pools of synaptic vesicles (Griesinger et al., 2002) and defects in this process would be expected to reduce the ability of IHCs to replenish the vesicle pools.

SynJ2 could also have a role in the sorting of internalised cargo in IHCs. In zebrafish with mutations in SynJ1, large vesicular structures accumulate in the inner segment of photoreceptors, associated with mislocalised synaptic proteins (George et al., 2014). This implicates SynJ1 in the sorting of internalised synaptic proteins, possibly at the late endosome stage and SynJ2 may have a similar role in IHCs.

SynJ2 may be expressed in non-sensory cells in the organ of Corti.

SynJ2 expression in the sensory epithelium of the organ of Corti has been shown by in-situ hybridisation in the cochleae of 4 week old mice, with the strongest expression observed in the sensory hair cell region (Manji et al., 2011). This suggested that SynJ2 is expressed in the sensory hair cells, however, due to the low resolution of the equipment and staining techniques used, it is possible that SynJ2 is in fact expressed in non-sensory cells in the cochlea. The Phalangeal cells and Deiters cells, which are located between the basilar membrane and IHCs and OHCs respectively, are the most likely cells to express SynJ2 other than the sensory hair cells. Phalangeal cells release neurotrophic factors that have been shown to promote synaptogenesis and hair cell survival in the cultured organ of Corti (Sobkowicz et al., 2002). The loss of SynJ2 may affect the release of neurotrophic

factors from phalangeal and Deiters cells in the adult cochlea, leading to the loss of the sensory hair cells.

Conclusion:

While the 5'-phosphatase activity of SynJ2 is important for the survival of auditory hair cells and ultimately hearing (Manji et al., 2011), the precise function of SynJ2 remains unclear. It is surprising that SynJ2 is not required for synaptic endocytosis, or vesicle replenishment at the ribbon synapse of IHCs. This suggests SynJ2 is involved in either non-synaptic endocytosis, or has a novel, as yet unidentified role in IHCs, such as the sorting of internalised cargo. Alternatively, SynJ2 may not be expressed in IHCs, but may have a role in supporting cells that release neurotrophic factors essential for survival of sensory hair cells.

Chapter 5 - The effect of Loss of Gap Junction Activity in the Cochlea on Synaptic Machinery of IHCs.

5.1 Introduction:

Mutations in connexin 26 (Cx26) and connexin 30 (Cx30), encoded by the genes GJB2 and GJB6 respectively, have long been known to cause autosomal non-syndromic hearing loss in humans (Kelsell et al., 1997; Grifa et al., 1999). Mutations in the DFNB1 locus where GJB2 is found account for over 50% of cases of nonsyndromic hearing loss in humans (Rabionet et al., 2000; del Castillo and del Castillo, 2011).

Connexins are transmembrane proteins that form the subunits of gap junction channels, which directly link the cytoplasm of neighbouring cells, allowing transfer of ions and small molecules between them (Maeda and Tsukihara, 2011). Cx26 and Cx30 are strongly expressed in the rat cochlea from E17. At this early age, supporting cells in the sensory epithelium express both Cx26 and Cx30 while only Cx26 is expressed in the lateral wall. Expression for both connexins increases and spreads to the stria vascularis, spiral ligament and spiral limbus before the onset of hearing, (Lautermann et al., 1998; Lautermann et al., 1999). In the cochlea, Cx26 and Cx30 are likely to form heteromeric gap junction channels and hemichannels in the supporting cells of the organ of Corti, stria vascularis and other areas (Nickel and Forge, 2008). Hemichannels have been shown to mediate ATP release by supporting cells, while gap junctions allow the transfer of second messengers between supporting cells. Both hemichannels and gap junctions are important for the propagation of calcium waves in the developing cochlea (Anselmi et al., 2008).

Early studies using mice carrying genetic mutations that disrupt Cx30 expression (Cx30 KO), showed these mice are severely deaf and fail to generate the endocochlear potential, essential for providing the driving force for ions to flow through the mechano-electrical transducer channel (Teubner et al., 2003). This may be due to disruption of the fluid-blood barrier in the stria vascularis (Cohen-Salmon et al., 2007). However it was later demonstrated that expression of Cx26 was reduced in the cochlea of Cx30 KO mice and almost completely abolished in the supporting cells of the outer sulcus (Ortolano et al., 2008). Further to this, mice deficient for Cx30, but where 50% of Cx26 expression is maintained, have normal

hearing thresholds (Boulay et al., 2013), suggesting Cx30 is dispensable for normal hearing.

The apparent redundancy for Cx30 is hard to reconcile with the fact that humans carrying the T5M mutation in Cx30 display a 20-50 dB threshold shift in hearing (Grifa et al., 1999), and that “knock-in” mice carrying the T5M mutation show a 15 dB hearing threshold shift, despite normal endocochlear potential (Schutz et al., 2010). However, it is possible that the T5M mutation in Cx30 has a dominant-negative effect on heteromeric gap-junction channels in the cochlea.

Genetic studies using Cx30 KO mice and a conditional Cx26 knockout strain, where expression of Cx26 was abolished after E19 - due to embryonic lethality of earlier removal - have revealed differences in the severity of the phenotype caused by deletion of the different connexins. In conditional Cx26 knockout animals, OHCs and supporting cells begin to degenerate in the cochlea at around P14, with almost total hair cell loss by 6 months. Conversely, in the cochlea of Cx30 KO mice, OHCs begin to deteriorate at around 1 month old, but some IHCs and supporting cells survive to 18 months (Sun et al., 2009). It is hard to explain why the conditional Cx26 knockout causes a more severe phenotype than that shown by the Cx30 KO mouse that also has reduced expression of Cx26, but supports the idea that Cx26 is more important for the development and/or maintenance of the cochlea than Cx30.

While the precise requirements of Cx26 and Cx30 expression remain to be shown, it is clear that loss of functional connexin gap-junctions and hemichannels leads to hearing loss and cochlear degeneration in mice and humans. Studies on the cochlea function of mice deficient for connexins have focused on supporting cells and generation of the endocochlear potential by the stria vascularis. While the expression of connexins is restricted to non-sensory cells, it is possible that the reduced gap-junctional activity in the cochlea of Cx30 KO mice has indirect consequences on the physiology and function of sensory hair cells.

I have investigated exocytosis from the presynaptic active zone of IHCs from Cx30 KO mice, to determine if the loss of gap junction activity in supporting cells of the cochlea affects the exocytotic machinery at the auditory ribbon synapse. Cx30 KO

mice (Teubner et al., 2003), were received from Professor F. Mammano and maintained on a C57Bl/6 background. Apical coil IHCs were studied in the acutely isolated organ of Corti from Cx30 control (Cx30+/+ and Cx30+/-) and Cx30 KO (Cx30-/-) adult mice (P17-P25). Hearing defects have not been detected in Cx30+/- mice (Teubner et al., 2003) and recordings of IHCs from Cx30+/- mice were compared to those from Cx30+/+ mice before results were pooled.

5.2 Results:

5.2.1 Electrical properties of IHCs from control and Cx30 KO mice:

IHCs from control and Cx30 KO mice were held in the patch-clamp configuration in near physiological conditions (1.3 mM Ca2+ at 37˚C), at a potential of -81 mV (Table 5.1). Some significant differences were observed between IHCs from control and DOC2B KO mice, IHCs from control mice had significantly ($P < 0.001$) smaller holding currents at -81 mV (-39.4 ± 6.3 pA, n = 15) than IHCs from Cx30 KO mice (-109.3 ± 9.3 pA, n = 17). This was coupled with significantly higher membrane resistances and lower leak conductance in IHCs from control mice (Rm = 920 ± 71 MΩ; gL = 1.2 ± 0.1 nS) compared to IHCs from Cx30 KO (Rm = 377 ± 22 MΩ; gL = 2.9 ± 0.2 nS) mice. However, the series resistance and membrane capacitance was similar between IHCs from control (Rs = 5.6 ± 0.3 MΩ; Cm = 10.3 ± 0.3pF) and Cx30 KO (Rs = 5.6 ± 0.4 MΩ; Cm = 9.1 ± 0.3 pF) mice.

These differences in the electrical properties of IHCs from control and Cx30 KO mice suggests that in our recording conditions, there is an increased conductance of ions through non-gated channels in the membranes of IHCs from Cx30 KO mice compared to controls. Further studies will be required to determine if this is the case.

Table 5.1: Electrical properties of Cx30 control and Cx30 KO IHCs in the whole-cell patch-clamp configuration.

Genotype	Rs (MΩ)	Cm (pF)	*I*h at -81 mV (pA)	Rm (MΩ)	gL (nS)	n
control	5.6 ± 0.3	10.3 ± 0.3	-39.4 ± 6.3	920 ± 71	1.2 ± 0.1	15
KO	5.6 ± 0.4	9.1 ± 0.3	-109.3 ± 9.3	377 ± 22	2.9 ± 0.2	17

5.2.2 IHCs from Cx30 KO mice display larger calcium currents and reduced exocytotic responses to depolarising voltage steps.

A series of 50 ms depolarising voltage steps in 10 mV increments was applied to IHCs from the apical coil of adult mice (P17 – 25). The peak of the calcium current elicited by depolarising the IHC to -11 mV was significantly smaller ($P < 0.001$, Student's two-tailed T-test) in control IHCs (I_{Ca} = -159.9 ± 8.4 pA, n = 15) than IHCs from Cx30 KO mice (I_{Ca} = -234.1 ± 19.8 pA, n = 7) (Figure 5.1). This suggests that more calcium channels were present in the membranes of IHCs from Cx30 KO mice, which could be due to either an increase in the surface area of the cell, with normal levels of calcium channels expressed, or an increase in the levels of calcium channel expression.

The capacitance of IHCs is directly proportional to the surface area of the cell and is measured prior to recordings of calcium currents and changes in membrane capacitance. The surface area of the cells from control mice is not significantly different from the surface area of IHCs from Cx30 KO mice (Cm = 10.3 ± 0.2 pF, n = 15 and Cm = 9.7 ± 0.5 pF, n = 7 respectively). However, calculating the current density (current ÷ capacitance) revealed that the current density of IHCs from control mice was significantly lower than IHCs from Cx30 KO mice (15.5 ± 0.8 pA pF^{-1}, n=15 and 23.9 ± 1.2 pA pF^{-1}, n = 7 respectively; $P < 0.001$, Student's two-tailed T-test). This strongly suggests there are lower levels of calcium channels expressed in the plasma membrane of IHCs from control mice compared to those from Cx30 KO mice.

Conversely, IHCs from control mice show significantly larger ($P < 0.001$, Student's two-tailed T-test) changes in membrane capacitance (ΔCm = 23.79 ± 2.02 fF, n = 15) compared to IHCs from Cx30 KO mice (ΔCm = 8.00 ± 2.66 fF, n = 5) (Figure 5.1), demonstrating that more vesicles fuse with the plasma membrane of control IHCs during the voltage step. This suggests that despite the larger influx of calcium during depolarising voltage steps, IHCs from Cx30 KO mice have a severely reduced exocytotic capacity.

Figure 5.1: Calcium currents and changes in membrane capacitance of IHCs from control and Cx30 KO mice in response to voltage steps.

A) Example of the step protocol applied to IHCs. A sinusoidal stimulus (37 mV peak to peak at 4 kHz) was applied to cells at a holding potential of -81 mV, which was interrupted for 50ms voltage steps in 10 mV increments (-11 mV in the example).
B) Example of the inward calcium current (top) and corresponding change in membrane capacitance (bottom) of an IHC from a control (black) and a Cx30 KO (grey) mouse in response to a 50 ms depolarising voltage step (to -11 mV). Each recording displayed is the average trace from two recordings of an individual cell.
C) Average peak of the calcium current elicited by applying 50ms voltage steps, in 10 mV increments, to IHCs from control (black, n=15) and Cx30 KO (grey, n = 7) mice (P17-P25).
D) Average change in membrane capacitance of IHCs from control (black, n = 15) and Cx30 KO (grey, n = 7) mice (P17-P25) in response to 50 ms voltage steps in 10 mV increments.

IHCs from Cx30 control mice show a significantly smaller amplitude peak calcium current than controls ($P < 0.001$) and a significantly larger exocytotic response ($P < 0.001$) when depolarised to -11 mV.

N.B The command voltage for each voltage step was corrected for the voltage drop across the series resistance, and each point has a voltage ± SEM, however the error bars are too small to be seen.

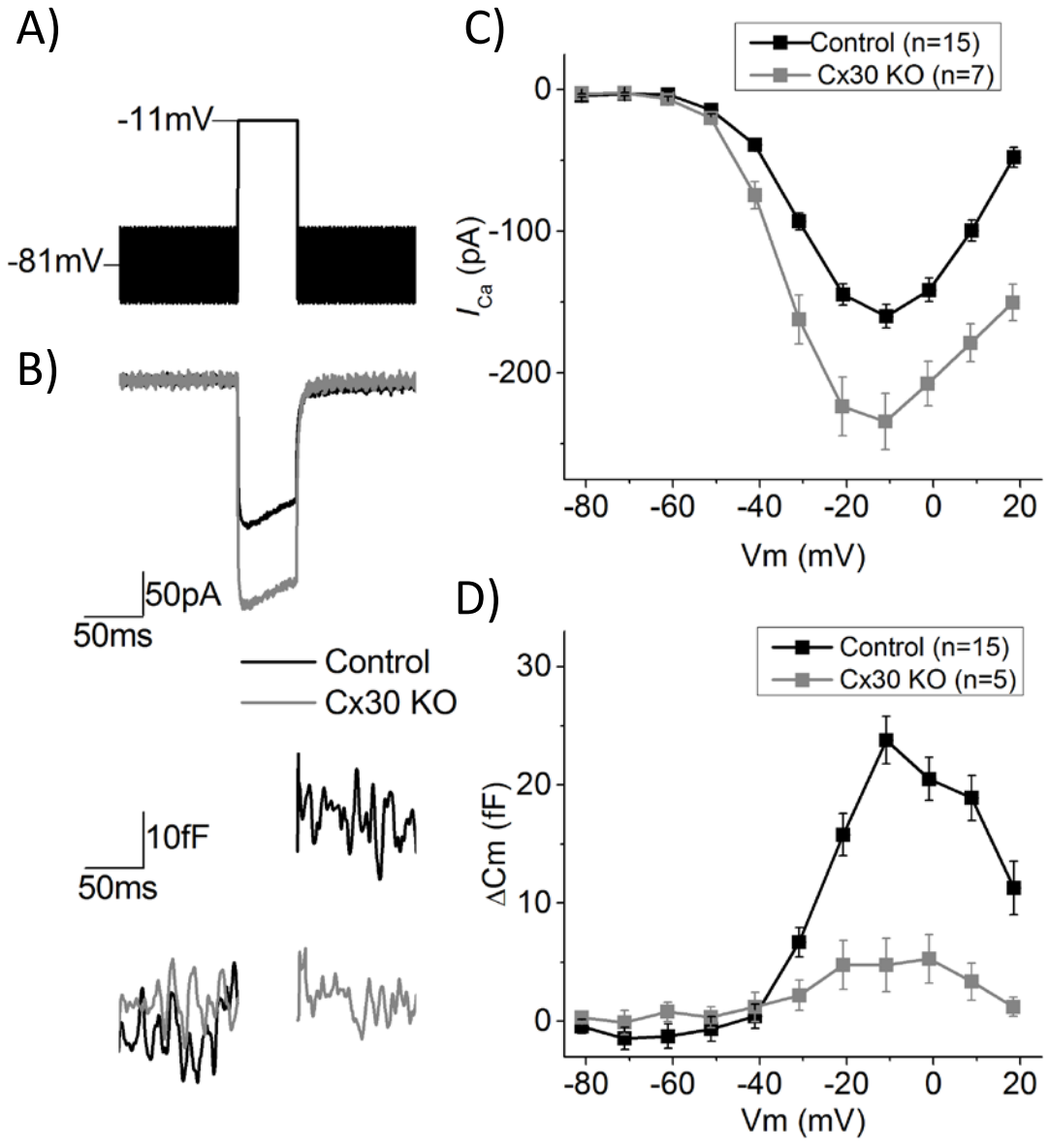
A)
-11mV
-81mV
B)
50pA
50ms
Control
Cx30 KO
10fF
50ms
C)
Control (n=15)
Cx30 KO (n=7)
I_{Ca} (pA)
0
-100
-200
-80
-60
-40
-20
0
20
Vm (mV)
D)
Control (n=15)
Cx30 KO (n=5)
ΔCm (fF)
30
20
10
0
-80
-60
-40
-20
0
20
Vm (mV)

5.2.3 Kinetics of vesicle fusion in IHCs from Cx30 KO mice

To further investigate the extent of the reduced exocytotic response of IHCs from Cx30 KO mice, I tested their ability to recruit and release vesicles from the different pools (RRP and SRP). Depolarising voltage steps to -11 mV were applied to IHCs with increasing durations, 2 – 3000 ms. Results were separated into shorter steps (2 – 100 ms), which elicited fusion of vesicles mainly from the RRP, and longer steps (0.1 – 3 s), which recruited vesicles from the SRP for release.

The exocytotic response of IHCs from control mice to short (2 – 100 ms) depolarising steps was significantly larger ($P < 0.001$, two-way ANOVA) than the exocytotic response of IHCs from Cx30 KO mice (Figure 5.2). A Bonferroni post-test was used to test which responses were significantly different and revealed that the responses to 50 ms and 100 ms voltage steps were significantly different ($P < 0.01$ and $P < 0.001$, respectively) between IHCs from control and Cx30 KO mice. This supports the previous experiments and demonstrates that IHCs from control mice have a significantly larger RRP of synaptic vesicles than IHCs from Cx30 KO mice.

In response to longer depolarising voltage steps (100 ms – 3 s), IHCs from control mice displayed significantly larger ($P < 0.01$, Two-way ANOVA) changes in membrane capacitance than IHCs from Cx30 KO mice. However, a Bonferroni post-test did not reveal any significant differences between the responses of IHCs from control and Cx30 KO mice to individual step durations. This shows that the IHCs from Cx30 KO mice display large exocytotic responses to long depolarising voltage steps, suggesting that they contain large numbers of synaptic vesicles, but require a prolonged influx of calcium to recruit vesicles for release.

Figure 5.2: Kinetics of exocytosis in IHCs from Cx30 KO mice.

A) Average change in membrane capacitance of IHCs from control (black, n = 12) and Cx30 KO (grey, n = 14) mice (P17-P25) in response to short (2 – 100 ms) depolarising voltage steps to -11 mV from a holding potential of -81 mV.
B) Average change in membrane capacitance of IHCs from control (black, n=10) and Cx30 KO (grey, n = 9) mice (P17-P25) in response to long (0.1 - 3 s) depolarising voltage steps to -11 mV from a holding potential of -81 mV

Two-way ANOVA was carried out and revealed there is a significant difference between the responses of IHCs from control and Cx30 KO mice to short depolarising steps ($P < 0.001$) and long depolarising steps ($P < 0.005$)

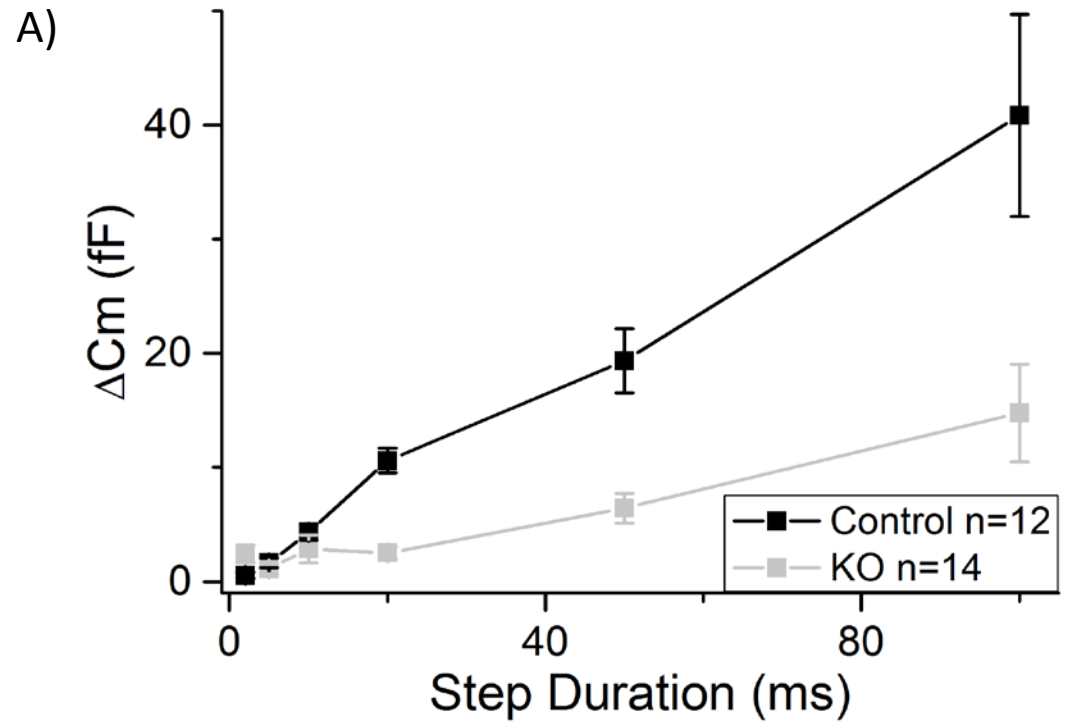
A)
40
20
0
ΔCm (fF)
0
40
80
Step Duration (ms)
Control n=12
KO n=14

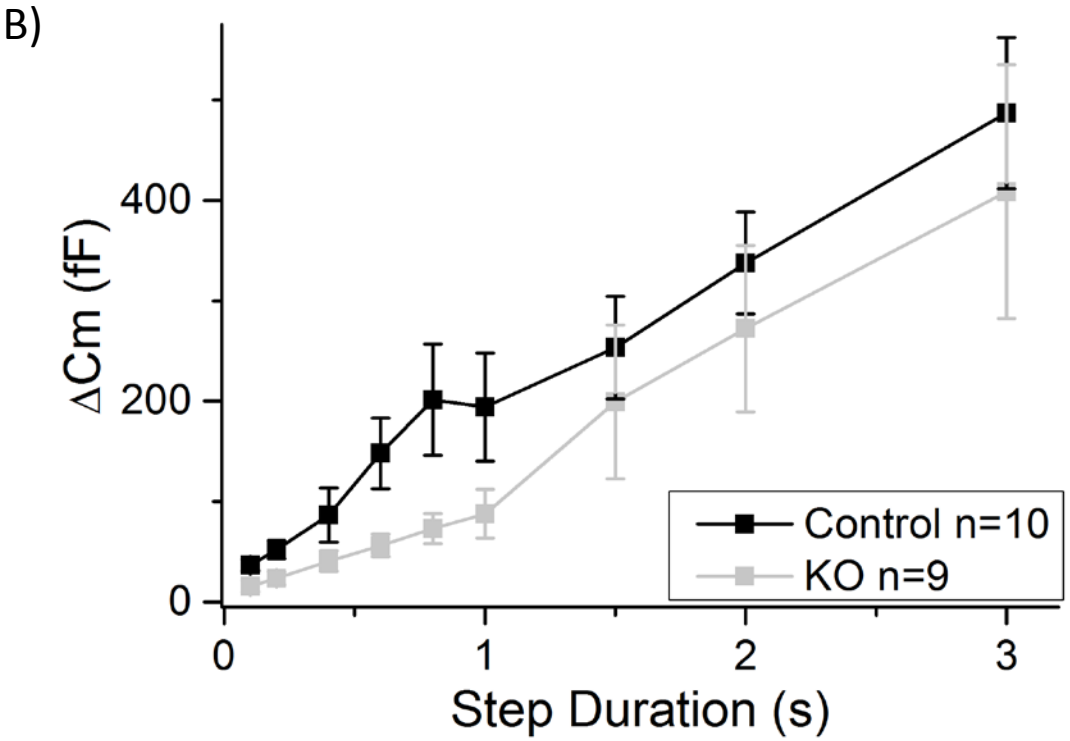
B)
400
200
0
ΔCm (fF)
0
1
2
3
Step Duration (s)
Control n=10
KO n=9

5.3 Discussion:

The expression and function of Cx26 and Cx30 in the cochlea has been studied extensively (Lautermann et al., 1998; Teubner et al., 2003; Cohen-Salmon et al., 2007) due the non-syndromic hearing loss observed in humans carrying genetic mutations in the genes that encode connexin 26 and 30 (Kelsell et al., 1997; Grifa et al., 1999). As connexins are expressed in non-sensory cells in the cochlea (Lautermann et al., 1998), studies have focused on their roles in the stria vascularis and supporting cells of the sensory epithelium, where they have important roles in maintaining the endocochlear potential and mediating intercellular calcium and ATP signalling respectively (Teubner et al., 2003; Cohen-Salmon et al., 2007; Piazza et al., 2007; Anselmi et al., 2008).

As connexin 26 and 30 are not expressed in mammalian IHCs, it is not obvious why deletion of Cx30 and downregulation of Cx26 expression in the supporting cells of Cx30 KO mice leads to larger calcium currents and reduces the exocytotic response of IHCs to depolarising voltage steps. ATP release from connexin hemichannels has been shown to regulate spontaneous developmental activity of IHCs and SGNs prior to the onset of hearing (Tritsch and Bergles, 2010). This “spontaneous” activity has been shown to be important for maturation of the presynaptic machinery at IHC ribbon synapses, particularly during the second postnatal week (Johnson et al., 2013b).

Normally, the expression of calcium channels decreases during the second postnatal week, prior to the onset of hearing (Johnson et al., 2005). This has been linked with maturation of the synaptic machinery and restriction of calcium channels to presynaptic active zones (Zampini et al., 2010; Wong et al., 2014). If calcium channel refinement is affected in IHCs from Cx30 KO mice, extrasynaptic calcium channels may persist beyond the normal onset of hearing.

The reduced availability of vesicles for release from the RRP, suggests that the mechanisms for recruiting and/or docking vesicles at the presynaptic active zone are disrupted by the loss of gap-junction activity in the cochlea of Cx30 KO mice. This is supported by further work from the lab of Professor Fabio Mammano, which

has revealed a reduction in the number of synaptic vesicles tethered to the synaptic ribbons in IHCs from Cx30 KO mice (unpublished). This could be due to a reduction in the expression of key presynaptic molecules, such as vesicle tethers, or priming factors in IHCs from Cx30 KO mice. The expression of these molecules could be linked to maturation of the synaptic machinery during the second postnatal week.

Further work will be needed to determine if the reduced presynaptic function in IHCs from Cx30 KO mice is due to aberrations in spontaneous activity in the developing cochlea, or other mechanisms, such as the loss of endocochlear potential. However it is clear that the exocytotic machinery at the auditory ribbon synapse is severely affected by reduced connexin expression in the cochlea and may be the primary cause of hearing loss in Cx30 KO mice.

Chapter 6 - The Transcriptional Co-activator Wbp2 may Regulate Expression of Key Synaptic Molecules at Auditory Ribbon Synapses.

6.1 Introduction:

Due to the complex structure of the organ of Corti, identifying molecules as specific regulators of synaptic function at auditory ribbon synapses is difficult. This is compounded by the apparent absence of a number of the conventional synaptic molecules that could be used for pull down assays to identify binding partners that form the fusion complex. One solution to this is to knockout specific genes of interest in mice, preventing the expression of molecules with unknown roles, then carry out phenotypic studies to determine the effect of each gene deletion. This approach is being pioneered by the mouse genetics project at the Wellcome Trust Sanger Institute.

The Sanger Institute mouse genetics project aims to identify novel regulators of many systems, including the auditory system, by applying high-throughput screening techniques to novel mouse mutants (White et al., 2013). One strain of mice generated by this project is the Wbp2 mutant (*Wbp2*$^{tm2a(EUCOMM)Wtsi}$), which lacks expression of the WW-domain binding protein 2 (Wbp2).

Wbp2 deletion in mice leads to hearing loss.

Measurements of ABRs are part of the phenotypic screening program used on mice generated by the Sanger Institute mouse genetics project and revealed that Wbp2 mutant (Wbp2 KO) mice had high frequency hearing loss. Further studies to determine the severity of the phenotype revealed that Wbp2 KO mice had normal hearing thresholds at P14, immediately after the onset of hearing, but began to lose high frequency hearing around 4 weeks, progressing to mid-frequency hearing loss by 44 weeks (Buniello et al., Under Revision). The cochlea of Wbp2 KO mice has no obvious gross morphological defects. However preliminary experiments have revealed abnormalities at the ribbon synapses of IHCs, including mislocalised synaptic ribbons, i.e. ribbons are not restricted to the basolateral portion of IHCs in Wbp2 KO, and swollen afferent boutons of type I SGNs.

Wbp2, a transcriptional co-activator.

WW domain binding proteins 1 and 2 (Wbp1 and Wbp2) were discovered by screening mouse embryos for ligands of the WW domain of yes-kinase associated protein (YAP). Wbp1 and 2 show little homology, except in their proline-rich WW binding domain (Chen et al., 1997). Wbp2 has been shown to mediate interactions between YAP and progesterone receptors, enhancing ligand dependent transcriptional activity of both oestrogen and progesterone receptors (Dhananjayan et al., 2006), suggesting it could have a role in regulating the transcription of target genes in signalling pathways, possibly as a co-activator.

Wbp2 has been shown to interact with Yorkie, the drosophila homologue of YAP, and enhance the transcriptional co-activator pathways of Yorkie (Zhang et al., 2011b). Yorkie is a downstream target of the Salvador-warts hippo (SWH) tumour suppressor pathway, implicated in regenerative tissue growth in drosophila. The SWH pathway suppresses activity of Yorkie to limit tissue growth (Grusche et al., 2011). These studies indirectly implicate Wbp2 in tissue growth that is normally supressed by the SWH tumour suppressor. Currently, the role of Wbp2 in normal tissue growth and development is unknown.

Investigating presynaptic function at the auditory ribbon synapse of Wbp2 KO mice.

The likely function of Wbp2 as a transcriptional coactivator suggests it has a role in regulating transcription of certain genes within the cochlea, possibly as part of a receptor mediated transcription pathway. The normal hearing thresholds of P14 Wbp2 KO mice shows it is not required for normal development of the cochlea, or ribbon synapses, but is likely to have a role in maintenance of the synapse after the onset of hearing. It is unclear if the synaptic defects observed in Wbp2 KO mice are due to a loss of the function of Wbp2 within IHCs, or type I SGNs. For example, mislocalised synaptic ribbons within the IHC may lead to defective coupling and signalling to type I SGNs, leading to the swelling of afferent terminals. On the other hand, it is possible that excessive outgrowth of type I SGNs in the absence of Wbp2 leads to afferent terminal swelling, which form mislocalised contacts with IHCs,

attracting functional presynaptic ribbons to active zones outside of the basolateral zone of IHCs.

To determine if Wbp2 deletion has an effect on the function of the presynaptic active zone of ribbon synapses, measurements of calcium currents and changes in membrane capacitance have been carried out on IHCs from Wbp2 KO mice. The Wbp2 KO strain of mice was kindly provided by our collaborator, Professor Karen Steel and maintained on a C57BL/6 background. IHCs from the basal coil of the organ of Corti from control (Wbp2+/+ and Wbp2+/-) and Wbp2 KO (Wbp2-/-) adult (P19-P33) mice were studied. Due to difficulties associated with maintaining cochlea preparations in older mice, it was not possible to assess the presynaptic function of IHCs from mice after the loss of hearing function. No defects were observed in the cochlea of Wbp2+/- mice (Buniello et al., Under Revision) and recordings of IHCs from Wbp2+/- mice were compared to those from Wbp2+/+ mice before pooling control data.

6.2 Results:

6.2.1 Electrical properties of IHCs from control and Wbp2 KO mice:

IHCs from control and Wbp2 KO mice were held in the patch-clamp configuration in near physiological conditions (1.3 mM Ca2+ at 37˚C), at a potential of -81 mV. No significant differences were observed between any of the electrical properties of IHCs from control mice compared to those from Wbp2 KO mice.

Table 6.1: Electrical properties of IHCs from control and Wbp2 KO mice.

Genotype	Rs (MΩ)	Cm (pF)	*I*h (pA)	Rm (MΩ)	gL (nS)	n
control	6.0 ± 0.3	7.2 ± 0.1	-10.7 ± 1.6	1786 ± 117	0.6 ± 0.0	12
KO	5.8 ± 0.2	6.7 ± 0.2	-12.5 ± 3.8	1633 ± 107	0.7 ± 0.1	13

6.2.2: Calcium currents and exocytosis from the ribbon synapse of Wbp2 KO mice.

To elicit calcium influx to trigger vesicle fusion, 50 ms voltage steps to different potentials were applied to basal coil IHCs from adult (P19 – 33) mice in 10 mV increments from a holding potential of -81 mV. As described previously, the peak of the current responses to voltage steps was measured and compared between IHCs from control and Wbp2 KO mice. No significant differences were observed in the maximal amplitude of the calcium current in IHCs from control (-142.2 ± 8.6 pA, n = 7) and Wbp2 KO (-159.2 ± 10.1 pA, n = 8) mice, elicited by a depolarising step to -11 mV (Figure 6.1). The shape of the IV curve generated in response to the different voltage steps was also similar between IHCs from control and Wbp2 KO mice. This suggests IHCs from Wbp2 KO mice express normal numbers of calcium channels in their plasma membrane. The corresponding maximal change in membrane capacitance triggered by the influx of calcium during the voltage step to -11 mV was also similar between IHCs from control (19.0 ± 1.5 fF, n = 7) and Wbp2 KO (18.1 ± 2.0 fF, n = 8) mice (Figure 6.1). These results suggest that exocytosis from the ribbon synapses of adult basal coil IHCs is normal in the absence of Wbp2, including functional synaptic machinery and normal expression of calcium channels at the ribbon synapses.

6.2.3: Vesicle release from the RRP and SRP at the IHC ribbon synapse.

In order to investigate whether the mislocalisation of some of the ribbon synapses of IHCs in Wbp2 KO mice affected the availability of vesicles for release, I investigated the kinetics of exocytosis from the ribbon synapses of IHCs from Wbp2 KO mice. For these experiments, IHCs were held at -81 mV and depolarised to -11 mV for increasing durations between 2 ms and 3 s. Changes in membrane capacitance in response to short (2 – 100 ms: revealing the RRP) and long (100 ms to 3s: revealing the SRP) depolarising steps were found to be similar between IHCs from control and Wbp2 KO mice (Figure 6.2). This suggests that ribbon synapses of IHCs from Wbp2 KO mice have normal numbers of synaptic vesicles in both the RRP and SRP. This indicates that expression and function of the presynaptic machinery for recruitment, priming and release does not require Wbp2.

Figure 6.1: Calcium currents and changes in membrane capacitance of IHCs from control and Wbp2 KO mice in response to voltage steps.

A) Example of the voltage protocol applied to IHCs. A sinusoidal stimulus (37 mV peak to peak at 4 kHz) was applied to cells at a holding potential of -81 mV, which was interrupted for 50ms voltage steps in 10 mV increments (-11 mV in the example).
B) Example of the inward calcium current (top) and corresponding change in membrane capacitance (bottom) of an IHC from a control (black) and a Wbp2 KO (grey) mouse in response to a 50 ms depolarising voltage step (to -11 mV). Each recording displayed is the average trace produced from two recordings from an individual cell.
C) Average peak of the calcium current elicited by applying 50ms voltage steps, in 10 mV increments, to IHCs from control (black, n=7) and Wbp2 KO (grey, n=8) mice (P19 – P33).
D) Average change in membrane capacitance from IHCs of control (black, n = 7) and Wbp2 KO (grey, n = 8) mice (P19 – 33) in response to 50 ms voltage steps in 10 mV increments.

No significant differences were observed between control and Wbp2 KO mutant in either the amplitude of the calcium current or the change in membrane capacitance.

N.B The command voltage for each voltage step was corrected for the voltage drop across the series resistance, and each point has a voltage ± SEM, however the error bars are too small to be seen.

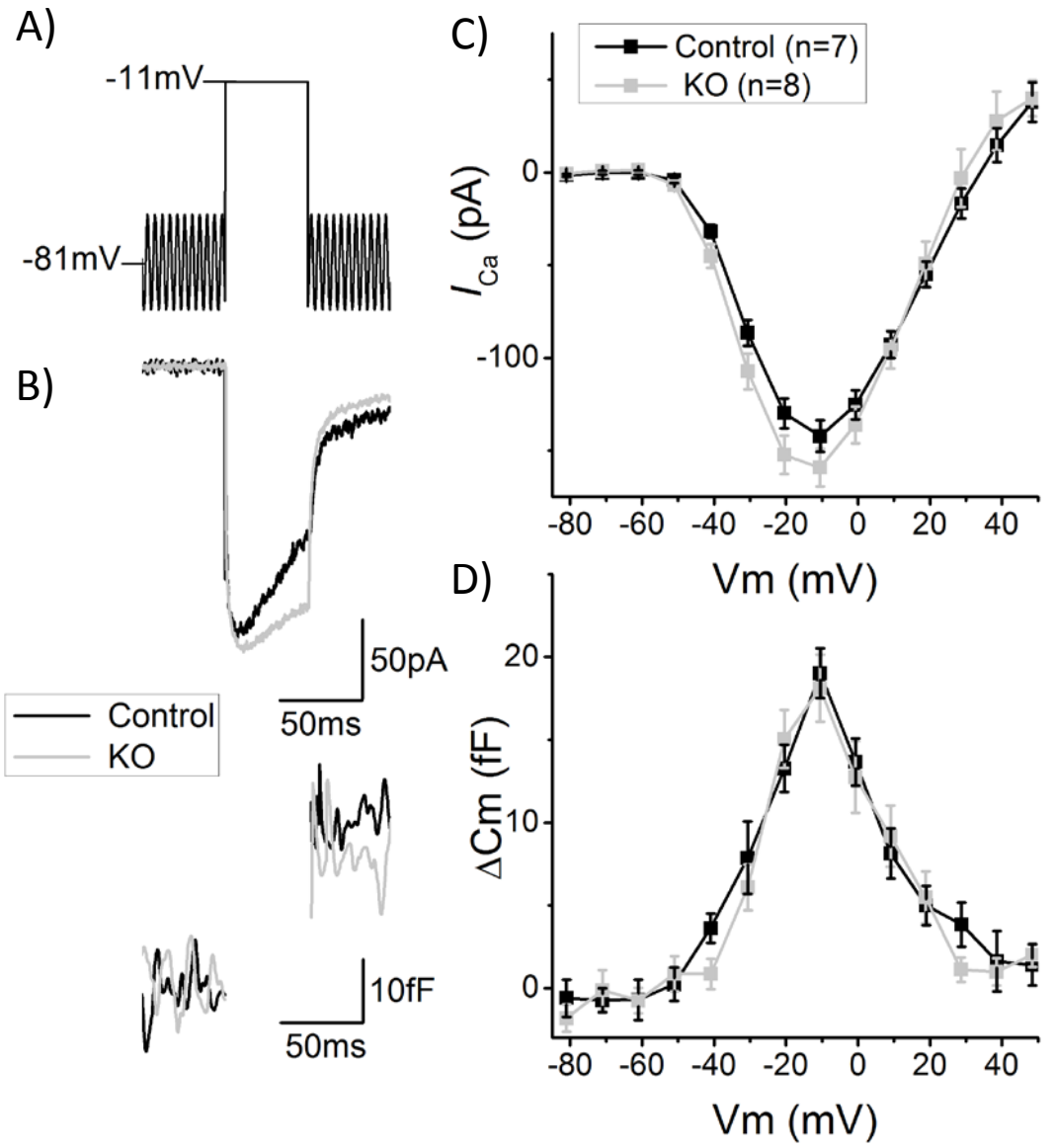
A)
-11mV
-81mV
B)
50pA
50ms
Control
KO
10fF
50ms
C)
Control (n=7)
KO (n=8)
I_{Ca} (pA)
0
-100
-80 -60 -40 -20 0 20 40
Vm (mV)
D)
ΔCm (fF)
20
10
0
-80 -60 -40 -20 0 20 40
Vm (mV)

Figure 6.2: Kinetics of exocytosis in IHCs from Wbp2 KO mice.

A) Average change in membrane capacitance of IHCs from control (black, n = 10) and Wbp2 KO (grey, n = 10) mice (P19 – P33) in response to short (2 – 100 ms) depolarising voltage steps to -11 mV from a holding potential of -81 mV.

B) Average change in membrane capacitance of IHCs from control (black, n = 8) and Wbp2 KO (grey, n = 8) mice (P19 – P33) in response to long (0.1 – 3 s) depolarising voltage steps to -11 mV from a holding potential of -81 mV.

No significant differences were observed between the responses of IHCs from control and Wbp2 KO mice to either short, or long depolarising voltage steps. The RRP and SRP respectively for IHCs from control mice is approximately 10.6 ± 1.5 fF and 269.3 ± 52.5 fF compared to 11.7 ± 1.1 fF and 263.6 ± 25.0 fF for IHCs from Wbp2 KO mice.

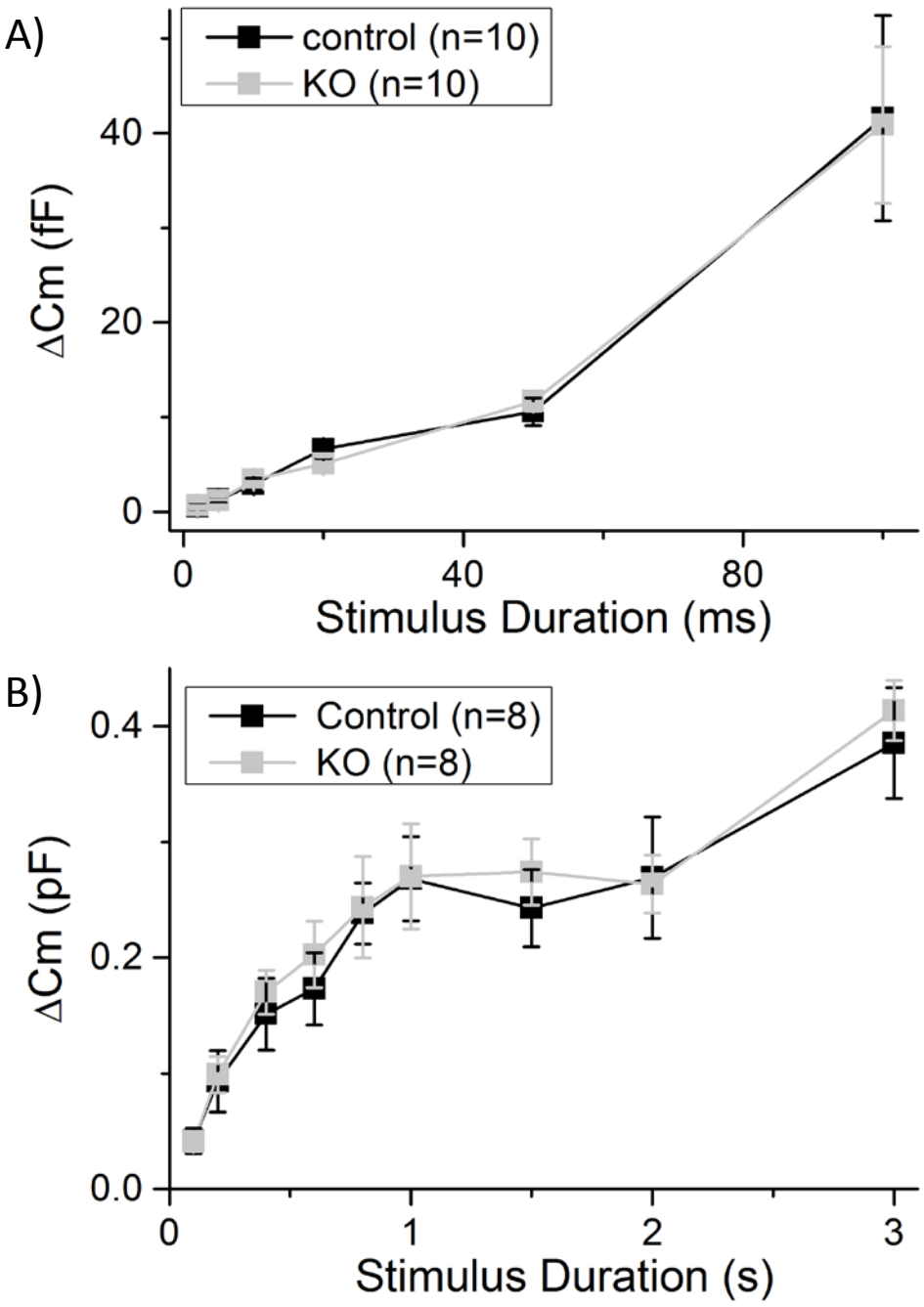
A)
control (n=10)
KO (n=10)
ΔCm (fF)
0
20
40
0
40
80
Stimulus Duration (ms)
B)
Control (n=8)
KO (n=8)
ΔCm (pF)
0.0
0.2
0.4
0
1
2
3
Stimulus Duration (s)

6.3 Discussion:

Wbp2 is a transcriptional co-activator with a novel role in expression of postsynaptic proteins.

The transcriptional co-activator Wbp2 acts in signalling pathways that regulate tissue growth (Zhang et al., 2011a), including the oestrogen receptor mediated transcription pathways (Dhananjayan et al., 2006). Little is known about the expression of Wbp2 and its role during normal development. The hearing loss observed in mice lacking Wbp2 and subsequent discovery of a Chinese child with profound hearing loss carrying mutations in both copies of the Wbp2 gene (Buniello et al., Under Revision) made Wbp2 an exciting candidate for a novel regulator of transcriptional pathways in the auditory system. The lack of any obvious gross morphological defects in the cochlea of Wbp2 KO mice and the normal hearing thresholds immediately after the onset of hearing suggests that the auditory system develops normally in the absence of Wbp2. However from 4 weeks, swelling of the postsynaptic terminals of type I SGNs and mislocalisation of synaptic ribbons can be observed throughout the cochlea of Wbp2 KO mice (Buniello et al., Under Revision). This suggests Wbp2 has a role in regulating the transcription of synaptic proteins, possibly after the onset of hearing; either in presynaptic IHCs, or postsynaptic SGNs.

We have provided evidence that shows Wbp2 is unlikely to be involved in the transcription of molecules essential for presynaptic function in IHCs. This suggests that Wbp2 is involved in transcription of molecules essential for formation, or maintenance of the afferent boutons of type I SGNs. Further work from the lab of Professor Karen Steel has revealed that the receptors for oestrogen and progesterone are down-regulated in the cochlea of 4-week old Wbp2 KO mice (Buniello et al., Under Revision). Oestrogen receptors are known to be expressed at the postsynaptic densities of glutamatergic synapses in the hippocampus (Adams and Morrison, 2003), where their activation has been shown to increase expression of key postsynaptic proteins; notably glutamate receptor subunits and the postsynaptic scaffold protein PSD-95 (Liu et al., 2008). Surprisingly, despite

decreased expression of oestrogen and progesterone receptors, expression of PSD-95 was significantly increased in the cochlea of Wbp2 KO mice (Buniello et al., Under Revision).

This suggests that the loss of Wbp2 leads to changes in the oestrogen and/or progesterone receptor mediated transcription in type I SGNs, including increased expression of PSD-95. Ultimately this leads to the excessive outgrowth (and swelling) of the afferent nerve terminals of type I SGNs and mislocalisation of the contacts they form with IHCs. The contacts of SGNs that lie outside of the basolateral region of the IHC may then “attract” presynaptic ribbons and synaptic machinery, leading to mislocalised, but functional presynaptic ribbons and active zones in the IHCs of Wbp2 KO mice.

Chapter 7 – Discussion.

7.1 Summary:

In this thesis, I have presented the results of electrophysiological investigations into the presynaptic function at the auditory ribbon synapse. I have attempted to identify novel molecular regulators of the synaptic machinery by recording the calcium currents and changes in membrane capacitance of IHCs from mice lacking a molecule of interest.

First, I have shown that deletion of the calcium sensor DOC2B has no discernible effect on exocytosis from IHCs, suggesting that unlike in neurons and secretory cells DOC2B has no role in fast, synchronous exocytosis in IHCs. These findings have demonstrated that this apparently ubiquitously expressed calcium sensor (Kojima et al., 1996) is not a regulator of vesicle fusion, priming or replenishment at auditory ribbon synapses.

I have also demonstrated that despite hearing loss and hair cell death in the cochlea of mice lacking the inositol-5'-phosphatase activity of SynJ2 (Manji et al., 2011), deletion of SynJ2 has no discernible effect on the physiology of mature hair cells in the high frequency region of the cochlea. SynJ2 is reported to regulate the formation of clathrin coated pits (Rusk et al., 2003), however internalisation of vesicle membranes and vesicle recycling appear normal in IHCs from SynJ2 KO mice. This suggests that SynJ2 may have a previously unidentified role in IHCs, possibly regulating the sorting of internalised cargo, or non-synaptic endocytosis. It is also possible that SynJ2 is expressed in non-sensory supporting cells in the cochlea. Loss of SynJ2 activity may affect the release of neurotrophic factors from supporting cells such as phalangeal cells and Deiters cells, which are essential for sensory hair cell survival (Sobkowicz et al., 2002).

In the cochlea of mice lacking Cx30 and with diminished expression of Cx26, IHCs have a larger calcium current and decreased exocytotic response to short depolarising steps, suggesting that the RRP of synaptic vesicles is reduced, despite normal numbers of vesicles present in the SRP. This demonstrates that loss of connexins prevents efficient function of the presynaptic machinery at the auditory ribbon synapse. These results suggest that connexin-based activity in the

supporting cells (Piazza et al., 2007) regulates development of presynaptic machinery in IHCs, revealing an indirect consequence of loss of connexins in the cochlea.

Finally, I have shown that Wbp2 deletion has no effect on exocytosis from the ribbon synapses of IHCs, despite the mislocalisation of synaptic ribbons and observed swelling of afferent terminals, demonstrating that Wbp2 is unlikely to be involved in regulation of transcription within IHCs. This led to further investigations that revealed the increased expression of postsynaptic proteins in the cochlea of Wbp2 KO mice and the decreased expression of the oestrogen and progesterone hormone receptors. Therefore, hormone receptor signalling mediated by Wbp2 appears to regulate transcriptional activity within type I SGNs and is important for the maintenance of adult ribbon synapses.

7.2 Future work:

The studies presented in this thesis have provided important insights into the regulation of ribbon synaptic function. However a number of questions regarding the role of these molecules remain, as well as questions regarding the general function of auditory ribbon synapses.

A novel role for SynJ2 in auditory hair cells.

Currently it is unclear why the loss of the phosphatase activity of SynJ2 leads to hair cell death and hearing loss (Manji et al., 2011). Using immunohistochemistry to determine the precise location of SynJ2 within the cochlea may provide more insight into its role. However suitable quality antibodies for SynJ2 have yet to be developed. Transmission electron microscopy (TEM) could also be used to investigate the ultrastructure of the cochlea in SynJ2 KO mice. If SynJ2 is responsible for sorting of synaptic components, similar to the role of SynJ1 in the retina (George et al., 2014), then TEM may reveal aberrations in these structures within IHCs from SynJ2 KO mice. While we would expect such aberrations to affect the recordings of membrane capacitance changes (Figure 4.5), it is possible that they affect cellular compartments not involved in the supply of synaptic vesicles. A

series of electron micrographs of the cochlea, taken at different ages would also reveal the progression of hair cell degeneration.

Alternatively, if SynJ2 is expressed in non-sensory cells, it may regulate CME in these cells. TEM studies may also help to determine if SynJ2 deletion leads to defects in CME in supporting cells, such as phalangeal cells, or Deiters cells.

Connexins in development of the cochlea.

As connexin gap junctions and hemichannels appear to have a role in calcium and ATP signalling within the prehearing cochlea, it seems likely that the loss of presynaptic function observed in IHCs (Figure 5.1) is due to abnormal development of the presynaptic machinery. This could be due to inefficient propagation of calcium waves in the developing cochlea (Piazza et al., 2007), which may regulate sensory independent activity of IHCs (Tritsch and Bergles, 2010). The dysregulation of sensory independent activity of IHCs in the cochlea, particularly during the critical period for synaptic development (second postnatal week) (Johnson et al., 2013b) may prevent expression, or maturation of the synaptic machinery in IHCs from Cx30 KO mice. It would be interesting to ascertain if the expression of calcium channels and synaptic machinery is normal in developing IHCs from Cx30 KO mice; this could be established by measuring calcium currents and membrane capacitance changes before the “critical period” of synaptic maturation (approximately P5).

Another question raised from this study is, if the SRP contains normal numbers of synaptic vesicles, why is the RRP so greatly diminished? Could this be due to a failure in vesicle tethering at the ribbons; or a failure to replenish the RRP? The vesicles are likely to be tethered by cytomatrix protein piccolo, possibly via interactions with bassoon, CtBP1, or Ribeye (Uthaiah and Hudspeth, 2010; Kantardzhieva et al., 2012). Using western blotting, or qPCR to analyse the expression levels of these cytomatrix proteins in the cochlea of Cx30 KO mice may determine if they are required for vesicle tethering at auditory ribbon synapses and if their expression is required for maturation of the synaptic machinery.

Another molecule suggested to have a role in vesicle pool replenishment is otoferlin (Pangrsic et al., 2010); it is possible that one of the consequences of the developmental failure of IHCs is a failure to develop efficient otoferlin dependent mechanisms for the replenishment of synaptic vesicles. Looking at otoferlin expression and localisation within IHCs from Cx30 KO mice may provide some insight into why the RRP is so diminished.

The sensitivity of high-frequency hair cells to hearing loss.

Two of the chapters in this study have focused on mice that show progressive hearing loss after deletion of a specific molecule; SynJ2 and Wbp2. In both cases, high frequency hearing (>36 kHz) deteriorates by 4 weeks, before progressive loss of lower frequency hearing. In the case of Wbp2 KO mice, swelling of afferent terminals is observed in both high and low frequency regions of the cochlea of 4 week old mice, while auditory thresholds at low frequencies (6-12 kHz) are normal until at least 44 weeks (Buniello et al., Under Revision). High-frequency hearing in humans is also particularly sensitive to noise-induced and age-related hearing loss (Gratton and Vazquez, 2003). Determining why high-frequency hearing is so much more sensitive to damage may help clinicians protect vulnerable individuals from hearing loss and potentially pave the way for future treatments.

Sensory hair cells in different frequency regions of the cochlea have been shown to display some physiological differences, such as the calcium-dependency of exocytosis (Johnson et al., 2008) and the number of ribbon synapses (Meyer et al., 2009). It is possible that these physiological differences make hair cells in the high frequency region more sensitive to stresses and ageing. These differences could be characterised using electrophysiology, which may reveal differences in the number, or regulation of ion channels. Alternatively, using qPCR to analyse gene expression in IHCs isolated from the different regions of the cochlea with laser capture microdissection (EmmertBuck et al., 1996), may reveal differences in the molecules expressed in IHCs from different regions of the cochlea. Determining why high-frequency hair cells are more sensitive to damage may help clinicians protect these

cells in individuals vulnerable to hearing loss and potentially pave the way for future treatments.

The synaptic ribbon.

One of the most obvious, yet most controversial questions regarding the ribbon synapse is the function of the ribbon itself. Early researchers proposed that the ribbon acted as a conveyor belt, driving vesicles towards the presynaptic active zone to rapidly replenish the RRP (Parsons and Sterling, 2003). IHCs with a loss of anchored ribbons show a marked reduction in the calcium current and exocytotic response to short (<50 ms) stimuli. However these IHCs display a normal exocytotic response to longer (50 ms) stimuli (Khimich et al., 2005). The authors use this evidence to suggest that the ribbon is important for fast, synchronous release of synaptic vesicles. However the mutated protein, bassoon, is a cytomatrix protein thought to be important for organisation of presynaptic active zones and later work, has suggested that it is the bassoon mutation, not the loss of ribbons that leads to the reduced exocytotic response from IHCs (Jing et al., 2013). Modelling of hair cell ribbon synapses has suggested that the ribbon increases the number of vesicles available for release, improving efficiency of postsynaptic spike generation by reducing spike latency during sustained stimuli (Wittig and Parsons, 2008). Similar modelling studies of ribbon synapses in rod bipolar cells of the retina have suggested that passive diffusion of tethered vesicles can account for maintaining an efficient supply of synaptic vesicles to release sites (Graydon et al., 2014). Determining the role of presynaptic ribbons in both the auditory and visual systems is crucial to understanding the physiological functions of ribbon synapses.

Identifying the full molecular profile of ribbon synapses may help to determine if the ribbons act passively as tethering sites for synaptic vesicles, or if they actively drive vesicles towards the presynaptic active zones. Knocking out candidate molecules for the different elements of the synaptic machinery can provide insight into the function of these molecules. However it can be difficult to determine if the effect seen is due to the loss of the specific molecule, or regulation of a downstream process; for example Rab3-interacting molecules (RIMs) have been

suggested to be vesicle tethers at photoreceptor ribbon synapses (Dieck et al., 2005), but have recently been shown to regulate calcium channel clustering and tethering by other molecules at the auditory ribbon synapse (Jung et al., 2015). An alternative technique for identifying synaptic molecules is isolating the synapses of interest by centrifugation of homogenised tissue samples using centrifugation, and then identifying the molecules found in the synaptic fraction, e.g. by western blotting. This technique was carried out on lysates of cochleae from chickens (Uthaiah and Hudspeth, 2010) and identified a number of synaptic molecules likely to be expressed at auditory ribbon synapses. However, some of the molecules identified in the synaptic fraction – notably SNARE proteins – have since been shown to be dispensable for presynaptic function in IHCs (Nouvian et al., 2011). This suggests that either SNARE proteins are expressed, but not required at auditory ribbon synapses, or that SNARE proteins from non-ribbon presynaptic active zones were identified, e.g. from the presynaptic terminals of olivocochlear efferents (Simmons et al., 1996).

Auditory thresholds for ribbon synapses.

Another interesting question regarding auditory ribbon synapses is how the differences in threshold and spontaneous rate of different SGNs are established? Are they due to intrinsic differences between the SGNs? Or differences in the ribbon synapses they receive input from? There is evidence for morphological differences both pre and post-synaptically, from the sizes of ribbons and postsynaptic AMPA receptor patches (Liberman et al., 2011) to differences in the diameter of SGNs (Liberman, 1980). However the impact of these differences on sound encoding by hair cells and SGNs is unclear. A simple model for sound encoding could be that as each hair cell responds to a characteristic frequency, each ribbon synapse within an IHC responds to a given threshold; i.e. low intensity sound stimulus only partially depolarises the IHC, which only triggers vesicle fusion at ribbon synapses on the pillar side of the IHC, leading to changes in the spike rate of large diameter, high-spontaneous rate fibres that form synapses here. While simple, this model relies on a single IHC being able to release neurotransmitters from different synapses depending on the level of the stimulus intensity the IHC

receives. To test for differences in neurotransmitter release from the different ribbon synapses, electrophysiological recordings from the postsynaptic boutons of afferent fibres, combined with recordings from the presynaptic IHC may reveal differences in the synaptic output of the different ribbon synapses. By depolarising IHCs to different levels, reflecting differences in the intensity of an auditory signal, it may be possible to determine if the different active zones within an IHC have different thresholds for neurotransmitter release.

7.3 Conclusions:

I have investigated a number of molecules as possible novel regulators of the auditory ribbon synapse in the mammalian cochlea. I have shown that the ubiquitous DOC2B is not required for fast, synchronous exocytosis at the auditory ribbon synapse. I have also provided evidence demonstrating that SynJ2 is not required for CME, or vesicle recycling at the auditory ribbon synapse. Investigations of exocytosis at the auditory ribbon synapses of IHCs from mice with reduced expression of connexins 30 and 26 in the cochlea have revealed dramatic consequences of a loss of gap-junctional activity on presynaptic function at the auditory ribbon synapse. Finally I have shown that Wbp2 deletion does not impair the presynaptic function of IHCs, showing it is not required for transcription of molecules essential for presynaptic function. This study has demonstrated the difficulties involved in advancing our understanding of this complex and unique synapse. Discovering the molecules that regulate vesicle priming, fusion, reuptake and recycling will vastly improve our understanding of how these synapses maintain the fidelity of auditory stimuli over long periods of stimulation.

References

Adams MM, Morrison JH (2003) Estrogen and the aging hippocampal synapse. Cerebral Cortex 13:1271-1275.

Akeroyd MA (2014) An overview of the major phenomena of the localization of sound sources by normal-hearing, hearing-impaired, and aided listeners. Trends in Hearing 18.

Allwardt BA, Lall AB, Brockerhoff SE, Dowling JE (2001) Synapse formation is arrested in retinal photoreceptors of the zebrafish nrc mutant. Journal of Neuroscience 21:2330-2342.

Anselmi F, Hernandez VH, Crispino G, Seydel A, Ortolano S, Roper SD, Kessaris N, Richardson W, Rickheit G, Filippov MA, Monyer H, Mammano F (2008) ATP release through connexin hemichannels and gap junction transfer of second messengers propagate Ca(2+) signals across the inner ear. Proceedings of the National Academy of Sciences of the United States of America 105:18770-18775.

Balla T (2013) Phosphoinositides: Tiny lipids with giant impact on cell regulation. Physiological Reviews 93:1019-1137.

Barlow HB (1953) Summation and inhibition in the frogs retina. Journal of Physiology-London 119:69-88.

Becher A, Drenckhahn A, Pahner I, Margittai M, Jahn R, Ahnert-Hilger G (1999) The synaptophysin-synaptobrevin complex: a hallmark of synaptic vesicle maturation. Journal of Neuroscience 19:1922-1931.

Beurg M, Michalski N, Safieddine S, Bouleau Y, Schneggenburger R, Chapman ER, Petit C, Dulon D (2010) Control of exocytosis by synaptotagmins and otoferlin in auditory hair cells. Journal of Neuroscience 30:13281-13290.

Billcliff PG, Lowe M (2014) Inositol lipid phosphatases in membrane trafficking and human disease. Biochemical Journal 461:159-175.

Blankenship AG, Feller MB (2010) Mechanisms underlying spontaneous patterned activity in developing neural circuits. Nature Reviews Neuroscience 11:18-29.

Boulay A-C, del Castillo FJ, Giraudet F, Hamard G, Giaume C, Petit C, Avan P, Cohen-Salmon M (2013) Hearing is normal without connexin30. Journal of Neuroscience 33:430-434.

Brandt A, Striessnig J, Moser T (2003) Ca(V)1.3 channels are essential for development and presynaptic activity of cochlear inner hair cells. Journal of Neuroscience 23:10832-10840.

Brandt A, Khimich D, Moser T (2005) Few Ca(V)1.3 channels regulate the exocytosis of a synaptic vesicle at the hair cell ribbon synapse. Journal of Neuroscience 25:11577-11585.

Brown MC, Ledwith JV (1990) Projections of thin (type-II) and thick (type-I) auditory-nerve fibers into the cochlear nucleus of the mouse. Hearing Research 49:105-118.

Brownell WE, Bader CR, Bertrand D, Deribaupierre Y (1985) Evoked mechanical responses of isolated cochlear outer hair cells. Science 227:194-196.

Buniello A, Ingham N, Huma A, Martinez-Vega R, Lewis M, Houston O, Bardhan T, Johnson S, Varela-Nieto I, Yuan H, White J, Marcotti W, Steel K (Under Revision) WBP2 controls the expression of key post-synaptic proteins of inner hair cell synapses and is crucial for hearing in mice and humans. EMBO Journal.

Cabezudo LM (1978) Ultrastructure of basilar-membrane in cat. Acta Oto-Laryngologica 86:160-175.

Carabelli V, Hernandez-Guijo JM, Baldelli P, Carbone E (2001) Direct autocrine inhibition and cAMP-dependent potentiation of single L-type Ca2+ channels in bovine chromaffin cells. Journal of Physiology-London 532:73-90.

Chapman ER (2002) Synaptotagmin: A Ca2+ sensor that triggers exocytosis? Nature Reviews Molecular Cell Biology 3:498-508.

Chapman ER (2008) How does synaptotagmin trigger neurotransmitter release? In: Annual Review of Biochemistry, pp 615-641.

Chen HI, Einbond A, Kwak SJ, Linn H, Koepf E, Peterson S, Kelly JW, Sudol M (1997) Characterization of the WW domain of human yes-associated protein and its polyproline-containing ligands. Journal of Biological Chemistry 272:17070-17077.

Choi SY, Borghuis B, Rea R, Levitan ES, Sterling P, Kramer RH (2005) Encoding light intensity by the cone photoreceptor synapse. Neuron 48:555-562.

Clause A, Kim G, Sonntag M, Weisz CJC, Vetter DE, Rubsamen R, Kandler K (2014) The precise temporal pattern of prehearing spontaneous activity is necessary for tonotopic map refinement. Neuron 82:822-835.

Cohen-Salmon M, Regnault B, Cayet N, Caille D, Demuth K, Hardelin J-P, Janel N, Meda P, Petit C (2007) Connexin30 deficiency causes instrastrial fluid-blood barrier disruption within the cochlear stria vascularis. Proceedings of the National Academy of Sciences of the United States of America 104:6229-6234.

Corey DP, Hudspeth AJ (1983) Kinetics of the receptor current in bullfrog saccular hair cells. Journal of Neuroscience 3:962-976.

Cremona O, Di Paolo G, Wenk MR, Luthi A, Kim WT, Takei K, Daniell L, Nemoto Y, Shears SB, Flavell RA, McCormick DA, De Camilli P (1999) Essential role of phosphoinositide metabolism in synaptic vesicle recycling. Cell 99:179-188.

Dallos P, Fay R (1996) The cochlea. Springer Handbook of Auditory Research 8:i-xii, 1-551.

del Castillo FJ, del Castillo I (2011) The DFNB1 subtype of autosomal recessive non-syndromic hearing impairment. Frontiers in Bioscience-Landmark 16:3252-3274.

Derosier DJ, Tilney LG (1989) The structure of the cuticular plate, an invivo actin gel. Journal of Cell Biology 109:2853-2867.

Dhananjayan SC, Ramamoorthy S, Khan OY, Ismail A, Sun J, Slingerland J, O'Malley BW, Nawaz Z (2006) WW domain binding protein-2, an E6-associated protein interacting protein, acts as a coactivator of estrogen and progesterone receptors. Molecular Endocrinology 20:2343-2354.

Di Paolo G, De Camilli P (2006) Phosphoinositides in cell regulation and membrane dynamics. Nature 443:651-657.

Dick O, Dieck ST, Altrock WD, Ammermuller J, Weiler R, Garner CC, Gundelfinger ED, Brandstatter JH (2003) The presynaptic active zone protein bassoon is essential for photoreceptor ribbon synapse formation in the retina. Neuron 37:775-786.

Dieck S, Altrock WD, Kessels MM, Qualmann B, Regus H, Brauner D, Fejtova A, Bracko O, Gundelfinger ED, Brandstatter JH (2005) Molecular dissection of the photoreceptor ribbon synapse: physical interaction of Bassoon and RIBEYE is essential for the assembly of the ribbon complex. The Journal of cell biology 168:825-836.

Duncker SV, Franz C, Kuhn S, Schulte U, Campanelli D, Brandt N, Hirt B, Fakler B, Blin N, Ruth P, Engel J, Marcotti W, Zimmermann U, Knipper M (2013) Otoferlin couples to clathrin-mediated endocytosis in mature cochlear inner hair cells. Journal of Neuroscience 33:9508-9519.

Eatock RA (2006) Vertebrate Hair Cells. Vertebrate Hair Cells 27.

Echteler SM (1992) Developmental segregation in the afferent-projections to mammalian auditory hair-cells. Proceedings of the National Academy of Sciences of the United States of America 89:6324-6327.

Echteler SM, Fay RR, Popper AN (1994) Structure of the mammalian cochlea. Springer Handbook of Auditory Research 4:134-171.

Edelmann L, Hanson PI, Chapman ER, Jahn R (1995) Synaptobrevin binding to synaptophysin - a potential mechanism for controlling the exocytotic fusion machine. Embo Journal 14:224-231.

EmmertBuck MR, Bonner RF, Smith PD, Chuaqui RF, Zhuang ZP, Goldstein SR, Weiss RA, Liotta LA (1996) Laser capture microdissection. Science 274:998-1001.

Euler T, Haverkamp S, Schubert T, Baden T (2014) Retinal bipolar cells: elementary building blocks of vision. Nature Reviews Neuroscience 15:507-519.

Fay RR, Popper AN (1994) Comparative hearing: mammals. Springer Handbook of Auditory Research 4:i-xi, 1-260.

Fettiplace R, Hackney CM (2006) The sensory and motor roles of auditory hair cells. Nature Reviews Neuroscience 7:19-29.

Fettiplace R, Kim KX (2014) The physiology of mechanoelectrical transduction channels in hearing. Physiological Reviews 94:951-986.

Flock A, Cheung HC (1977) Actin filaments in sensory hairs of inner-ear receptor cells. Journal of Cell Biology 75:339-343.

Frank T, Rutherford MA, Strenzke N, Neef A, Pangrsic T, Khimich D, Fetjova A, Gundelfinger ED, Liberman MC, Harke B, Bryan KE, Lee A, Egner A, Riedel D, Moser T (2010) Bassoon and the synaptic ribbon organize Ca2+ channels and vesicles to add release sites and promote refilling. Neuron 68:724-738.

Friedrich R, Groffen AJ, Connell E, van Weering JRT, Gutman O, Henis YI, Davletov B, Ashery U (2008) DOC2B acts as a calcium switch and enhances vesicle fusion. Journal of Neuroscience 28:6794-6806.

Fuchs M, Brandstaetter JH, Regus-Leidig H (2014) Evidence for a Clathrin-independent mode of endocytosis at a continuously active sensory synapse. Frontiers in Cellular Neuroscience 8.

Fuchs PA (1996) Synaptic transmission at vertebrate hair cells. Current Opinion in Neurobiology 6:514-519.

Furness DN, Hackney CM (2006) The structure and composition of the stereociliary bundle of vertebrate hair cells. Vertebrate Hair Cells 27:95-153.

Galambos R, Davis H (1943) The response of single auditory-nerve fibers to acoustic stimulation. Journal of Neurophysiology 6:39-57.

Gale JE, Piazza V, Ciubotaru CD, Mammano F (2004) A mechanism for sensing noise damage in the inner ear. Current Biology 14:526-529.

George AA, Hayden S, Holzhausen LC, Ma EY, Suzuki SC, Brockerhoff SE (2014) Synaptojanin 1 is required for endolysosomal trafficking of synaptic proteins in cone photoreceptor inner segments. Plos One 9.

Glowatzki E, Fuchs PA (2000) Cholinergic synaptic inhibition of inner hair cells in the neonatal mammalian cochlea. Science 288:2366-2368.

Glowatzki E, Fuchs PA (2002) Transmitter release at the hair cell ribbon synapse. Nature Neuroscience 5:147-154.

Goutman JD, Glowatzki E (2007) Time course and calcium dependence of transmitter release at a single ribbon synapse. Proceedings of the National Academy of Sciences of the United States of America 104:16341-16346.

Gratton MA, Vazquez AE (2003) Age-related hearing loss: current research. Current opinion in otolaryngology & head and neck surgery 11:367-371.

Graydon CW, Zhang J, Oesch NW, Sousa AA, Leapman RD, Diamond JS (2014) Passive diffusion as a mechanism underlying ribbon synapse vesicle release and resupply. Journal of Neuroscience 34:8948-8962.

Griesinger CB, Richards CD, Ashmore JF (2002) FM1-43 reveals membrane recycling in adult inner hair cells of the mammalian cochlea. Journal of Neuroscience 22:3939-3952.

Griesinger CB, Richards CD, Ashmore JF (2005) Fast vesicle replenishment allows indefatigable signalling at the first auditory synapse. Nature 435:212-215.

Grifa A, Wagner CA, D'Ambrosio L, Melchionda S, Bernardi F, Lopez-Bigas N, Rabionet R, Arbones M, Della Monica M, Estivill X, Zelante L, Lang F, Gasparini P (1999) Mutations in GJB6 cause nonsyndromic autosomal dominant deafness at DFNA3 locus. Nature Genetics 23:16-18.

Groffen AJ, Martens S, Arazola RD, Cornelisse LN, Lozovaya N, de Jong APH, Goriounova NA, Habets RLP, Takai Y, Borst JG, Brose N, McMahon HT, Verhage M (2010) Doc2b is a high-affinity Ca2+ sensor for spontaneous neurotransmitter release. Science 327:1614-1618.

Groffen AJA, Friedrich R, Brian EC, Ashery U, Verhage M (2006) DOC2A and DOC2B are sensors for neuronal activity with unique calcium-dependent and kinetic properties. Journal of Neurochemistry 97:818-833.

Groffen AJA, Brian EC, Dudok JJ, Kampmeijer J, Toonen RF, Verhage M (2004) Ca2+-induced recruitment of the secretory vesicle protein DOC2B to the target membrane. Journal of Biological Chemistry 279:23740-23747.

Grusche FA, Degoutin JL, Richardson HE, Harvey KF (2011) The Salvador/Warts/Hippo pathway controls regenerative tissue growth in Drosophila melanogaster. Developmental Biology 350:255-266.

Guild SR (1927) The width of the basilar membrane. Science 65:67-69.

Gundersen CB, Umbach JA (2013) Synaptotagmins 1 and 2 as mediators of rapid exocytosis at nerve terminals: The dyad hypothesis. Journal of Theoretical Biology 332:149-160.

Guo SL, Stolz LE, Lemrow SM, York JD (1999) SAC1-like domains of yeast SAC1, INP52, and INP53 and of human synaptojanin encode polyphosphoinositide phosphatases. Journal of Biological Chemistry 274:12990-12995.

Haffner C, Takei K, Chen H, Ringstad N, Hudson A, Butler MH, Salcini AE, Di Fiore PP, De Camilli P (1997) Synaptojanin 1: localization on coated endocytic intermediates in nerve terminals and interaction of its 170 kDa isoform with Eps15. FEBS Lett 419:175-180.

Hallermann S, Fejtova A, Schmidt H, Weyhersmuller A, Silver RA, Gundelfinger ED, Eilers J (2010) Bassoon speeds vesicle reloading at a central excitatory synapse. Neuron 68:710-723.

Hamill OP, Marty A, Neher E, Sakmann B, Sigworth FJ (1981) Improved patch-clamp techniques for high-resolution current recording from cells and cell-free membrane patches. Pflugers Archiv-European Journal of Physiology 391:85-100.

Heidelberger R (1998) Adenosine triphosphate and the late steps in calcium-dependent exocytosis at a ribbon synapse. Journal of General Physiology 111:225-241.

Heidrych P, Zimmermann U, Kuhn S, Franz C, Engel J, Duncker SV, Hirt B, Pusch CM, Ruth P, Pfister M, Marcotti W, Blin N, Knipper M (2009) Otoferlin interacts with myosin VI: implications for maintenance of the basolateral synaptic structure of the inner hair cell. Human Molecular Genetics 18:2779-2790.

Heil P, Neubauer H (2010) Summing across different active zones can explain the quasi-linear Ca-dependencies of exocytosis by receptor cells. Frontiers in synaptic neuroscience 2:148-148.

Heil P, Neubauer H, Irvine DRF, Brown M (2007) Spontaneous activity of auditory-nerve fibers: Insights into Stochastic processes at ribbon synapses. Journal of Neuroscience 27:8457-8474.

Heuser JE, Reese TS (1973) Evidence for recycling of synaptic vesicle membrane during transmitter release at frog neuromuscular junction. Journal of Cell Biology 57:315-344.

Hibino H, Nin F, Tsuzuki C, Kurachi Y (2010) How is the highly positive endocochlear potential formed? The specific architecture of the stria vascularis and the roles of the ion-transport apparatus. Pflugers Archiv-European Journal of Physiology 459:521-533.

Holley M (2000) Hearing - Tuning in with motor proteins. Nature 405:130-133.

Hori T, Takai Y, Takahashi T (1999) Presynaptic mechanism for phorbol ester-induced synaptic potentiation. Journal of Neuroscience 19:7262-7267.

Horowitz P, Hill W (1980) The art of electronics, First Edition: Cambridge University Press.

Huang L-C, Barclay M, Lee K, Peter S, Housley GD, Thorne PR, Montgomery JM (2012) Synaptic profiles during neurite extension, refinement and retraction in the developing cochlea. Neural Development 7.

Hudspeth AJ (2014) Integrating the active process of hair cells with cochlear function. Nat Rev Neurosci 15:600-614.

Hudspeth AJ, Corey DP (1977) Sensitivity, polarity and conductance change in response of vertebrate hair cells to controlled mechanical stimuli. Proceedings of the National Academy of Sciences of the United States of America 74:2407-2411.

Hui E, Johnson CP, Yao J, Dunning FM, Chapman ER (2009) Synaptotagmin-mediated bending of the target membrane is a critical step in Ca2+-regulated fusion. Cell 138:709-721.

Ito M, Spicer SS, Schulte BA (1995) Cytological changes related to maturation of the organ of Corti and opening of Cortis tunnel. Hearing Research 88:107-123.

Jackman SL, Choi S-Y, Thoreson WB, Rabl K, Bartoletti TM, Kramer RH (2009) Role of the synaptic ribbon in transmitting the cone light response. Nature Neuroscience 12:303-310.

Jaffe LA, Hagiwara S, Kado RT (1978) Time course of cortical vesicle fusion in sea-urchin eggs observed as membrane capacitance changes. Developmental Biology 67:243-248.

Jing ZZ, Rutherford MA, Takago H, Frank T, Fejtova A, Khimich D, Moser T, Strenzke N (2013) Disruption of the presynaptic cytomatrix protein bassoon degrades ribbon anchorage, multiquantal release, and sound encoding at the hair cell afferent synapse. Journal of Neuroscience 33:4456-4467.

Johnson SL, Thomas MV, Kros CJ (2002) Membrane capacitance measurement using patch clamp with integrated self-balancing lock-in amplifier. Pflugers Archiv-European Journal of Physiology 443:653-663.

Johnson SL, Marcotti W, Kros CJ (2005) Increase in efficiency and reduction in Ca2+ dependence of exocytosis during development of mouse inner hair cells. Journal of Physiology-London 563:177-191.

Johnson SL, Adelman JP, Marcotti W (2007) Genetic deletion of SK2 channels in mouse inner hair cells prevents the developmental linearization in the Ca2+ dependence of exocytosis. Journal of Physiology-London 583:631-646.

Johnson SL, Forge A, Knipper M, Munker S, Marcotti W (2008) Tonotopic variation in the calcium dependence of neurotransmitter release and vesicle pool replenishment at mammalian auditory ribbon synapses. Journal of Neuroscience 28:7670-7678.

Johnson SL, Kennedy HJ, Holley MC, Fettiplace R, Marcotti W (2012) The resting transducer current drives spontaneous activity in prehearing mammalian cochlear inner hair cells. Journal of Neuroscience 32:10479-10483.

Johnson SL, Wedemeyer C, Vetter DE, Adachi R, Holley MC, Elgoyhen AB, Marcotti W (2013a) Cholinergic efferent synaptic transmission regulates the maturation of auditory hair cell ribbon synapses. Open Biology 3.

Johnson SL, Kuhn S, Franz C, Ingham N, Furness DN, Knipper M, Steel KP, Adelman JP, Holley MC, Marcotti W (2013b) Presynaptic maturation in auditory hair cells requires a critical period of sensory-independent spiking activity. Proceedings of the National Academy of Sciences of the United States of America 110:8720-8725.

Johnson SL, Eckrich T, Kuhn S, Zampini V, Franz C, Ranatunga KM, Roberts TP, Masetto S, Knipper M, Kros CJ, Marcotti W (2011) Position-dependent patterning of spontaneous action potentials in immature cochlear inner hair cells. Nature Neuroscience 14:711-U386.

Johnson SL, Franz C, Kuhn S, Furness DN, Ruttiger L, Munkner S, Rivolta MN, Seward EP, Herschman HR, Engel J, Knipper M, Marcotti W (2010) Synaptotagmin IV determines the linear Ca2+ dependence of vesicle fusion at auditory ribbon synapses. Nature Neuroscience 13:45-U201.

Jung S, Oshima-Takago T, Chakrabarti R, Wong AB, Jing Z, Yamanbaeva G, Picher MM, Wojcik SM, Goettfert F, Predoehl F, Michel K, Hell SW, Schoch S, Strenzke N, Wichmann C, Moser T (2015) Rab3-interacting molecules 2 alpha and 2 beta promote the abundance of voltage-gated Ca(V)1.3 Ca2+ channels at hair cell active zones. Proceedings of the National Academy of Sciences of the United States of America 112:7347-7347.

Kachar B, Battaglia A, Fex J (1997) Compartmentalized vesicular traffic around the hair cell cuticular plate. Hear Res 107:102-112.

Kamp TJ, Hell JW (2000) Regulation of cardiac L-type calcium channels by protein kinase A and protein kinase C. Circulation Research 87:1095-1102.

Kaneko A (1970) Physiological and morphological identification of horizontal, bipolar and amacrine cells in goldfish retina. Journal of Physiology-London 207:623-&.

Kantardzhieva A, Peppi M, Lane WS, Sewell WF (2012) Protein composition of immunoprecipitated synaptic ribbons. Journal of Proteome Research 11:1163-1174.

Katz E, Elgoyhen ABN, Gomez-Casati ME, Knipper M, Vetter DE, Fuchs PA, Glowatzki E (2004) Developmental regulation of nicotinic synapses on cochlear inner hair cells. Journal of Neuroscience 24:7814-7820.

Katz LC, Shatz CJ (1996) Synaptic activity and the construction of cortical circuits. Science 274:1133-1138.

Ke B, Oh E, Thurmond DC (2007) Doc2 beta is a novel Munc18c-interacting partner and positive effector of syntaxin 4-mediated exocytosis. Journal of Biological Chemistry 282:21786-21797.

Kelley MW (2006) Regulation of cell fate in the sensory epithelia of the inner ear. Nature Reviews Neuroscience 7:837-849.

Kelsell DP, Dunlop J, Stevens HP, Lench NJ, Liang JN, Parry G, Mueller RF, Leigh IM (1997) Connexin 26 mutations in hereditary non-syndromic sensorineural deafness. Nature 387:80-83.

Kennedy HJ, Evans MG, Crawford AC, Fettiplace R (2006) Depolarization of cochlear outer hair cells evokes active hair bundle motion by two mechanisms. Journal of Neuroscience 26:2757-2766.

Khimich D, Nouvian R, Pujol R, Dieck ST, Egner A, Gundelfinger ED, Moser T (2005) Hair cell synaptic ribbons are essential for synchronous auditory signalling. Nature 434:889-894.

Kiang NY-S (1966) Research Monograph: Discharge patterns of single fibers in the cat's auditory nerve.xvii+154p. Illus.-xvii+154p. Illus.

Kiang NYS, Clark LF, Watanabe T, Thomas EC (1962) Stimulus coding in cats auditory nerve - preliminary report. Annals of Otology Rhinology and Laryngology 71:1009-&.

Kiang NYS, Rho JM, Northrop CC, Liberman MC, Ryugo DK (1982) Hair-cell innervation by spiral ganglion-cells in adult cats. Science 217:175-177.

Kojima T, Fukuda M, Aruga J, Mikoshiba K (1996) Calcium-dependent phospholipid binding to the C2A domain of a ubiquitous form of double C2 protein (Doc2 beta). Journal of Biochemistry 120:671-676.

Kononenko NL, Haucke V (2015) Molecular mechanisms of presynaptic membrane retrieval and synaptic vesicle reformation. Neuron 85:484-496.

Kros CJ, Ruppersberg JP, Rusch A (1998) Expression of a potassium current in inner hair cells during development of hearing in mice. Nature 394:281-284.

Kudo M, Saito S, Sakagami H, Suzaki H, Kondo H (1999) Localization of mRNAs for synaptojanin isoforms in the brain of developing and mature rats. Brain Res Mol Brain Res 64:179-185.

Kujawa SG, Liberman MC (2009) Adding Insult to Injury: Cochlear Nerve Degeneration after "Temporary" Noise-Induced Hearing Loss. Journal of Neuroscience 29:14077-14085.

Kurtz R, Warzecha AK, Egelhaaf M (2001) Transfer of visual motion information via graded synapses operates linearly in the natural activity range. Journal of Neuroscience 21:6957-6966.

Lautermann J, Frank HG, Jahnke K, Traub O, Winterhager E (1999) Developmental expression patterns of connexin26 and-30 in the rat cochlea. Developmental Genetics 25:306-311.

Lautermann J, ten Cate WJF, Altenhoff P, Grummer R, Traub O, Frank HG, Jahnke K, Winterhager E (1998) Expression of the gap-junction connexins 26 and 30 in the rat cochlea. Cell and Tissue Research 294:415-420.

Li L, Chin LS, Shupliakov O, Brodin L, Sihra TS, Hvalby O, Jensen V, Zheng D, McNamara JO, Greengard P, Andersen P (1995) Impairment of synaptic vesicle clustering and of synaptic transmission, and increased seizure propensity, in synapsin I-deficient mice. Proceedings of the National Academy of Sciences of the United States of America 92:9235-9239.

Liberman LD, Wang HB, Liberman MC (2011) Opposing gradients of ribbon size and AMPA receptor expression underlie sensitivity differences among cochlear-nerve/hair-cell synapses. Journal of Neuroscience 31:801-808.

Liberman MC (1978) Auditory-nerve response from cats raised in a low-noise chamber. Journal of the Acoustical Society of America 63:442-455.

Liberman MC (1980) Morphological differences among radial afferent-fibers in the cat cochlea - an electron - microscopic study of serial sections. Hearing Research 3:45-63.

Liberman MC (1982) Single-neuron labelling in in the cat auditory nerve. Science 216:1239-1241.

Liberman MC, Dodds LW, Pierce S (1990) Afferent and efferent innervation of the cat cochlea - quantitative analysis with light and electron-microscopy. Journal of Comparative Neurology 301:443-460.

Lindau M, Neher E (1988) Patch-clamp techniques for time-resolved capacitance measurements in single cells. Pflugers Archiv-European Journal of Physiology 411:137-146.

Liu F, Day M, Muniz LC, Bitran D, Arias R, Revilla-Sanchez R, Grauer S, Zhang G, Kelley C, Pulito V, Sung A, Mervis RF, Navarra R, Hirst WD, Reinhart PH, Marquis KL, Moss SJ, Pangalos MN, Brandon NJ (2008) Activation of estrogen receptor-beta regulates

hippocampal synaptic plasticity and improves memory. Nature Neuroscience 11:334-343.

Maeda S, Tsukihara T (2011) Structure of the gap junction channel and its implications for its biological functions. Cellular and Molecular Life Sciences 68:1115-1129.

Mani M, Lee SY, Lucast L, Cremona O, Di Paolo G, De Camlli P, Ryan TA (2007) The dual phosphatase activity of synaptojanin1 is required for both efficient synaptic vesicle endocytosis and reavailability at nerve terminals. Neuron 56:1004-1018.

Manji SSM, Williams LH, Miller KA, Ooms LM, Bahlo M, Mitchell CA, Dahl H-HM (2011) A mutation in synaptojanin 2 causes progressive hearing loss in the ENU-mutagenised mouse strain mozart. Plos One 6.

Marcotti W (2012) Functional assembly of mammalian cochlear hair cells. Experimental Physiology 97:438-451.

Marcotti W, Johnson SL, Kros CJ (2004) A transiently expressed SK current sustains and modulates action potential activity in immature mouse inner hair cells. Journal of Physiology-London 560:691-708.

Marcotti W, Johnson SL, Holley MC, Kros CJ (2003a) Developmental changes in the expression of potassium currents of embryonic, neonatal and mature mouse inner hair cells. Journal of Physiology-London 548:383-400.

Marcotti W, Johnson SL, Rusch A, Kros CJ (2003b) Sodium and calcium currents shape action potentials in immature mouse inner hair cells. Journal of Physiology-London 552:743-761.

Matthews G, Sterling P (2008) Evidence that vesicles undergo compound fusion on the synaptic ribbon. Journal of Neuroscience 28:5403-5411.

Matthews G, Fuchs P (2010) The diverse roles of ribbon synapses in sensory neurotransmission. Nature Reviews Neuroscience 11:812-822.

McMahon HT, Boucrot E (2011) Molecular mechanism and physiological functions of clathrin-mediated endocytosis. Nature Reviews Molecular Cell Biology 12:517-533.

McPherson PS, Takei K, Schmid SL, De Camilli P (1994) p145, a major Grb2-binding protein in brain, is co-localized with dynamin in nerve terminals where it undergoes activity-dependent dephosphorylation. J Biol Chem 269:30132-30139.

McPherson PS, Garcia EP, Slepnev VI, David C, Zhang X, Grabs D, Sossin WS, Bauerfeind R, Nemoto Y, De Camilli P (1996) A presynaptic inositol-5-phosphatase. Nature 379:353-357.

Meyer AC, Frank T, Khimich D, Hoch G, Riedel D, Chapochnikov NM, Yarin YM, Harke B, Hell SW, Egner A, Moser T (2009) Tuning of synapse number, structure and function in the cochlea. Nature Neuroscience 12:444-453.

Morgans CW (2000) Neurotransmitter release at ribbon synapses in the retina. Immunology and Cell Biology 78:442-446.

Morsli H, Choo D, Ryan A, Johnson R, Wu DK (1998) Development of the mouse inner ear and origin of its sensory organs. Journal of Neuroscience 18:3327-3335.

Moser T, Beutner D (2000) Kinetics of exocytosis and endocytosis at the cochlear inner hair cell afferent synapse of the mouse. Proceedings of the National Academy of Sciences of the United States of America 97:883-888.

Neef J, Jung S, Wong AB, Reuter K, Pangrsic T, Chakrabarti R, Kuegler S, Lenz C, Nouvian R, Boumil RM, Frankel WN, Wichmann C, Moser T (2014) Modes and regulation of endocytic membrane retrieval in mouse auditory hair cells. Journal of Neuroscience 34:705-716.

Nemoto Y, Arribas M, Haffner C, DeCamilli P (1997) Synaptojanin 2, a novel synaptojanin isoform with a distinct targeting domain and expression pattern. J Biol Chem 272:30817-30821.

Nickel R, Forge A (2008) Gap junctions and connexins in the inner ear: their roles in homeostasis and deafness. Current Opinion in Otolaryngology & Head and Neck Surgery 16:452-457.

Nouvian R, Neef J, Bulankina AV, Reisinger E, Pangrsic T, Frank T, Sikorra S, Brose N, Binz T, Moser T (2011) Exocytosis at the hair cell ribbon synapse apparently operates without neuronal SNARE proteins. Nature Neuroscience 14:411-413.

Oarih (2004) Cochlea-crosssection. In. Wikipedia.

Open University T (2013) The role of the basilar membrane in sound reception. In: Structure and Function of the inner ear.

Orita S, Sasaki T, Komuro R, Sakaguchi G, Maeda M, Igarashi H, Takai Y (1996) Doc2 enhances Ca2+-dependent exocytosis from PC12 cells. Journal of Biological Chemistry 271:7257-7260.

Orita S, Sasaki T, Naito A, Komuro R, Ohtsuka T, Maeda M, Suzuki H, Igarashi H, Takai Y (1995) DOC2 - A novel brain protein having 2 repeated C-2-like domains. Biochemical and Biophysical Research Communications 206:439-448.

Ortolano S, Di Pasquale G, Crispino G, Anselmi F, Mammano F, Chiorini JA (2008) Coordinated control of connexin 26 and connexin 30 at the regulatory and functional level in the inner ear. Proceedings of the National Academy of Sciences of the United States of America 105:18776-18781.

Palmer AR, Russell IJ (1986) Phase-locking in the cochlear nerve of the guinea-pig and its relation to the receptor potential of inner hair cells. Hearing Research 24:1-15.

Pangrsic T, Reisinger E, Moser T (2012) Otoferlin: a multi-C-2 domain protein essential for hearing. Trends in Neurosciences 35:671-680.

Pangrsic T, Lasarow L, Reuter K, Takago H, Schwander M, Riedel D, Frank T, Tarantino LM, Bailey JS, Strenzke N, Brose N, Muller U, Reisinger E, Moser T (2010) Hearing requires otoferlin-dependent efficient replenishment of synaptic vesicles in hair cells. Nature Neuroscience 13:869-U116.

Parnas H, Parnas I (1994) Neurotransmitter release at fast synapses. Journal of Membrane Biology 142:267-279.

Parsons TD, Sterling P (2003) Synaptic ribbon: Conveyor belt or safety belt? Neuron 37:379-382.

Parsons TD, Lenzi D, Almers W, Roberts WM (1994) Calcium-triggered exocytosis and endocytosis in an isolated presynaptic cell - capacitance measurements in saccular hair-cells. Neuron 13:875-883.

Perkins RE, Morest DK (1975) Study of cochlear innervation patterns in cats and rats with golgi method and nomarski optics. Journal of Comparative Neurology 163:129-158.

Petit C, Richardson GP (2009) Linking genes underlying deafness to hair-bundle development and function. Nature Neuroscience 12:703-710.

Piazza V, Ciubotaru CD, Gale JE, Mammano F (2007) Purinergic signalling and intercellular Ca2+ wave propagation in the organ of Corti. Cell Calcium 41:77-86.

Pinheiro PS, de Wit H, Walter AM, Groffen AJ, Verhage M, Sorensen JB (2013) Doc2b synchronizes secretion from chromaffin cells by stimulating fast and inhibiting sustained release. Journal of Neuroscience 33:16459-16470.

Platzer J, Engel J, Schrott-Fischer A, Stephan K, Bova S, Chen H, Zheng H, Striessnig J (2000) Congenital deafness and sinoatrial node dysfunction in mice lacking class D L-type Ca2+ channels. Cell 102:89-97.

Pujol R, Lavigne-Rebellard M, Lenoir M (1998) Development of sensory and neural structures in the mammalian cochlea. Springer Handbook of Auditory Research 9:146-192.

Rabbitt RD, Brownell WE (2011) Efferent modulation of hair cell function. Current Opinion in Otolaryngology & Head and Neck Surgery 19:376-381.

Rabionet R, Gasparini P, Estivill X (2000) Molecular genetics of hearing impairment due to mutations in gap junction genes encoding beta connexins. Human Mutation 16:190-202.

Rama S, Zbili M, Debanne D (2015) Modulation of spike-evoked synaptic transmission: The role of presynaptic calcium and potassium channels. Biochimica Et Biophysica Acta-Molecular Cell Research 1853:1933-1939.

Ramalingam L, Oh E, Thurmond DC (2014) Doc2b enrichment enhances glucose homeostasis in mice via potentiation of insulin secretion and peripheral insulin sensitivity. Diabetologia 57:1476-1484.

Richardson GP, Lukashkin AN, Russell IJ (2008) The tectorial membrane: one slice of a complex cochlear sandwich. Current Opinion in Otolaryngology & Head and Neck Surgery 16:458-464.

Rizzoli SO (2014) Synaptic vesicle recycling: steps and principles. Embo Journal 33:788-822.

Robles L, Ruggero MA (2001) Mechanics of the mammalian cochlea. Physiological Reviews 81:1305-1352.

Rosahl TW, Spillane D, Missler M, Herz J, Selig DK, Wolff JR, Hammer RE, Malenka RC, Sudhof TC (1995) Essential function of synapsin-I and synapsin-II in synaptic vesicle regulation. Nature 375:488-493.

Rose JE, Brugge JF, Anderson DJ, Hind JE (1967) Phase-locked response to low-frequency tones in single auditory nerve fibers of squirrel monkey. Journal of Neurophysiology 30:769-&.

Roux I, Safieddine S, Nouvian R, Grati Mh, Simmler M-C, Bahloul I, Perfettini I, Le Gall M, Rostaing P, Hamard G, Triller A, Avan P, Moser T, Petit C (2006) Otoferlin, defective in a human deafness form, is essential for exocytosis at the auditory ribbon synapse. Cell 127:277-289.

Rubel EW, Fritzsch B (2002) Auditory system development: Primary auditory neurons and their targets. Annual Review of Neuroscience 25:51-101.

Rupert A, Galambos R, Moushegian G (1963) Unit responses to sound from auditory nerve of cat. Journal of Neurophysiology 26:449-&.

Rusk N, Le PU, Mariggio S, Guay G, Iurisci C, Nabi IR, Corda D, Symons M (2003) Synaptojanin 2 functions at an early step of clathrin-mediated endocytosis (vol 13, pg 659, 2003). Current Biology 13:1746-1746.

Russell IJ, Sellick PM (1977) Tuning properties of cochlear hair cells. Nature 267:858-860.

Russell IJ, Sellick PM (1978) Intracellular studies of hair cells in mammalian cochlea. Journal of Physiology-London 284:261-290.

Rutherford MA, Chapochnikov NM, Moser T (2012) Spike encoding of neurotransmitter release timing by spiral ganglion neurons of the cochlea. Journal of Neuroscience 32:4773-4789.

Safieddine S, Wenthold RJ (1999) SNARE complex at the ribbon synapses of cochlear hair cells: analysis of synaptic vesicle- and synaptic membrane-associated proteins. European Journal of Neuroscience 11:803-812.

Safieddine S, El-Amraoui A, Petit C (2012) The auditory hair cell ribbon synapse: From assembly to function. In: Annual Review of Neuroscience, Vol 35 (Hyman SE, ed), pp 509-528. Palo Alto: Annual Reviews.

Saszik S, DeVries SH (2012) A mammalian retinal bipolar cell uses both graded changes in membrane voltage and all-or-nothing Na+ spikes to encode light. Journal of Neuroscience 32:297-307.

Schmid AC, Wise HM, Mitchell CA, Nussbaum R, Woscholski R (2004) Type II phosphoinositide 5-phosphatases have unique sensitivities towards fatty acid composition and head group phosphorylation. Febs Letters 576:9-13.

Schmitz F (2014) Presynaptic Ca(2+) and GCAPs: aspects on the structure and function of photoreceptor ribbon synapses. Frontiers in molecular neuroscience 7:3-3.

Schmitz F, Konigstorfer A, Sudhof TC (2000) RIBEYE, a component of synaptic ribbons: A protein's journey through evolution provides insight into synaptic ribbon function. Neuron 28:857-872.

Schug N, Braig C, Zimmermann U, Engel J, Winter H, Ruth P, Blin N, Pfister M, Kalbacher H, Knipper M (2006) Differential expression of otoferlin in brain, vestibular system, immature and mature cochlea of the rat. European Journal of Neuroscience 24:3372-3380.

Schutz M, Scimemi P, Majumder P, De Siati RD, Crispino G, Rodriguez L, Bortolozzi M, Santarelli R, Seydel A, Sonntag S, Ingham N, Steel KP, Willecke K, Mammano F (2010) The human deafness-associated connexin 30 T5M mutation causes mild hearing loss and reduces biochemical coupling among cochlear non-sensory cells in knock-in mice. Human Molecular Genetics 19:4759-4773.

Sher AE (1971) The embryonic and postnatal development of the inner ear of the mouse. Acta oto-laryngologica Supplementum 285:1-77.

Simmons DD, Mansdorf NB, Kim JH (1996) Olivocochlear innervation of inner and outer hair cells during postnatal maturation: Evidence for a waiting period. Journal of Comparative Neurology 370:551-562.

Sjostrand FS (1958) Ultrastructure of retinal rod synapses of the guinea pig eye as revealed by 3-dimensional reconstructions from serial sections. Journal of Ultrastructure Research 2:122-170.

Snellman J, Mehta B, Babai N, Bartoletti TM, Akmentin W, Francis A, Matthews G, Thoreson W, Zenisek D (2011) Acute destruction of the synaptic ribbon reveals a role for the ribbon in vesicle priming. Nature Neuroscience 14:1135-U1262.

Sobkowicz HM, August BK, Slapnick SM (2002) Influence of neurotrophins on the synaptogenesis of inner hair cells in the deaf Bronx waltzer (bv) mouse organ of Corti in culture. International Journal of Developmental Neuroscience 20:537-554.

Sobkowicz HM, Rose JE, Scott GE, Slapnick SM (1982) Ribbon synapses in the developing intact and cultured organ of Corti in the mouse. Journal of Neuroscience 2:942-957.

Spoendlin H (1972) Innervation densities of the cochlea. Acta Otolaryngol 73:235-248.

Stellwagen D, Shatz CJ (2002) An instructive role for retinal waves in the development of retinogeniculate connectivity. Neuron 33:357-367.

Sudhof TC (2013) Neurotransmitter release: The last millisecond in the life of a synaptic vesicle. Neuron 80:675-690.

Sudhof TC, Rothman JE (2009) Membrane Fusion: Grappling with SNARE and SM Proteins. Science 323:474-477.

Sun Y, Tang W, Chang Q, Wang Y, Kong W, Lin X (2009) Connexin30 null and conditional connexin26 null nice display distinct pattern and time course of cellular degeneration in the cochlea. Journal of Comparative Neurology 516:569-579.

Teubner B, Michel V, Pesch J, Lautermann J, Cohen-Salmon M, Sohl G, Jahnke K, Winterhager E, Herberhold C, Hardelin JP, Petit C, Willecke K (2003) Connexin30 (Gjb6)-deficiency causes severe hearing impairment and lack of endocochlear potential. Human Molecular Genetics 12:13-21.

Thuronyi B (2010) Phosphatidylinositol. In. Wikipedia.

Tilney LG, Tilney MS (1986) Functional-organization of the cytoskeleton. Hearing Research 22:55-77.

Torres M, Giraldez F (1998) The development of the vertebrate inner ear. Mechanisms of Development 71:5-21.

Trapani JG, Obholzer N, Mo W, Brockerhoff SE, Nicolson T (2009) Synaptojanin1 is required for temporal fidelity of synaptic transmission in hair cells. Plos Genetics 5.

Tritsch NX, Bergles DE (2010) Developmental regulation of spontaneous activity in the mammalian cochlea. Journal of Neuroscience 30:1539-1550.

Tritsch NX, Yi E, Gale JE, Glowatzki E, Bergles DE (2007) The origin of spontaneous activity in the developing auditory system. Nature 450:50-+.

Tritsch NX, Rodriguez-Contreras A, Crins TTH, Wang HC, Borst JGG, Bergles DE (2010) Calcium action potentials in hair cells pattern auditory neuron activity before hearing onset. Nature Neuroscience 13:1050-1052.

Ubach J, Garcia J, Nittler MP, Sudhof TC, Rizo J (1999) Structure of the Janus-faced C2B domain of rabphilin. Nature Cell Biology 1:106-112.

Uthaiah RC, Hudspeth AJ (2010) Molecular anatomy of the hair cell's ribbon synapse. Journal of Neuroscience 30:12387-12399.

Van Epps HA, Yim CM, Hurley JB, Brockerhoff SE (2001) Investigations of photoreceptor synaptic transmission and light adaptation in the zebrafish visual mutant nrc. Investigative Ophthalmology & Visual Science 42:868-874.

Van Epps HA, Hayashi M, Lucast L, Stearns GW, Hurley JB, De Camilli P, Brockerhoff SE (2004) The zebrafish nrc mutant reveals a role for the polyphosphoinositide phosphatase synaptojanin 1 in cone photoreceptor ribbon anchoring. J Neurosci 24:8641-8650.

VanDewater T, Popper A, Richard R (1996) Springer Handbook of Auditory Research, Vol. 7. Clinical aspects of hearing. Springer Handbook of Auditory Research; Clinical aspects of hearing 7:xiv+317p-xiv+317p.

Verhage M, deVries KJ, Roshol H, Burbach JPH, Gispen WH, Sudhof TC (1997) DOC2 proteins in rat brain: Complementary distribution and proposed function as vesicular adapter proteins in early stages of secretion. Neuron 18:453-461.

Vogl C, Cooper BH, Neef J, Wojcik SM, Reim K, Reisinger E, Brose N, Rhee J-S, Moser T, Wichmann C (2015) Unconventional molecular regulation of synaptic vesicle replenishment in cochlear inner hair cells. Journal of cell science 128:638-644.

White JK et al. (2013) Genome-wide generation and systematic phenotyping of knockout mice reveals new roles for many genes. Cell 154:452-464.

Wittig JH, Parsons TD (2008) Synaptic ribbon enables temporal precision of hair cell afferent synapse by increasing the number of readily releasable vesicles: A modeling study. Journal of Neurophysiology 100:1724-1739.

Wong AB, Rutherford MA, Gabrielaitis M, Pangrsic T, Goettfert F, Frank T, Michanski S, Hell S, Wolf F, Wichmann C, Moser T (2014) Developmental refinement of hair cell synapses tightens the coupling of Ca2+ influx to exocytosis. Embo Journal 33:247-264.

Wu Y, Gu YW, Morphew MK, Yao J, Yeh FL, Dong M, Chapman ER (2012) All three components of the neuronal SNARE complex contribute to secretory vesicle docking. Journal of Cell Biology 198:323-330.

Yasunaga S, Grati M, Chardenoux S, Smith TN, Friedman TB, Lalwani AK, Wilcox ER, Petit C (2000) OTOF encodes multiple long and short isoforms: Genetic evidence that the long ones underlie recessive deafness DFNB9. American Journal of Human Genetics 67:591-600.

Yasunaga S, Grati M, Cohen-Salmon M, El-Amraoui A, Mustapha M, Salem N, El-Zir E, Loiselet J, Petit C (1999) A mutation in OTOF, encoding otoferlin, a FER-1-like protein, causes DFNB9, a nonsyndromic form of deafness. Nature Genetics 21:363-369.

Yikrazuul (2010) Myo-Inositol and Inositol-1,4,5 trisphosphate. In. Wikipedia.

Yu H, Rathore SS, Davis EM, Ouyang Y, Shen J (2013) Doc2b promotes GLUT4 exocytosis by activating the SNARE-mediated fusion reaction in a calcium-and membrane bending-dependent manner. Molecular Biology of the Cell 24:1176-1184.

Zampini V, Johnson SL, Franz C, Knipper M, Holley MC, Magistretti J, Masetto S, Marcotti W (2013) Burst activity and ultrafast activation kinetics of Ca(V)1.3 Ca2+ channels support presynaptic activity in adult gerbil hair cell ribbon synapses. Journal of Physiology-London 591:3811-3820.

Zampini V, Johnson SL, Franz C, Lawrence ND, Munkner S, Engel J, Knipper M, Magistretti J, Masetto S, Marcotti W (2010) Elementary properties of Ca(V)1.3 Ca2+channels expressed in mouse cochlear inner hair cells. Journal of Physiology-London 588:187-199.

Zerlin S (1969) Travelling-wave velocity in the human cochlea. Journal of the Acoustical Society of America 46:1011-&.

Zhang X, Milton CC, Poon CLC, Hong W, Harvey KF (2011a) Wbp2 cooperates with Yorkie to drive tissue growth downstream of the Salvador-Warts-Hippo pathway. Cell Death and Differentiation 18:1346-1355.

Zhang Z, Wu Y, Wang Z, Dunning FM, Rehfuss J, Ramanan D, Chapman ER, Jackson MB (2011b) Release mode of large and small dense-core vesicles specified by different synaptotagmin isoforms in PC12 cells. Molecular Biology of the Cell 22:2324-2336.

Zheng J, Shen WX, He DZZ, Kevin BL, Madison LD, Dallos P (2000) Prestin is the motor protein of cochlear outer hair cells. Nature 405:149-155.